



The Compact Muon Solenoid Experiment  
**Analysis Note**

The content of this note is intended for CMS internal use and distribution only



October 12, 2012

# Search for Direct Stop Quark Pair Production in the Single Lepton Channel at 8 TeV

L. Bauerdick, K. Burkett, I. Fisk, Y. Gao, O. Gutsche, B. Hooberman, S. Jindariani, J. Linacre, V. Martinez Outschoorn

*Fermilab National Accelerator Laboratory, Batavia, USA*

C. Campagnari, A. George, F. Golf, D. Kovalskyi, V. Krutelyov

*University of California, Santa Barbara, Santa Barbara, USA*

G. Cerati, M. D'Alfonso, D. Evans, R. Kelley, I. MacNeill, S. Padhi, Y. Tu, F. Würthwein, V. Welke, A. Yagil, J. Yoo

*University of California, San Diego, San Diego, USA*

## Abstract

This note describes a search for direct stop quark pair production in the single lepton channel using  $9.7 \text{ fb}^{-1}$  of pp collision data at  $\sqrt{s} = 8 \text{ TeV}$  taken with the CMS detector in 2012. A search for an excess of events over the Standard Model prediction is performed in a sample with a single isolated electron or muon, several jets including a b-tagged jet, missing transverse energy, and large transverse mass.

# Contents

<b>1</b>	<b>Introduction</b>	<b>3</b>
<b>2</b>	<b>Overview and Strategy for Background Determination</b>	<b>3</b>
2.1	$\ell$ + jets background . . . . .	4
2.2	Dilepton background . . . . .	5
2.3	Other backgrounds . . . . .	5
2.4	Future improvements . . . . .	6
<b>3</b>	<b>Data Samples</b>	<b>6</b>
<b>4</b>	<b>Event Selection</b>	<b>8</b>
4.1	Single Lepton Selection . . . . .	8
4.2	Isolated track veto . . . . .	8
4.3	Signal Region Selection . . . . .	8
4.4	Control Region Selection . . . . .	9
4.5	Definition of $M_T$ peak region . . . . .	10
4.6	Default $t\bar{t}$ MC sample . . . . .	10
4.7	MC Corrections . . . . .	10
4.7.1	Corrections to Jets and $E_T^{\text{miss}}$ . . . . .	10
4.8	Lepton Selection Efficiency Measurements . . . . .	10
4.9	Trigger Efficiency Measurements . . . . .	16
<b>5</b>	<b>Signal reach</b>	<b>18</b>
<b>6</b>	<b>Control Region Studies</b>	<b>22</b>
6.1	W+Jets MC Modelling Validation from CR1 . . . . .	22
6.2	Single Lepton Top MC Modelling Validation from CR2 . . . . .	27
6.3	Dilepton studies in CR4 . . . . .	30
6.3.1	Modeling of Additional Hard Jets in Top Dilepton Events . . . . .	30
6.3.2	Validation of the “Physics” Modelling of the $t\bar{t} \rightarrow \ell\ell$ MC in CR4 . . . . .	32
6.4	Test of control region with isolated track in CR5 . . . . .	35
<b>7</b>	<b>Other Backgrounds</b>	<b>39</b>
<b>8</b>	<b>Tail-to-Peak ratio for lepton + jets top and W events</b>	<b>39</b>
<b>9</b>	<b>Background Prediction</b>	<b>40</b>
<b>10</b>	<b>Systematic Uncertainties on the Background</b>	<b>44</b>
10.1	Statistical uncertainties on the event counts in the $M_T$ peak regions . . . . .	44
10.2	Uncertainty from the choice of $M_T$ peak region . . . . .	44

10.3	Uncertainty on the Wjets cross-section and the rare MC cross-sections . . . . .	44
10.4	Scale factors for the tail-to-peak ratios for lepton + jets top and W events . . . . .	44
10.5	Uncertainty on extra jet radiation for dilepton background . . . . .	45
10.6	Uncertainty from MC statistics . . . . .	45
10.7	Uncertainty on the $t\bar{t} \rightarrow \ell\ell$ Acceptance . . . . .	45
10.8	Uncertainty from the isolated track veto . . . . .	51
10.8.1	Isolated Track Veto: Tag and Probe Studies . . . . .	51
<b>11</b>	<b>Results</b>	<b>55</b>
<b>12</b>	<b>Conclusion</b>	<b>59</b>
<b>A</b>	<b>Performance of the Isolation Requirement</b>	<b>60</b>
<b>B</b>	<b>Additional CR Data and MC Comparisons</b>	<b>61</b>
<b>C</b>	<b>Glossary of abbreviations</b>	<b>67</b>

# 1 Introduction

This note presents a search for the production of supersymmetric (SUSY) stop quark pairs in events with a single isolated lepton, several jets, missing transverse energy, and large transverse mass. We use a data sample corresponding to an integrated luminosity of  $9.7 \text{ fb}^{-1}$ . This search is of theoretical interest because of the critical role played by the stop quark in solving the hierarchy problem in SUSY models. This solution requires that the stop quark be light, less than a few hundred GeV and hence within reach for direct pair production. We focus on two decay modes  $\tilde{t} \rightarrow t\chi_1^0$  and  $\tilde{t} \rightarrow b\chi_1^+$  which are expected to have large branching fractions if they are kinematically accessible, leading to:

- $pp \rightarrow \tilde{t}\tilde{t} \rightarrow t\bar{t}\chi_1^0\chi_1^0$ , and
- $pp \rightarrow \tilde{t}\tilde{t} \rightarrow b\bar{b}\chi_1^+\chi_1^- \rightarrow b\bar{b}W^+W^-\chi_1^0\chi_1^0$ .

Both of these signatures contain high transverse momentum ( $p_T$ ) jets including two b-jets, and missing transverse energy ( $E_T^{\text{miss}}$ ) due to the invisible  $\chi_1^0$  lightest SUSY particles (LSP's). In addition, the presence of two W bosons leads to a large branching fraction to the single lepton final state. Hence we require the presence of exactly one isolated, high  $p_T$  electron or muon, which provides significant suppression of several backgrounds that are present in the all-hadronic channel. The largest backgrounds for this signature are semi-leptonic  $t\bar{t}$  and  $W$ +jets. These backgrounds contain a single leptonically-decaying W boson, and the transverse mass ( $M_T$ ) of the lepton-neutrino system has a kinematic endpoint requiring  $M_T < M_W$ . For signal stop quark events, the presence of additional LSP's in the final states allows the  $M_T$  to exceed  $M_W$ . Hence we search for an excess of events with large  $M_T$ . The dominant background in this kinematic region is dilepton  $t\bar{t}$  where one of the leptons is not identified, since the presence of two neutrinos from leptonically-decaying W bosons allows the  $M_T$  to exceed  $M_W$ . Backgrounds are estimated from Monte Carlo (MC) simulation, with careful validation and determination of scale factors (where necessary) and corresponding uncertainties based on data control samples.

The expected stop quark pair production cross section (see Fig. 1) varies between 18 pb for  $m_{\tilde{t}} = 200 \text{ GeV}$  and 0.09 pb for  $m_{\tilde{t}} = 500 \text{ GeV}$  [1]. The critical challenge of this analysis is due to the fact that for light stop quarks ( $m_{\tilde{t}} \approx m_t$ ), the production cross section is large but the kinematic distributions, in particular  $M_T$ , are very similar to SM  $t\bar{t}$  production. In this regime it becomes very difficult to distinguish the signal and background. For large stop quark mass the kinematic distributions differ from those in SM  $t\bar{t}$  production, but the cross section decreases rapidly, reducing the signal-to-background ratio.

## 2 Overview and Strategy for Background Determination

We are searching for a  $t\bar{t}\chi^0\chi^0$  or  $WbW\bar{b}\chi^0\chi^0$  final state (after top decay in the first mode, the final states are actually the same). So to first order this is “ $t\bar{t}$ + extra  $E_T^{\text{miss}}$ ”.

We work in the  $\ell$ + jets final state, where the main background is  $t\bar{t}$ . We look for  $E_T^{\text{miss}}$  inconsistent with  $W \rightarrow \ell\nu$ . We do this by concentrating on the  $\ell\nu$  transverse mass ( $M_T$ ), since except for resolution and W-off-shell effects,  $M_T < M_W$  for  $W \rightarrow \ell\nu$ . Thus, the initial analysis is simply a counting experiment in the tail of the  $M_T$  distribution.

The event selection is one-and-only-one high  $p_T$  isolated lepton, four or more jets, and an  $E_T^{\text{miss}}$  cut. At least one of the jets has to be b tagged to reduce  $W$ + jets. The event sample is then dominated by  $t\bar{t}$ , but there are also contributions from  $W$ + jets, single top, dibosons, as well as rare SM processes such as  $ttW$ .

The  $t\bar{t}$  events in the  $M_T$  tail can be broken up into two categories: (i)  $t\bar{t} \rightarrow \ell$ + jets, and (ii)  $t\bar{t} \rightarrow \ell^+\ell^-$  where one of the two leptons is not found by the second-lepton-veto (here the second lepton can be a hadronically decaying  $\tau$ ). For a reasonable  $M_T$  cut, say  $M_T > 150 \text{ GeV}$ , the dilepton background is approximately 80% of the total. This is because in dileptons there are two neutrinos from W decay, thus  $M_T$  is not bounded by  $M_W$ . This is a very important point: while it is true that we are looking in the tail of  $M_T$ , the bulk of the background events end up there not because of some exotic  $E_T^{\text{miss}}$  reconstruction failure, but because of well understood physics processes. This means that the background estimate can be taken from Monte Carlo (MC) after carefully accounting for possible data/MC differences.

The search is performed in a number of Signal Regions (SRs) defined by minimum requirements on  $E_T^{\text{miss}}$  and  $M_T$ . The SRs are defined in Section 4.3.



Figure 1: The stop quark pair production cross section as a function of the stop quark mass [2].

In Section 6 we will describe the analysis of various Control Regions (CRs) that are used to test the Monte Carlo model and, if necessary, to extract data/MC scale factors. In this section we give a general description of the procedure. The details of how the final background prediction is assembled are given in Section 9.

One general point is that in order to minimize systematic uncertainties, the MC background predictions are whenever possible normalized to the bulk of the  $t\bar{t}$  data, i.e., events passing all of the requirements but with  $M_T \approx 80$  GeV. This (mostly) removes uncertainties due to  $\sigma(t\bar{t})$ , lepton ID, trigger efficiency, luminosity, etc.

## 2.1 $\ell$ + jets background

The  $\ell$ + jets background is dominated by  $t\bar{t} \rightarrow \ell + \text{jets}$ , but also includes some  $W$ + jets as well as single top. The MC input used in the background estimation is the ratio of the number of events with  $M_T$  in the signal region to the number of events with  $M_T \approx 80$  GeV. This ratio is (possibly) corrected by a data/MC scale factor obtained from a study of CRs, as outlined below.

Note that the ratio described above is actually different for  $t\bar{t}$ /single top and  $W$ + jets. This is because in  $W$  events there is a significant contribution to the  $M_T$  tail from very off-shell  $W$ s. This contribution is much smaller in top events because  $M(\ell\nu)$  cannot exceed  $M_{top} - M_b$ . Therefore the large  $M_T$  tail in  $t\bar{t}$ /single top is dominated by jet resolution effects, while for  $W$ +jets events the large  $M_T$  tail is dominated by off-shell  $W$  production.

For  $W$ + jets the ability of the Monte Carlo to model this ratio ( $R_{wjet}$ ) is tested in a sample of  $\ell$ + jets enriched in  $W$ + jets by the application of a b-veto. The equivalent ratio for top events ( $R_{top}$ ) is validated in a sample of well identified  $Z \rightarrow \ell\ell$  with one lepton added to the  $E_T^{\text{miss}}$  calculation. This sample is well suited to testing the resolution effects on the  $M_T$  tail, since off-shell effects are eliminated by the  $Z$ -mass requirement.

Note that the fact that the ratios are different for  $t\bar{t}$ /single top and  $W$ + jets introduces a systematic uncertainty in the background calculation because one needs to know the relative fractions of these two components in the  $M_T \approx 80$  GeV lepton + jets sample.

## 2.2 Dilepton background

To suppress dilepton backgrounds, we veto events with an isolated track of  $p_T > 10$  GeV (see Sec. 4.2 for details). Being the common feature for electron, muon, and one-prong tau decays, this veto is highly efficient for rejecting  $t\bar{t}$  to dilepton events. The remaining dilepton background can be classified into the following categories:

- lepton is out of acceptance ( $|\eta| > 2.5$ )
- lepton has  $p_T < 10$  GeV, and is inside the acceptance
- lepton has  $p_T > 10$  GeV, is inside the acceptance, but survives the additional isolated track veto

The last category includes 1-prong and 3-prong hadronic tau decays, as well as electrons and muons either from direct  $W$  decay or via  $W \rightarrow \tau \rightarrow \ell$  decay that fail the isolation requirement. We note that at present we do not attempt to veto 3-prong tau decays as they are about 15% of the total dilepton background according to the MC.

The high  $M_T$  dilepton background predictions come from MC, but their rate is normalized to the  $M_T \approx 80$  GeV peak. In order to perform this normalization in data, the rare background events in the  $M_T$  peak are subtracted off. This also introduces a systematic uncertainty.

There are two types of effects that can influence the MC dilepton prediction: physics effects and instrumental effects. We discuss these next, starting from physics.

First of all, many of our  $t\bar{t}$  MC samples (e.g. MadGraph) have  $\text{BR}(W \rightarrow \ell\nu) = \frac{1}{9} = 0.1111$ . PDG says  $\text{BR}(W \rightarrow \ell\nu) = 0.1080 \pm 0.0009$ . This difference matters, so the  $t\bar{t}$  MC must be corrected to account for this.

Second, our selection is  $\ell + 4$  or more jets. A dilepton event passes the selection only if there are two additional jets from ISR, or one jet from ISR and one jet which is reconstructed from the unidentified lepton, *e.g.*, a three-prong tau. Therefore, all MC dilepton  $t\bar{t}$  samples used in the analysis must have their jet multiplicity corrected (if necessary) to agree with what is seen in  $t\bar{t}$  data. We use a data control sample of well identified dilepton events with  $E_T^{\text{miss}}$  and at least one jet (including at least one b-tag) as a template to “adjust” the  $N_{jet}$  distribution of the  $t\bar{t} \rightarrow$  dileptons MC samples.

The final physics effect has to do with the modeling of  $t\bar{t}$  production and decay. Different MC models could in principle result in different BG predictions. Therefore we use several different  $t\bar{t}$  MC samples using different generators and different parameters, to test the stability of the dilepton BG prediction. All these predictions, **after** corrections for branching ratio and  $N_{jet}$  dependence, are compared to each other. The spread is a measure of the systematic uncertainty associated with the  $t\bar{t}$  generator modeling.

The main instrumental effect is associated with the efficiency of the isolated track veto. We use tag-and-probe to compare the isolated track veto performance in  $Z + 4$  jets data and MC. Note that the performance of the isolated track veto is not exactly the same on  $e/\mu$  and on one prong hadronic tau decays. This is because the pions from one-prong taus are often accompanied by  $\pi^0$ 's that can then result in extra tracks due to photon conversions. We let the simulation take care of that. Note that JES uncertainties are effectively “calibrated away” by the  $N_{jet}$  rescaling described above.

## 2.3 Other backgrounds

Other backgrounds are  $tW$ ,  $t\bar{t}V$ , dibosons, tribosons, and Drell Yan. These are small. They are taken from MC with appropriate scale factors for trigger efficiency, and reweighting to match the distribution of reconstructed primary vertices in data.

## 2.4 Future improvements

Finally, there are possible improvements to this basic analysis strategy that can be added in the future:

- Move from counting experiment to shape analysis. But first, we need to get the counting experiment under control.
- Add an explicit three prong tau veto
- Do something to require that three of the jets in the event be consistent with  $t \rightarrow Wb, W \rightarrow q\bar{q}$ . This could help reject some of the dilepton BG in the search for  $\tilde{t} \rightarrow t\chi^0$ , but is not applicable to the  $\tilde{t} \rightarrow b\chi^+$  search.
- Consider the  $M(\ell b)$  variable, which is not bounded by  $M_{top}$  in  $\tilde{t} \rightarrow b\chi^+$

## 3 Data Samples

The datasets used for this analysis are summarized in Tables 1 (data) and 2 (MC). The total integrated luminosity is  $9.7 \text{ fb}^{-1}$  after applying the official good run list. The main  $t\bar{t}$  Monte Carlo sample is generated with Powheg since this sample has the largest number of events, though samples with alternative generators such as Madgraph are also used for the derivation of systematic uncertainties in the  $t\bar{t}$  background prediction. The triggers used to select both the signal and control samples are also summarized in Table 3.

Dataset Name
Single Lepton Samples
/SingleElectron/Run2012A-13Jul2012-v1/AOD
/SingleMu/Run2012A-13Jul2012-v1/AOD
/SingleElectron/Run2012B-13Jul2012-v1/AOD
/SingleMu/Run2012B-13Jul2012-v1/AOD
/SingleElectron/Run2012C-PromptReco-v1/AOD
/SingleMu/Run2012C-PromptReco-v1/AOD
/SingleElectron/Run2012C-PromptReco-v2/AOD
/SingleMu/Run2012C-PromptReco-v2/AOD
Dilepton Samples (only used for dilepton control region)
/DoubleElectron/Run2012A-13Jul2012-v1/AOD
/DoubleMu/Run2012A-13Jul2012-v1/AOD
/MuEG/Run2012A-13Jul2012-v1/AOD
/DoubleElectron/Run2012B-13Jul2012-v1/AOD
/DoubleMu/Run2012B-13Jul2012-v1/AOD
/MuEG/Run2012B-13Jul2012-v1/AOD
/DoubleElectron/Run2012C-PromptReco-v1/AOD
/DoubleMu/Run2012C-PromptReco-v1/AOD
/MuEG/Run2012C-PromptReco-v1/AOD
/DoubleElectron/Run2012C-PromptReco-v2/AOD
/DoubleMu/Run2012C-PromptReco-v2/AOD
/MuEG/Run2012C-PromptReco-v2/AOD

Table 1: Summary of data datasets used.

With Pileup: Processed dataset name is		
(53) Summer12_DR53X-PU_S10.START53.V7A-v*/AODSIM		
(52) Summer12-START52.V9.FSIM-v*/AODSIM		
Description	Primary Dataset Name	cross-section [pb]
tt	/TT_CT10_TuneZ2Star_8TeV-powheg-tauola (53)	225.2
$W \rightarrow \ell\nu$	/WJetsToLNu_TuneZ2Star_8TeV-madgraph-tauola (53)	37509
$W \rightarrow \ell\nu + 3 \text{ jets}$	/W3JetsToLNu_TuneZ2Star_8TeV-madgraph-tauola (53)	640
$W \rightarrow \ell\nu + \geq 4 \text{ jets}$	/W4JetsToLNu_TuneZ2Star_8TeV-madgraph-tauola (53)	264
WW	/WWJetsTo2L2Nu_TuneZ2star_8TeV-madgraph-tauola (53)	5.8
WZ	/WZJetsTo3LNu_TuneZ2.8TeV-madgraph-tauola (53)	1.1
	/WZJetsTo2L2Q_TuneZ2star_8TeV-madgraph-tauola (53)	1.1
ZZ	/ZZJetsTo2L2Nu_TuneZ2star_8TeV-madgraph-tauola (53)	0.4
	/ZZJetsTo4L_TuneZ2star_8TeV-madgraph-tauola (53)	0.2
	/ZZJetsTo2L2Q_TuneZ2star_8TeV-madgraph-tauola (53)	2.4
$t \text{ (s-chan)}$	/T_TuneZ2Star_s-channel_8TeV-powheg-tauola (53)	3.9
$\bar{t} \text{ (s-chan)}$	/Tbar_TuneZ2Star_s-channel_8TeV-powheg-tauola (53)	1.8
$t \text{ (t-chan)}$	/T_TuneZ2Star_t-channel_8TeV-powheg-tauola (53)	55.5
$\bar{t} \text{ (t-chan)}$	/Tbar_TuneZ2Star_t-channel_8TeV-powheg-tauola (53)	30.0
$tW$	/T_TuneZ2Star_tW-channel-DR_8TeV-powheg-tauola (53)	11.2
$\bar{t}W$	/Tbar_TuneZ2Star_tW-channel-DR_8TeV-powheg-tauola (53)	11.2
$Z/\gamma^* \rightarrow \ell\ell$	/DYJetsToLL_TuneZ2Star_M-50.8TeV-madgraph-tarball (53)	3532.8
$Z/\gamma^* \rightarrow \ell\ell + \geq 4 \text{ jets}$	/DY4JetsToLL_TuneZ2Star_M-50.8TeV-madgraph-tarball (53)	27.6
ttW	/TTW_TuneZ2Star_8TeV-madgraph (53)	0.23
ttZ	/TTZ_TuneZ2Star_8TeV-madgraph (53)	0.21
tt $\gamma$	/TTGJets_TuneZ2Star_8TeV-madgraph (53)	0.65
WWW	/WWW_TuneZ2Star_8TeV-madgraph (53)	0.082
WWZ	/WWZNoGstar_TuneZ2Star_8TeV-madgraph (53)	0.063
WZZ	/WZZNoGstar_TuneZ2Star_8TeV-madgraph (53)	0.019
ZZZ	/ZZZNoGstar_TuneZ2Star_8TeV-madgraph (53)	0.019
$t\bar{t} \rightarrow t\bar{t}\chi_1^0\chi_1^0$	/SMS-T2tt_FineBin_Mstop-225to1200_mLSP-0to1000.8TeV-Pythia6Z (52)	scan
$t\bar{t} \rightarrow b\bar{b}\chi_1^+\chi_1^-$	/SMS-T2bw_FineBin_Mstop-100to600_mLSP-0to500.8TeV-Pythia6Z (52)	scan
tt	/TTJets_MassiveBinDECAY_TuneZ2Star_8TeV-madgraph-tauola (53)	225.2
tt ( $Q^2 \times 2$ )	/TTjets_TuneZ2Star_scaleup_8TeV-madgraph-tauola (53)	225.2
tt ( $Q^2 \times 0.5$ )	/TTjets_TuneZ2Star_scaledown_8TeV-madgraph-tauola (53)	225.2
tt ( $x_q > 40 \text{ GeV}$ )	/TTjets_TuneZ2Star_matchingup_8TeV-madgraph-tauola (53)	225.2
tt ( $x_q > 10 \text{ GeV}$ )	/TTjets_TuneZ2Star_matchingdown_8TeV-madgraph-tauola (53)	225.2
tt ( $m_{\text{top}} = 178.5 \text{ GeV}$ )	/TTJets_TuneZ2Star_mass178.5_8TeV-madgraph-tauola (53)	225.2
tt ( $m_{\text{top}} = 166.5 \text{ GeV}$ )	/TTJets_TuneZ2Star_mass166.5_8TeV-madgraph-tauola (53)	225.2

Table 2: Summary of Monte Carlo datasets used.

Triggers
Single Muon Sample
HLT_IsoMu24_v*
HLT_IsoMu24_eta2p1_v*
Single Electron Sample
HLT_Ele27_WP80_v*
Dilepton Sample (only used for dilepton control regions)
HLT_Mu17_Mu8_v*
HLT_Mu17_Ele8_CaloIdT_CaloIsoVL_TrkIdVL_TrkIsoVL_v*
HLT_Mu8_Ele17_CaloIdT_CaloIsoVL_TrkIdVL_TrkIsoVL*
HLT_Ele17_CaloIdT_CaloIsoVL_TrkIdVL_TrkIsoVL_Ele8_CaloIdT_CaloIsoVL_TrkIdVL_TrkIsoVL_v*

Table 3: Summary of triggers used.



## 4 Event Selection

Here we define the selections of leptons, jets, and  $E_T^{\text{miss}}$ . We also describe our measurements of the lepton and trigger efficiency. The analysis uses several different Control Regions (CRs) in addition to the Signal Regions (SRs). All of these different regions are defined in this section. This section also includes some information on the basic MC corrections that we apply.

### 4.1 Single Lepton Selection

The single lepton selection is based on the following criteria, starting from the requirements described on [https://twiki.cern.ch/twiki/bin/viewauth/CMS/SUSYstop#SINGLE\\_LEPTON\\_CHANNEL](https://twiki.cern.ch/twiki/bin/viewauth/CMS/SUSYstop#SINGLE_LEPTON_CHANNEL) (revision r20)

- satisfy the trigger requirement (see Table 3). Note that the analysis triggers are inclusive single lepton triggers. Dilepton triggers are used only for the dilepton control region.
- select events with one high  $p_T$  electron or muon, requiring
  - $p_T > 30 \text{ GeV}/c$  and  $|\eta| < 1.4442(2.1)$  for electrons (muons). The restriction to the barrel for electrons is motivated by an observed excess of events with large  $M_T$  with endcap electrons in the b-veto control region, and does not significantly reduce the signal acceptance since the leptons tend to be central.
  - muon ID criteria is based on the 2012 POG recommended tight working point
  - electron ID criteria is based on the 2012 POG recommended medium working point
  - PF-based isolation ( $\Delta R < 0.3$ ) relative isolation  $< 0.15$  and absolute isolation  $< 5 \text{ GeV}$ . PU corrections are performed with the  $\Delta\beta$  scheme for muons and effective-area fastjet rho scheme for electrons (as recommended by the relevant POGs).
  - $|p_T(\text{PF}_{\text{lep}}) - p_T(\text{RECO}_{\text{lep}})| < 10 \text{ GeV}$
  - $E/p_{\text{in}} < 4$  (electrons only)
  - We remove electron events with  $E_T^{\text{miss}} > 50 \text{ GeV}$  and  $M_T > 100 \text{ GeV}$  with at least one crystal in the supercluster with laser correction  $> 2.1$
- require at least 4 PF jets in the event with  $p_T > 30 \text{ GeV}$  within  $|\eta| < 2.5$  out of which at least 1 satisfies the CSV medium working point b-tagging requirement
- require moderate  $E_T^{\text{miss}} > 50 \text{ GeV}$  (type1-corrected pfmet with  $\phi$  corrections applied as described in Sec. 4.7.1).
- Isolated track veto, see Section 4.2

### 4.2 Isolated track veto

The isolated track veto is intended to remove top dilepton events. Looking for an isolated track is an effective way of identifying  $W \rightarrow e$ ,  $W \rightarrow \mu$ ,  $W \rightarrow \tau \rightarrow \ell$ , and  $W \rightarrow \tau \rightarrow h^\pm + n\pi^0$ . The requirements on the track are

- $P_T > 10 \text{ GeV}$
- Relative track isolation  $< 10\%$  computed from charged PF candidates with  $dZ < 0.05 \text{ cm}$  from the primary vertex.

### 4.3 Signal Region Selection

The signal regions (SRs) are selected to improve the sensitivity for the single lepton requirements and cover a range of scalar top scenarios. The  $M_T$  and  $E_T^{\text{miss}}$  variables are used to define the signal regions and the requirements are listed in Table 4.

---

<sup>1)</sup> This is an ad-hoc removal based on run-event numbers, since the problem was found very recently and the filter was not available when we processed the events.

Signal Region	Minimum $M_T$ [GeV]	Minimum $E_T^{\text{miss}}$ [GeV]
SRA	150	100
SRB	120	150
SRC	120	200
SRD	120	250
SRE	120	300
SRF	120	350
SRG	120	400

Table 4: Signal region definitions based on  $M_T$  and  $E_T^{\text{miss}}$  requirements. These requirements are applied in addition to the baseline single lepton selection.

Table 5 shows the expected number of SM background yields for the SRs. A few stop signal yields for four values of the parameters are also shown for comparison. The signal regions with looser requirements are sensitive to lower stop masses  $M(\tilde{t})$ , while those with tighter requirements are more sensitive to higher  $M(\tilde{t})$ .

Sample	SRA	SRB	SRC	SRD	SRE	SRF	SRG
$t\bar{t} \rightarrow \ell\bar{\ell}$	$619 \pm 9$	$366 \pm 7$	$127 \pm 4$	$44 \pm 2$	$17 \pm 1$	$7 \pm 1$	$4 \pm 1$
$t\bar{t} \rightarrow \ell + \text{jets} \ \& \ \text{single top} \ (1\ell)$	$95 \pm 3$	$67 \pm 3$	$15 \pm 1$	$6 \pm 1$	$2 \pm 1$	$1 \pm 1$	$1 \pm 0$
$W + \text{jets}$	$29 \pm 2$	$15 \pm 2$	$6 \pm 1$	$3 \pm 1$	$1 \pm 0$	$0 \pm 0$	$0 \pm 0$
Rare	$59 \pm 3$	$38 \pm 3$	$16 \pm 2$	$8 \pm 1$	$4 \pm 1$	$2 \pm 0$	$1 \pm 0$
Total	$802 \pm 10$	$486 \pm 8$	$164 \pm 5$	$62 \pm 3$	$23 \pm 2$	$10 \pm 1$	$6 \pm 1$
Yield UL (optimistic)	147 (10%)	94 (10%)	47 (15%)	25 (20%)	14 (25%)	8.6 (30%)	7.5 (50%)
Yield UL (pessimistic)	200 (15%)	152 (20%)	64 (25%)	30 (30%)	15 (35%)	9.7 (50%)	8.2 (100%)
T2tt m(stop) = 250 m( $\chi^0$ ) = 0	$315 \pm 18$	$193 \pm 14$	$53 \pm 8$	$13 \pm 4$	$2 \pm 2$	$0 \pm 0$	$0 \pm 0$
T2tt m(stop) = 300 m( $\chi^0$ ) = 50	$296 \pm 11$	$236 \pm 10$	$88 \pm 6$	$28 \pm 3$	$10 \pm 2$	$2 \pm 1$	$0 \pm 0$
T2tt m(stop) = 300 m( $\chi^0$ ) = 100	$128 \pm 7$	$93 \pm 6$	$29 \pm 3$	$10 \pm 2$	$5 \pm 1$	$2 \pm 1$	$1 \pm 1$
T2tt m(stop) = 350 m( $\chi^0$ ) = 0	$224 \pm 6$	$206 \pm 6$	$119 \pm 4$	$52 \pm 3$	$20 \pm 2$	$8 \pm 1$	$3 \pm 1$
T2tt m(stop) = 450 m( $\chi^0$ ) = 0	$71 \pm 2$	$71 \pm 2$	$53 \pm 1$	$36 \pm 1$	$21 \pm 1$	$11 \pm 1$	$5 \pm 0$

Table 5: Expected SM background contributions and signal yields for a few sample points, including both muon and electron channels. This is “dead reckoning” MC with no correction. It is meant only as a general guide. The uncertainties are statistical only. The signal yield expected upper limits are also shown for two values of the total background systematic uncertainty, indicated in parentheses.

## 4.4 Control Region Selection

Control regions (CRs) are used to validate the background estimation procedure and derive systematic uncertainties for some contributions. The CRs are selected to have similar kinematics to the SRs, but have a different requirement in terms of number of b-tags and number of leptons, thus enhancing them in different SM contributions. The four CRs used in this analysis are summarized in Table 6.

Selection Criteria	exactly 1 lepton	exactly 2 leptons	1 lepton + isolated track
0 b-tags	CR1) W+Jets dominated: Validate W+Jets $M_T$ tail	CR2) apply Z-mass constraint $\rightarrow$ Z+Jets dominated: Validate $t\bar{t} \rightarrow \ell + \text{jets} \ M_T$ tail comparing data vs. MC “pseudo- $M_T$ ”	CR3) not used
$\geq 1$ b-tags	SIGNAL REGION	CR4) Apply Z-mass veto $\rightarrow$ $t\bar{t} \rightarrow \ell\bar{\ell}$ dominated: Validate “physics” modelling of $t\bar{t} \rightarrow \ell\bar{\ell}$	CR5) $t\bar{t} \rightarrow \ell\bar{\ell}$ , $t\bar{t} \rightarrow \ell\tau$ and $t\bar{t} \rightarrow \ell\text{fake}$ dominated: Validate $\tau$ and fake lepton modeling/detector effects in $t\bar{t} \rightarrow \ell\bar{\ell}$

Table 6: Summary of signal and control regions.

## 4.5 Definition of $M_T$ peak region

This region is defined as  $50 < M_T < 80$  GeV.

## 4.6 Default $t\bar{t}$ MC sample

Our default  $t\bar{t}$  MC sample is Powheg.

## 4.7 MC Corrections

All MC samples are corrected for trigger efficiency. In the case of single lepton selections, we apply the  $P_T$  and  $\eta$ -dependent scale factors that we measure ourselves, see Section 4.9. In the case of dilepton selections that require the dilepton triggers, we apply overall scale factors of 0.95, 0.88, and 0.92 for  $ee$ ,  $\mu\mu$ , and  $e\mu$  respectively [3].

The leptonic branching fraction used in some of the  $t\bar{t}$  MC samples differs from the value listed in the PDG ( $10.80 \pm 0.09\%$ ). Table. 7 summarizes the branching fractions used in the generation of the various  $t\bar{t}$  MC samples. For  $t\bar{t}$  samples with the incorrect leptonic branching fraction, event weights are applied based on the number of true leptons and the ratio of the corrected and incorrect branching fractions.

$t\bar{t}$ Sample - Event Generator	Leptonic Branching Fraction
Madgraph	0.111
MC@NLO	0.111
Pythia	0.108
Powheg	0.108

Table 7: Leptonic branching fractions for the various  $t\bar{t}$  samples used in the analysis. The  $t\bar{t}$  MC samples produced with Madgraph and MC@NLO has a branching fraction that is almost 3% higher than the PDG value.

All  $t\bar{t}$  dilepton samples are corrected (when needed and appropriate) in order to have the correct jet multiplicity distribution. This correction procedure is described in Section 6.3.1.

### 4.7.1 Corrections to Jets and $E_T^{\text{miss}}$

The official recommendations from the Jet/MET group are used for the data and MC samples. In particular, the jet energy corrections (JEC) are updated using the official recipe. L1FastL2L3Residual (L1FastL2L3) corrections are applied for data (MC), based on the global tags GR\_R\_52\_V9 (START52\_V9B) for data (MC). In addition, these jet energy corrections are propagated to the  $E_T^{\text{miss}}$  calculation, following the official prescription for deriving the Type I corrections.

Events with anomalous “rho” pile-up corrections are excluded from the sample since these correspond to events with unphysically large  $E_T^{\text{miss}}$  and  $M_T$  tail signal region. In addition, the recommended MET filters are applied. A correction to remove the  $\phi$  modulation in  $E_T^{\text{miss}}$  is also applied to the data.

## 4.8 Lepton Selection Efficiency Measurements

In this section we measure the identification and isolation efficiencies for muons and electrons in data and MC using tag-and-probe studies. The tag is required to pass the full offline analysis selection and have  $p_T > 30$  GeV,  $|\eta| < 2.1$ , and be matched to the single lepton trigger, HLT\_IsoMu24(.eta2p1) for muons and HLT\_Ele27\_WP80 for electrons. The probe is required to have  $|\eta| < 2.1$  and  $p_T > 20$  GeV. To measure the identification efficiency we require the probe to pass the isolation requirement, to measure the isolation efficiency we require the probe to pass the identification requirement.

The tag-probe pair is required to have opposite-sign and an invariant mass in the range 76–106 GeV. In order to suppress lepton pairs from sources other than Z boson decays, we require the event to have  $E_T^{\text{miss}} < 30$  GeV and no b-tagged jets (CSV loose working point).

The muon efficiencies are summarized in Table 8 for inclusive events (i.e. no jet requirements). These efficiencies are displayed in Fig. 2 for several different jet multiplicity requirements. We currently observe

good agreement for muons with  $p_T$  up to about 300 GeV. For high  $p_T$  muons we observe a source of background in the data with large impact parameters, which we suppress by requiring muon  $d_0 < 0.02$  cm and  $d_Z < 0.5$  cm. We are currently investigating the source of this inefficiency. The electron efficiencies are summarized in Table 9 for inclusive events (i.e. no jet requirements). These efficiencies are displayed in Fig. 3 for several different jet multiplicity requirements. In general we observe good agreement between the data and MC identification and isolation efficiencies.

We do not correct the MC for differences in lepton efficiency. In the background calculation, we do not take any systematics due to lepton selection efficiency uncertainties. This is because all backgrounds except the rare MC background are normalized to the  $M_T$  peak, thus the lepton identification uncertainty cancels out. For the rare MC these uncertainties are negligible compared to the assumed cross-section uncertainty (Section 7).

Table 8: Summary of the data and MC muon identification and isolation efficiencies measured with tag-and-probe studies.

MC ID			
$p_T$ range [GeV]	$ \eta  < 0.8$	$0.8 <  \eta  < 1.5$	$1.5 <  \eta  < 2.1$
20 - 30	$0.9672 \pm 0.0005$	$0.9640 \pm 0.0006$	$0.9471 \pm 0.0008$
30 - 40	$0.9684 \pm 0.0002$	$0.9657 \pm 0.0003$	$0.9446 \pm 0.0004$
40 - 50	$0.9704 \pm 0.0002$	$0.9687 \pm 0.0002$	$0.9432 \pm 0.0004$
50 - 60	$0.9684 \pm 0.0005$	$0.9640 \pm 0.0005$	$0.9414 \pm 0.0009$
60 - 80	$0.9678 \pm 0.0009$	$0.9640 \pm 0.0010$	$0.9354 \pm 0.0018$
80 - 100	$0.9709 \pm 0.0021$	$0.9642 \pm 0.0027$	$0.9234 \pm 0.0051$
100 - 150	$0.9679 \pm 0.0029$	$0.9654 \pm 0.0035$	$0.9261 \pm 0.0069$
150 - 200	$0.9643 \pm 0.0069$	$0.9568 \pm 0.0088$	$0.9045 \pm 0.0198$
200 - 300	$0.9647 \pm 0.0116$	$0.9388 \pm 0.0171$	$0.8906 \pm 0.0390$
300 - 10000	$1.0000 \pm 0.0000$	$1.0000 \pm 0.0000$	$1.0000 \pm 0.0000$
MC ISO			
$p_T$ range [GeV]	$ \eta  < 0.8$	$0.8 <  \eta  < 1.5$	$1.5 <  \eta  < 2.1$
20 - 30	$0.8966 \pm 0.0007$	$0.9153 \pm 0.0008$	$0.9298 \pm 0.0009$
30 - 40	$0.9610 \pm 0.0002$	$0.9632 \pm 0.0003$	$0.9707 \pm 0.0003$
40 - 50	$0.9876 \pm 0.0001$	$0.9897 \pm 0.0001$	$0.9912 \pm 0.0002$
50 - 60	$0.9921 \pm 0.0002$	$0.9927 \pm 0.0003$	$0.9939 \pm 0.0003$
60 - 80	$0.9927 \pm 0.0004$	$0.9937 \pm 0.0004$	$0.9947 \pm 0.0005$
80 - 100	$0.9920 \pm 0.0012$	$0.9921 \pm 0.0013$	$0.9932 \pm 0.0016$
100 - 150	$0.9898 \pm 0.0017$	$0.9923 \pm 0.0017$	$0.9933 \pm 0.0022$
150 - 200	$0.9901 \pm 0.0037$	$0.9922 \pm 0.0039$	$0.9950 \pm 0.0050$
200 - 300	$0.9919 \pm 0.0057$	$1.0000 \pm 0.0000$	$0.9828 \pm 0.0171$
300 - 10000	$1.0000 \pm 0.0000$	$1.0000 \pm 0.0000$	$1.0000 \pm 0.0000$
DATA ID			
$p_T$ range [GeV]	$ \eta  < 0.8$	$0.8 <  \eta  < 1.5$	$1.5 <  \eta  < 2.1$
20 - 30	$0.9530 \pm 0.0005$	$0.9517 \pm 0.0006$	$0.9369 \pm 0.0008$
30 - 40	$0.9556 \pm 0.0003$	$0.9519 \pm 0.0003$	$0.9362 \pm 0.0005$
40 - 50	$0.9584 \pm 0.0002$	$0.9558 \pm 0.0003$	$0.9355 \pm 0.0004$
50 - 60	$0.9540 \pm 0.0005$	$0.9487 \pm 0.0006$	$0.9314 \pm 0.0010$
60 - 80	$0.9536 \pm 0.0010$	$0.9466 \pm 0.0012$	$0.9307 \pm 0.0019$
80 - 100	$0.9505 \pm 0.0028$	$0.9414 \pm 0.0035$	$0.9289 \pm 0.0053$
100 - 150	$0.9472 \pm 0.0038$	$0.9454 \pm 0.0045$	$0.9149 \pm 0.0079$
150 - 200	$0.9628 \pm 0.0073$	$0.9675 \pm 0.0089$	$0.8950 \pm 0.0217$
200 - 300	$0.9463 \pm 0.0157$	$0.9290 \pm 0.0206$	$0.8889 \pm 0.0468$
300 - 10000	$0.9412 \pm 0.0404$	$1.0000 \pm 0.0000$	$0.4000 \pm 0.2191$
DATA ISO			
$p_T$ range [GeV]	$ \eta  < 0.8$	$0.8 <  \eta  < 1.5$	$1.5 <  \eta  < 2.1$
20 - 30	$0.8939 \pm 0.0007$	$0.9144 \pm 0.0008$	$0.9361 \pm 0.0008$
30 - 40	$0.9598 \pm 0.0002$	$0.9646 \pm 0.0003$	$0.9744 \pm 0.0003$
40 - 50	$0.9870 \pm 0.0001$	$0.9901 \pm 0.0001$	$0.9920 \pm 0.0002$
50 - 60	$0.9912 \pm 0.0002$	$0.9933 \pm 0.0002$	$0.9953 \pm 0.0003$
60 - 80	$0.9920 \pm 0.0004$	$0.9934 \pm 0.0005$	$0.9956 \pm 0.0005$
80 - 100	$0.9926 \pm 0.0011$	$0.9933 \pm 0.0013$	$0.9955 \pm 0.0014$
100 - 150	$0.9913 \pm 0.0016$	$0.9949 \pm 0.0015$	$0.9965 \pm 0.0017$
150 - 200	$0.9969 \pm 0.0022$	$0.9974 \pm 0.0026$	$0.9944 \pm 0.0055$
200 - 300	$1.0000 \pm 0.0000$	$1.0000 \pm 0.0000$	$1.0000 \pm 0.0000$
300 - 10000	$1.0000 \pm 0.0000$	$1.0000 \pm 0.0000$	$1.0000 \pm 0.0000$
Scale Factor ID			
$p_T$ range [GeV]	$ \eta  < 0.8$	$0.8 <  \eta  < 1.5$	$1.5 <  \eta  < 2.1$
20 - 30	$0.9853 \pm 0.0007$	$0.9872 \pm 0.0009$	$0.9893 \pm 0.0012$
30 - 40	$0.9868 \pm 0.0003$	$0.9857 \pm 0.0005$	$0.9911 \pm 0.0007$
40 - 50	$0.9877 \pm 0.0003$	$0.9866 \pm 0.0004$	$0.9918 \pm 0.0006$
50 - 60	$0.9851 \pm 0.0007$	$0.9841 \pm 0.0009$	$0.9894 \pm 0.0014$
60 - 80	$0.9853 \pm 0.0014$	$0.9820 \pm 0.0017$	$0.9949 \pm 0.0028$
80 - 100	$0.9790 \pm 0.0036$	$0.9763 \pm 0.0046$	$1.0059 \pm 0.0080$
100 - 150	$0.9786 \pm 0.0049$	$0.9793 \pm 0.0059$	$0.9879 \pm 0.0113$
150 - 200	$0.9984 \pm 0.0104$	$1.0112 \pm 0.0131$	$0.9894 \pm 0.0323$
200 - 300	$0.9810 \pm 0.0201$	$0.9896 \pm 0.0284$	$0.9981 \pm 0.0684$
300 - 10000	$0.9412 \pm 0.0404$	$1.0000 \pm 0.0000$	$0.4000 \pm 0.2191$
Scale Factor ISO			
$p_T$ range [GeV]	$ \eta  < 0.8$	$0.8 <  \eta  < 1.5$	$1.5 <  \eta  < 2.1$
20 - 30	$0.9970 \pm 0.0012$	$0.9989 \pm 0.0012$	$1.0068 \pm 0.0013$
30 - 40	$0.9987 \pm 0.0004$	$1.0014 \pm 0.0004$	$1.0038 \pm 0.0005$
40 - 50	$0.9994 \pm 0.0002$	$1.0004 \pm 0.0002$	$1.0008 \pm 0.0002$
50 - 60	$0.9991 \pm 0.0003$	$1.0006 \pm 0.0003$	$1.0013 \pm 0.0004$
60 - 80	$0.9993 \pm 0.0006$	$0.9997 \pm 0.0006$	$1.0009 \pm 0.0008$
80 - 100	$1.0006 \pm 0.0016$	$1.0012 \pm 0.0018$	$1.0023 \pm 0.0022$
100 - 150	$1.0015 \pm 0.0023$	$1.0027 \pm 0.0023$	$1.0032 \pm 0.0028$
150 - 200	$1.0068 \pm 0.0044$	$1.0053 \pm 0.0047$	$0.9994 \pm 0.0075$
200 - 300	$1.0081 \pm 0.0058$	$1.0000 \pm 0.0000$	$1.0175 \pm 0.0177$
300 - 10000	$1.0000 \pm 0.0000$	$1.0000 \pm 0.0000$	$1.0000 \pm 0.0000$

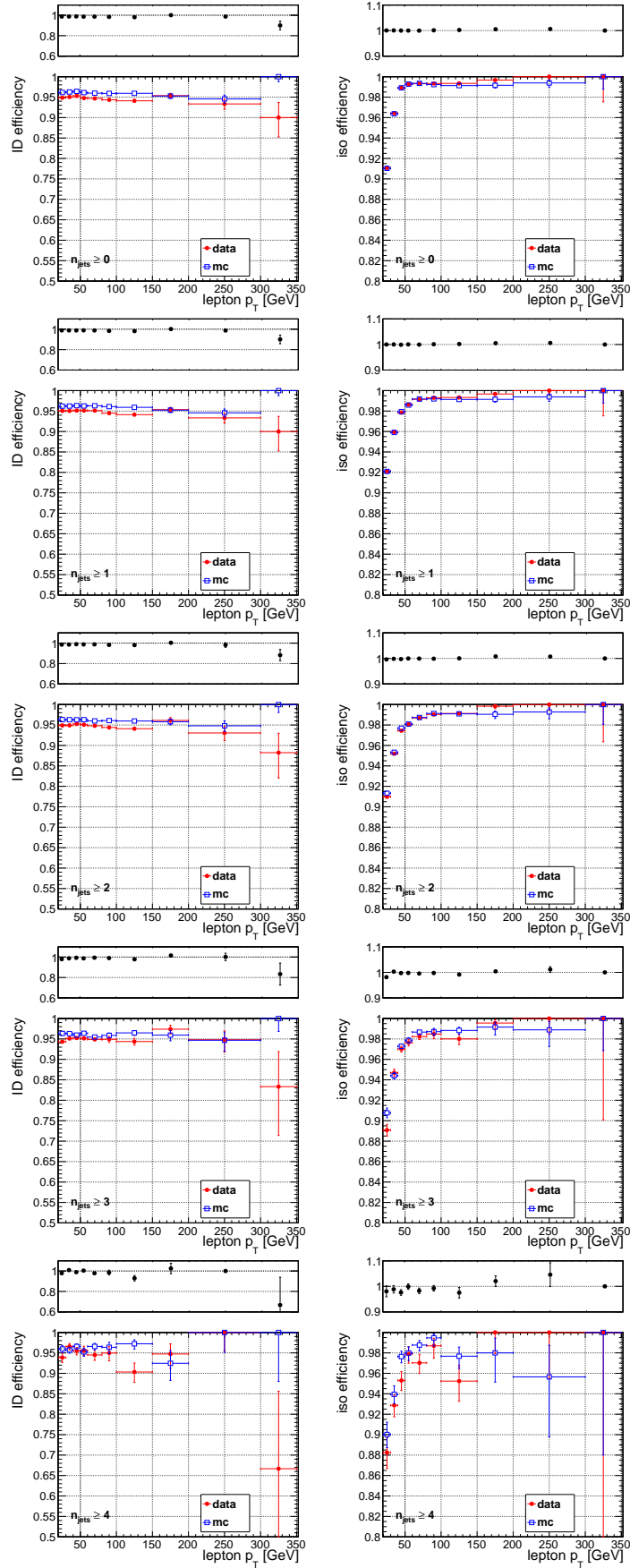


Figure 2: Comparison of the muon identification and isolation efficiencies in data and MC for various jet multiplicity requirements.

Table 9: Summary of the data and MC electron identification and isolation efficiencies measured with tag-and-probe studies.

MC ID		
$p_T$ range [GeV]	$ \eta  < 1.5$	$1.5 <  \eta  < 2.1$
20 - 30	$0.8156 \pm 0.0008$	$0.6565 \pm 0.0019$
30 - 40	$0.8670 \pm 0.0004$	$0.7450 \pm 0.0010$
40 - 50	$0.8922 \pm 0.0003$	$0.7847 \pm 0.0008$
50 - 60	$0.9023 \pm 0.0006$	$0.7956 \pm 0.0018$
60 - 80	$0.9097 \pm 0.0011$	$0.8166 \pm 0.0034$
80 - 100	$0.9203 \pm 0.0028$	$0.8196 \pm 0.0090$
100 - 150	$0.9162 \pm 0.0037$	$0.8378 \pm 0.0117$
150 - 200	$0.9106 \pm 0.0087$	$0.8111 \pm 0.0292$
200 - 300	$0.9304 \pm 0.0119$	$0.9153 \pm 0.0363$
300 - 10000	$0.8684 \pm 0.0388$	$0.8000 \pm 0.1789$
MC ISO		
$p_T$ range [GeV]	$ \eta  < 1.5$	$1.5 <  \eta  < 2.1$
20 - 30	$0.9245 \pm 0.0006$	$0.9466 \pm 0.0011$
30 - 40	$0.9682 \pm 0.0002$	$0.9741 \pm 0.0004$
40 - 50	$0.9876 \pm 0.0001$	$0.9883 \pm 0.0002$
50 - 60	$0.9909 \pm 0.0002$	$0.9912 \pm 0.0005$
60 - 80	$0.9916 \pm 0.0004$	$0.9930 \pm 0.0008$
80 - 100	$0.9915 \pm 0.0010$	$0.9908 \pm 0.0025$
100 - 150	$0.9929 \pm 0.0012$	$0.9894 \pm 0.0035$
150 - 200	$0.9919 \pm 0.0029$	$0.9932 \pm 0.0068$
200 - 300	$0.9953 \pm 0.0033$	$1.0000 \pm 0.0000$
300 - 10000	$1.0000 \pm 0.0000$	$1.0000 \pm 0.0000$
DATA ID		
$p_T$ range [GeV]	$ \eta  < 1.5$	$1.5 <  \eta  < 2.1$
20 - 30	$0.8145 \pm 0.0008$	$0.6528 \pm 0.0018$
30 - 40	$0.8676 \pm 0.0004$	$0.7462 \pm 0.0010$
40 - 50	$0.8955 \pm 0.0003$	$0.7922 \pm 0.0008$
50 - 60	$0.9049 \pm 0.0006$	$0.8072 \pm 0.0018$
60 - 80	$0.9110 \pm 0.0011$	$0.8212 \pm 0.0035$
80 - 100	$0.9156 \pm 0.0028$	$0.8358 \pm 0.0091$
100 - 150	$0.9257 \pm 0.0036$	$0.8507 \pm 0.0116$
150 - 200	$0.9186 \pm 0.0084$	$0.8929 \pm 0.0292$
200 - 300	$0.9106 \pm 0.0149$	$0.7576 \pm 0.0746$
300 - 10000	$0.9400 \pm 0.0336$	$1.0000 \pm 0.0000$
DATA ISO		
$p_T$ range [GeV]	$ \eta  < 1.5$	$1.5 <  \eta  < 2.1$
20 - 30	$0.9201 \pm 0.0006$	$0.9419 \pm 0.0011$
30 - 40	$0.9667 \pm 0.0002$	$0.9734 \pm 0.0004$
40 - 50	$0.9872 \pm 0.0001$	$0.9892 \pm 0.0002$
50 - 60	$0.9904 \pm 0.0002$	$0.9922 \pm 0.0004$
60 - 80	$0.9923 \pm 0.0004$	$0.9916 \pm 0.0009$
80 - 100	$0.9914 \pm 0.0010$	$0.9921 \pm 0.0024$
100 - 150	$0.9945 \pm 0.0011$	$1.0000 \pm 0.0000$
150 - 200	$0.9908 \pm 0.0031$	$1.0000 \pm 0.0000$
200 - 300	$0.9941 \pm 0.0042$	$1.0000 \pm 0.0000$
300 - 10000	$0.9792 \pm 0.0206$	$1.0000 \pm 0.0000$
Scale Factor ID		
$p_T$ range [GeV]	$ \eta  < 1.5$	$1.5 <  \eta  < 2.1$
20 - 30	$0.9987 \pm 0.0014$	$0.9944 \pm 0.0040$
30 - 40	$1.0007 \pm 0.0006$	$1.0015 \pm 0.0019$
40 - 50	$1.0036 \pm 0.0005$	$1.0096 \pm 0.0015$
50 - 60	$1.0029 \pm 0.0010$	$1.0146 \pm 0.0031$
60 - 80	$1.0014 \pm 0.0018$	$1.0057 \pm 0.0060$
80 - 100	$0.9949 \pm 0.0043$	$1.0197 \pm 0.0158$
100 - 150	$1.0104 \pm 0.0057$	$1.0154 \pm 0.0198$
150 - 200	$1.0087 \pm 0.0134$	$1.1008 \pm 0.0535$
200 - 300	$0.9786 \pm 0.0203$	$0.8277 \pm 0.0879$
300 - 10000	$1.0824 \pm 0.0619$	$1.2500 \pm 0.2795$
Scale Factor ISO		
$p_T$ range [GeV]	$ \eta  < 1.5$	$1.5 <  \eta  < 2.1$
20 - 30	$0.9952 \pm 0.0009$	$0.9950 \pm 0.0016$
30 - 40	$0.9984 \pm 0.0003$	$0.9992 \pm 0.0006$
40 - 50	$0.9996 \pm 0.0002$	$1.0009 \pm 0.0003$
50 - 60	$0.9995 \pm 0.0003$	$1.0009 \pm 0.0006$
60 - 80	$1.0006 \pm 0.0005$	$0.9985 \pm 0.0012$
80 - 100	$0.9999 \pm 0.0014$	$1.0013 \pm 0.0035$
100 - 150	$1.0016 \pm 0.0016$	$1.0108 \pm 0.0036$
150 - 200	$0.9989 \pm 0.0042$	$1.0068 \pm 0.0069$
200 - 300	$0.9987 \pm 0.0053$	$1.0000 \pm 0.0000$
300 - 10000	$0.9792 \pm 0.0206$	$1.0000 \pm 0.0000$

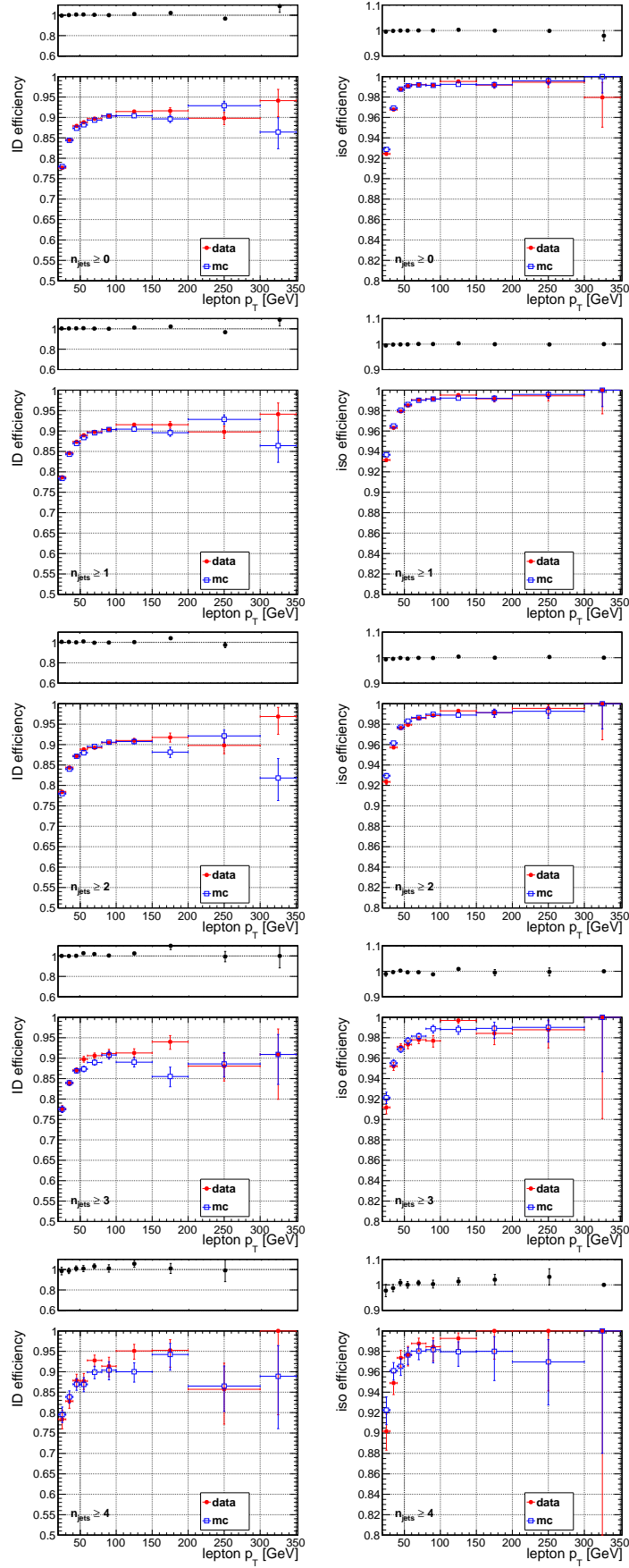


Figure 3: Comparison of the electron identification and isolation efficiencies in data and MC for various jet multiplicity requirements.



## 4.9 Trigger Efficiency Measurements

In this section we measure the efficiencies of the single lepton triggers, HLT\_IsoMu24(.eta2p1) for muons and HLT\_Ele27\_WP80 for electrons, using a tag-and-probe approach. The tag is required to pass the full offline analysis selection and have  $p_T > 30$  GeV,  $|\eta| < 2.1$ , and be matched to the single lepton trigger. The probe is also required to pass the full offline analysis selection and have  $|\eta| < 2.1$ , but the  $p_T$  requirement is relaxed to 20 GeV in order to measure the  $p_T$  turn-on curve. The tag-probe pair is required to have opposite-sign and an invariant mass in the range 76–106 GeV.

The measured trigger efficiencies are displayed in Fig. 4 and summarized in Table 10 (muons) and Table 11 (electrons). These trigger efficiencies are applied to the MC when used to predict data yields selected by single lepton triggers.

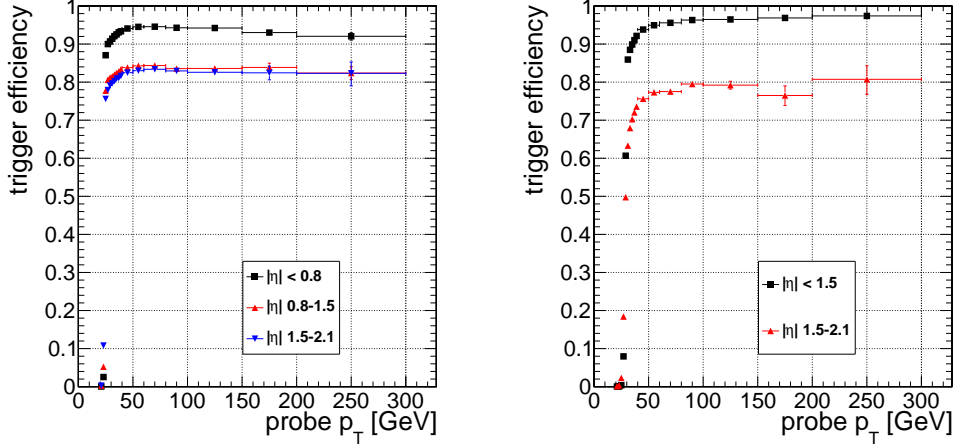


Figure 4: Efficiency for the single muon trigger HLT\_IsoMu24(.eta2p1) (left) and single electron trigger HLT\_Ele27\_WP80 (right) as a function of lepton  $p_T$ , for several bins in lepton  $|\eta|$ .

Table 10: Summary of the single muon trigger efficiency HLT\_IsoMu24(\_eta2p1). Uncertainties are statistical.

$p_T$ range [GeV]	$ \eta  < 0.8$	$0.8 <  \eta  < 1.5$	$1.5 <  \eta  < 2.1$
20 - 22	$0.00 \pm 0.000$	$0.00 \pm 0.000$	$0.00 \pm 0.000$
22 - 24	$0.03 \pm 0.001$	$0.05 \pm 0.001$	$0.11 \pm 0.002$
24 - 26	$0.87 \pm 0.002$	$0.78 \pm 0.002$	$0.76 \pm 0.003$
26 - 28	$0.90 \pm 0.001$	$0.81 \pm 0.002$	$0.78 \pm 0.002$
28 - 30	$0.91 \pm 0.001$	$0.81 \pm 0.002$	$0.79 \pm 0.002$
30 - 32	$0.91 \pm 0.001$	$0.81 \pm 0.001$	$0.80 \pm 0.002$
32 - 34	$0.92 \pm 0.001$	$0.82 \pm 0.001$	$0.80 \pm 0.002$
34 - 36	$0.93 \pm 0.001$	$0.82 \pm 0.001$	$0.81 \pm 0.001$
36 - 38	$0.93 \pm 0.001$	$0.83 \pm 0.001$	$0.81 \pm 0.001$
38 - 40	$0.93 \pm 0.001$	$0.83 \pm 0.001$	$0.82 \pm 0.001$
40 - 50	$0.94 \pm 0.000$	$0.84 \pm 0.000$	$0.82 \pm 0.001$
50 - 60	$0.95 \pm 0.000$	$0.84 \pm 0.001$	$0.83 \pm 0.001$
60 - 80	$0.95 \pm 0.001$	$0.84 \pm 0.002$	$0.83 \pm 0.002$
80 - 100	$0.94 \pm 0.002$	$0.84 \pm 0.004$	$0.83 \pm 0.006$
100 - 150	$0.94 \pm 0.003$	$0.84 \pm 0.005$	$0.83 \pm 0.008$
150 - 200	$0.93 \pm 0.006$	$0.84 \pm 0.011$	$0.82 \pm 0.018$
>200	$0.92 \pm 0.010$	$0.82 \pm 0.017$	$0.82 \pm 0.031$

Table 11: Summary of the single electron trigger efficiency HLT\_Ele27\_WP80. Uncertainties are statistical.

$p_T$ range [GeV]	$ \eta  < 1.5$	$1.5 <  \eta  < 2.1$
20 - 22	$0.00 \pm 0.000$	$0.00 \pm 0.000$
22 - 24	$0.00 \pm 0.000$	$0.00 \pm 0.001$
24 - 26	$0.00 \pm 0.000$	$0.02 \pm 0.001$
26 - 28	$0.08 \pm 0.001$	$0.18 \pm 0.003$
28 - 30	$0.61 \pm 0.002$	$0.50 \pm 0.004$
30 - 32	$0.86 \pm 0.001$	$0.63 \pm 0.003$
32 - 34	$0.88 \pm 0.001$	$0.68 \pm 0.003$
34 - 36	$0.90 \pm 0.001$	$0.70 \pm 0.002$
36 - 38	$0.91 \pm 0.001$	$0.72 \pm 0.002$
38 - 40	$0.92 \pm 0.001$	$0.74 \pm 0.002$
40 - 50	$0.94 \pm 0.000$	$0.76 \pm 0.001$
50 - 60	$0.95 \pm 0.000$	$0.77 \pm 0.002$
60 - 80	$0.96 \pm 0.001$	$0.78 \pm 0.003$
80 - 100	$0.96 \pm 0.002$	$0.80 \pm 0.008$
100 - 150	$0.96 \pm 0.002$	$0.79 \pm 0.010$
150 - 200	$0.97 \pm 0.004$	$0.76 \pm 0.026$
>200	$0.97 \pm 0.005$	$0.81 \pm 0.038$

## 5 Signal reach

In this Section we take a first look at the reach of this search for the T2tt and T2bw simplified models (Figure 5). Since this is a first look, not all the i's are dotted and not all the t's are crossed (and the T2bw MC is still missing). However, it is instructive to get a first feeling for where the sensitivity of this search is. We do this in terms of “expected limits”, assuming a null result. The case of an excess is quite different and more complicated.

The signal efficiency in the stop vs LSP mass plane for T2tt are shown in Fig. 6. This figure shows clearly how difficult it is to have sensitivity near the kinematical boundaries. The expected limits, under two different scenarios for the uncertainty on the background, are shown in Fig. 7 and 8. The complementarity of the different signal regions is readily apparent. The sensitivity to low (high) stop masses comes from the low (high)  $E_T^{\text{miss}}$  signal regions.

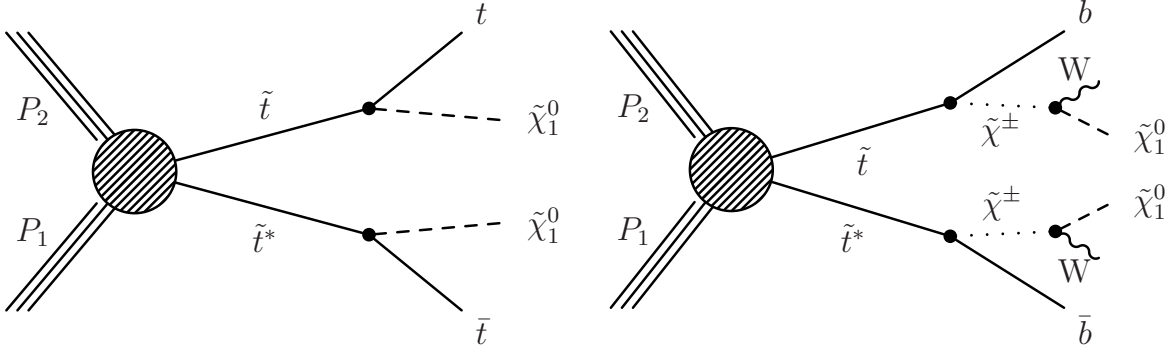


Figure 5: Diagram for the T2tt and T2bw simplified model.

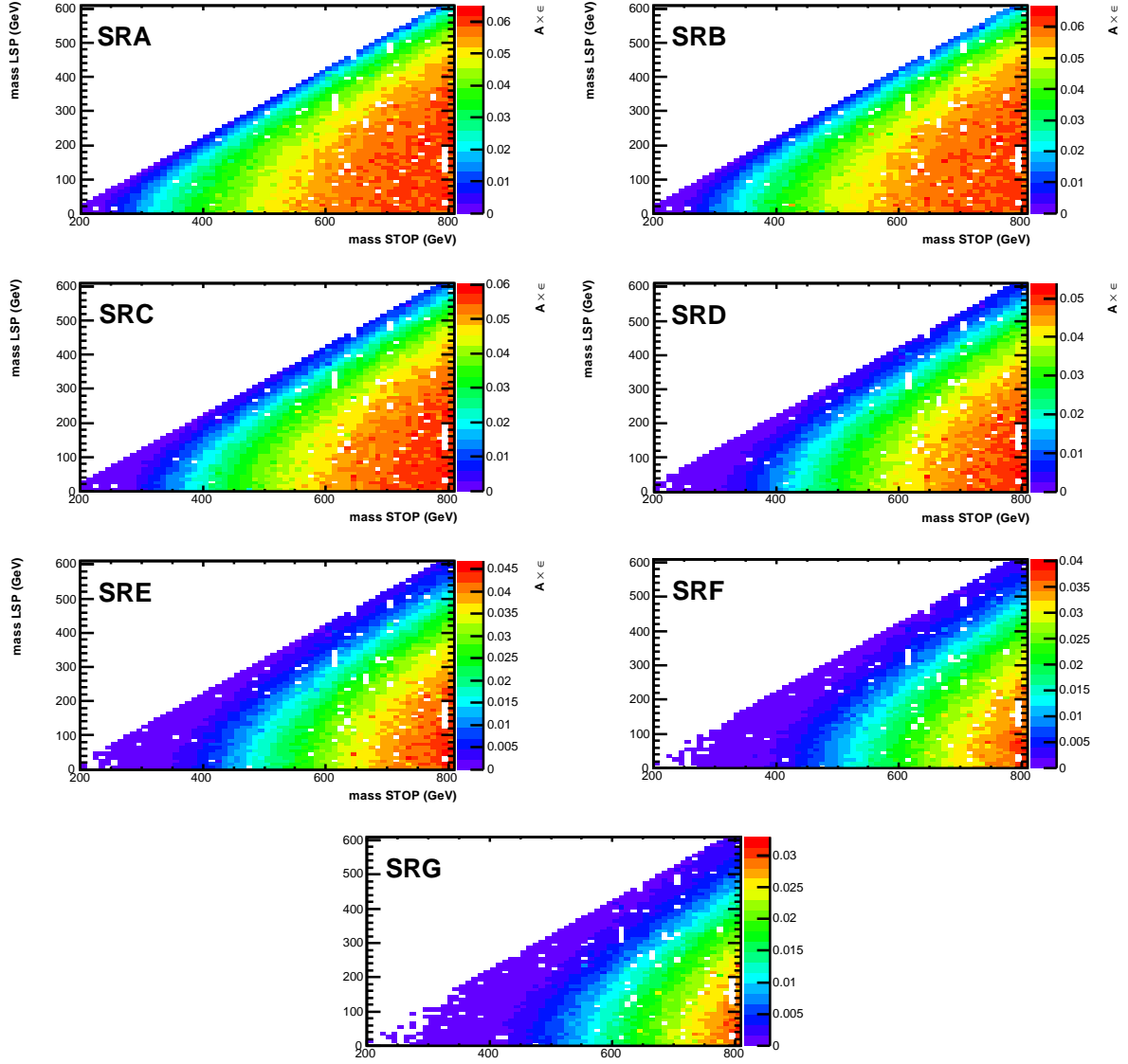


Figure 6: Signal efficeincy in for the T2tt

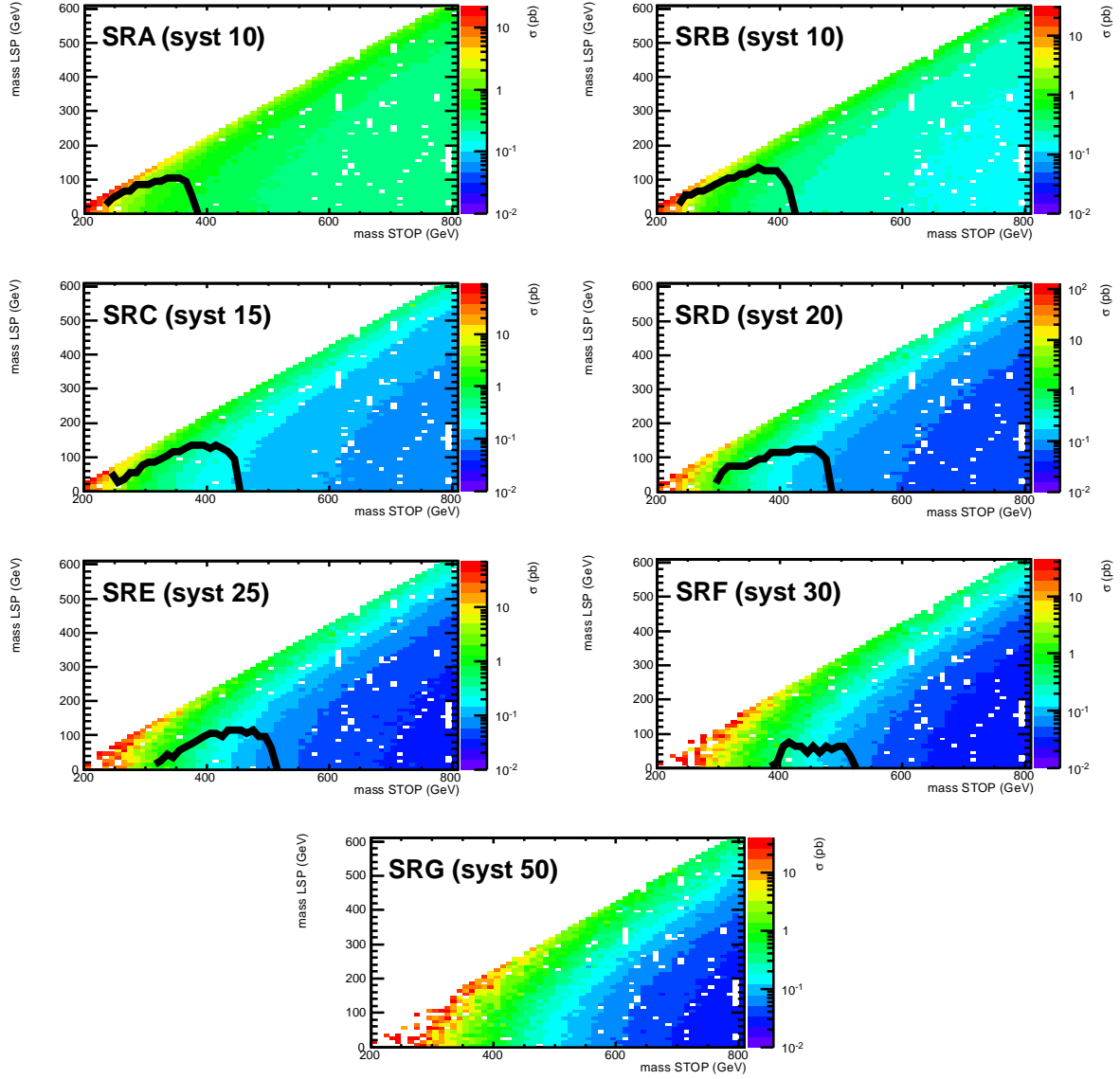


Figure 7: Expected upper limit on the cross section for the T2tt. A somewhat optimistic scenario is considered as systematics on the background. The assumed uncertainties on the background (in percent) is indicated on the plot.

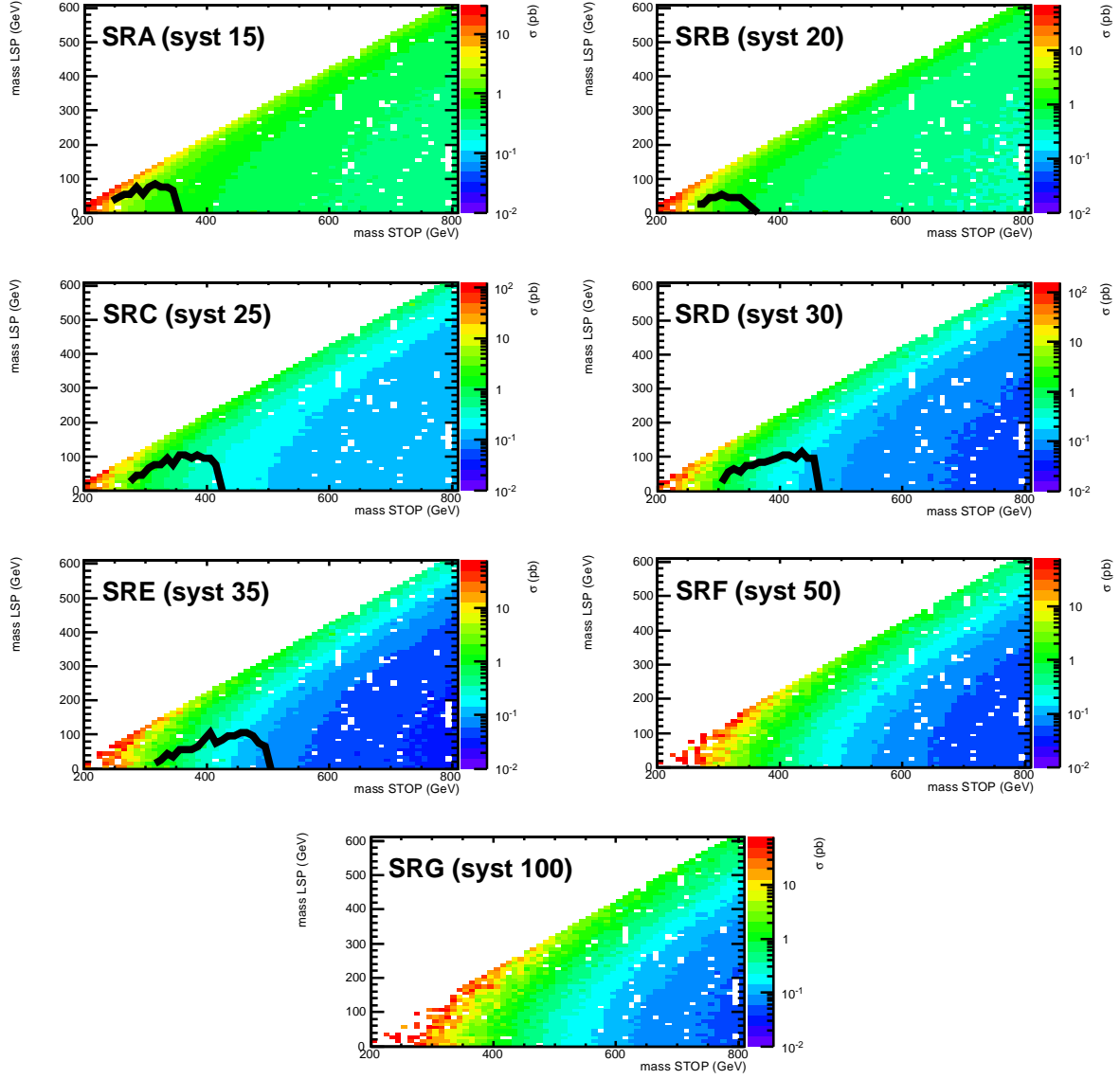


Figure 8: Expected upper limit on the cross section for the T2tt. A less optimistic scenario is considered as systematics on the background. (compared to Fig 7). The assumed uncertainties on the background (in percent) is indicated on the plots.

## 6 Control Region Studies

The CR studies described in this Section are key to validating the background predictions. The CRs are defined in Section 6.

CR1 and CR2 are designed to test the  $M_T$  tail in  $W$ +jets and  $t\bar{t}$  respectively. Note that, as explained in Section 2.1, these tails are different in the two samples because the off-shell effects are much more pronounced for  $W$ +jets (the s- and t-channel single top have the same  $M_T$  tail as  $t\bar{t}$ ). To put things in perspective, keep in mind that these backgrounds are only about 15% of the total, see Table 5.

CR4 and CR5 address the dominant  $t\bar{t}$  dilepton background. In CR4 we test the  $M_T$  tail in well identified dilepton events. In CR5 we test the same quantity, but in events where the second lepton is identified as an isolated track. Clearly CR4 and CR5 overlap.

### 6.1 W+Jets MC Modelling Validation from CR1

The estimate of the uncertainty on this background is based on CR1, defined by applying the full signal selection, including the isolated track veto, but requiring 0 b-tags (CSV medium working point as described in Sec. 4). The sample is dominated by  $W$ +jets and is thus used to validate the MC modelling of this background.

In Table 12 we show the amount that we need to scale the Wjets MC by in order to have agreement between data and Monte Carlo in the  $M_T$  peak region, defined as  $50 < M_T < 80$  GeV, for the different signal regions. (Recall, the signal regions have different  $E_T^{\text{miss}}$  requirements). These scale factors are not terribly important, but it is reassuring that they are not too different from 1.

Sample	CR1PRESEL	CR1A	CR1B	CR1C	CR1D	CR1E	CR1F	CR1G
$\mu$ $M_T$ -SF	$0.92 \pm 0.02$	$0.97 \pm 0.03$	$0.90 \pm 0.04$	$0.91 \pm 0.06$	$0.93 \pm 0.09$	$0.98 \pm 0.13$	$0.94 \pm 0.18$	$0.96 \pm 0.25$
e $M_T$ -SF	$0.94 \pm 0.02$	$0.90 \pm 0.04$	$0.84 \pm 0.05$	$0.80 \pm 0.07$	$0.83 \pm 0.10$	$0.77 \pm 0.13$	$0.86 \pm 0.20$	$0.87 \pm 0.29$

Table 12:  $M_T$  peak Data/MC scale factors applied to Wjets samples. The MC is used for backgrounds from rare processes. CR1PRESEL refers to a sample with  $E_T^{\text{miss}} > 50$  GeV. The uncertainties are statistical only.

Next, in Fig 9, 10, and 11, we show plots of  $E_T^{\text{miss}}$  and then  $M_T$  for different  $E_T^{\text{miss}}$  requirements corresponding to those defining our signal regions. It is clear that there are more events in the  $M_T$  tail than predicted from MC. This implies that we need to rescale the MC Wjets background in the tail region.

The rescaling is explored in Table 13. Here we compare the data and MC yields in the  $M_T$  signal regions and in a looser control region. Note that the MC is normalized in the  $M_T$  peak region by rescaling the  $W$ +jets component according to Table 12.

We also derive data/MC scale factors. These are derived in two different ways, separately for muons and electrons and then combined, as follows;

- For the first three sets of scale factors, above the triple horizontal line, we calculate the scale factor as the amount by which we would need to rescale **all** MC ( $W$ +jets,  $t\bar{t}$ , single top, rare) in order to have data-MC agreement in the  $M_T$  tail.
- For the next three set of scale factors, below the triple horizontal line, we calculate the scale factor as the amount by which we would need to scale  $W$ +jets keeping all other components fixed in order to have data-MC agreement in the tail.

The true  $W$ +jets scale factor is somewhere in between these two extremes. We also note that there is no statistically significant difference between the electron and muon samples. We use these data to extract a data/MC scale factor for  $W$ +jets which will be used to rescale the  $W$ +jets MC tail. This scale factor is listed in the last line of the Table, and is called  $SFR_{\text{wjets}}$ . It is calculated as follows.

- Separately for each signal region
- As the average of the two methods described above

Sample	CR1PRESEL	CR1A	CR1B	CR1C	CR1D	CR1E	CR1F	CR1G
$\mu$ MC	$480 \pm 22$	$173 \pm 5$	$114 \pm 4$	$40 \pm 2$	$16 \pm 1$	$8 \pm 1$	$4 \pm 1$	$2 \pm 1$
$\mu$ Data	629	238	139	45	12	8	3	2
$\mu$ Data/MC	$1.31 \pm 0.08$	$1.37 \pm 0.10$	$1.22 \pm 0.11$	$1.12 \pm 0.18$	$0.75 \pm 0.23$	$0.99 \pm 0.37$	$0.75 \pm 0.45$	$0.96 \pm 0.72$
e MC	$330 \pm 8$	$118 \pm 4$	$79 \pm 3$	$29 \pm 2$	$13 \pm 1$	$5 \pm 1$	$3 \pm 1$	$2 \pm 0$
e Data	473	174	100	36	16	5	5	2
e Data/MC	$1.43 \pm 0.07$	$1.47 \pm 0.12$	$1.27 \pm 0.14$	$1.23 \pm 0.22$	$1.26 \pm 0.34$	$1.07 \pm 0.51$	$1.80 \pm 0.91$	$1.26 \pm 0.97$
$\mu$ +e MC	$810 \pm 23$	$291 \pm 7$	$192 \pm 5$	$69 \pm 3$	$29 \pm 2$	$13 \pm 1$	$7 \pm 1$	$4 \pm 1$
$\mu$ +e Data	1102	412	239	81	28	13	8	4
$\mu$ +e Data/MC	$1.36 \pm 0.08$	$1.42 \pm 0.13$	$1.24 \pm 0.15$	$1.17 \pm 0.23$	$0.97 \pm 0.31$	$1.02 \pm 0.51$	$1.18 \pm 0.69$	$1.09 \pm 0.96$
$\mu$ W MC	$300 \pm 23$	$84 \pm 5$	$52 \pm 4$	$20 \pm 2$	$9 \pm 2$	$5 \pm 1$	$3 \pm 1$	$1 \pm 1$
$\mu$ W Data	$449 \pm 26$	$149 \pm 16$	$78 \pm 12$	$25 \pm 7$	$5 \pm 4$	$5 \pm 3$	$2 \pm 2$	$1 \pm 1$
$\mu$ W Data/MC	$1.50 \pm 0.14$	$1.77 \pm 0.21$	$1.49 \pm 0.26$	$1.25 \pm 0.38$	$0.56 \pm 0.39$	$0.98 \pm 0.62$	$0.60 \pm 0.73$	$0.94 \pm 1.14$
e W MC	$192 \pm 8$	$55 \pm 4$	$36 \pm 3$	$14 \pm 2$	$6 \pm 1$	$3 \pm 1$	$2 \pm 1$	$1 \pm 0$
e W Data	$335 \pm 22$	$111 \pm 13$	$58 \pm 10$	$20 \pm 6$	$10 \pm 4$	$3 \pm 2$	$4 \pm 2$	$1 \pm 1$
e W Data/MC	$1.74 \pm 0.14$	$2.02 \pm 0.29$	$1.58 \pm 0.32$	$1.49 \pm 0.50$	$1.50 \pm 0.70$	$1.10 \pm 0.80$	$2.27 \pm 1.55$	$1.51 \pm 1.96$
$\mu$ +e W MC	$493 \pm 24$	$139 \pm 6$	$89 \pm 5$	$33 \pm 3$	$16 \pm 2$	$8 \pm 1$	$4 \pm 1$	$2 \pm 1$
$\mu$ +e W Data	$785 \pm 59$	$260 \pm 37$	$135 \pm 28$	$45 \pm 16$	$15 \pm 9$	$8 \pm 7$	$6 \pm 5$	$3 \pm 3$
$\mu$ +e W Data/MC	$1.59 \pm 0.14$	$1.87 \pm 0.28$	$1.53 \pm 0.33$	$1.35 \pm 0.50$	$0.95 \pm 0.58$	$1.03 \pm 0.83$	$1.29 \pm 1.13$	$1.16 \pm 1.65$
$SFR_{wjet}$	$1.48 \pm 0.26$	$1.64 \pm 0.38$	$1.38 \pm 0.30$	$1.26 \pm 0.39$	$0.96 \pm 0.45$	$1.02 \pm 0.67$	$1.23 \pm 0.92$	$1.12 \pm 1.31$

Table 13: Yields in  $M_T$  tail comparing the MC prediction (after applying SFs) to data. CR1PRESEL refers to a sample with  $E_T^{\text{miss}} > 50$  GeV and  $M_T > 150$  GeV. See text for details.

- Including the statistical uncertainty
- Adding in quadrature to the uncertainty one-half of the deviation from 1.0



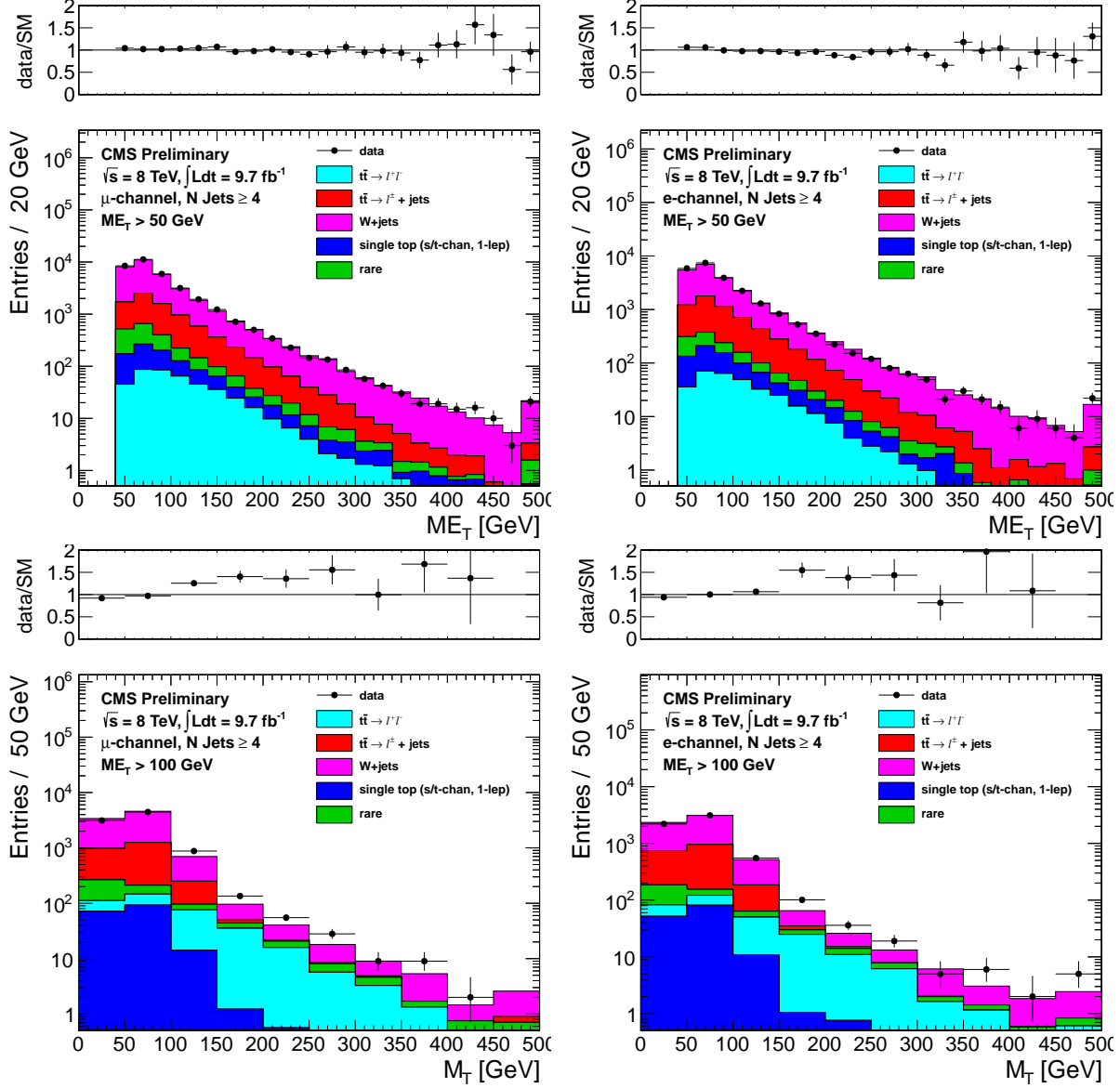


Figure 9: Comparison of the  $E_T^{\text{miss}}$  (top) and  $M_T$  for  $E_T^{\text{miss}} > 100$  (bottom) distributions in data vs. MC for events with a leading muon (left) and leading electron (right) satisfying the requirements of CR1.

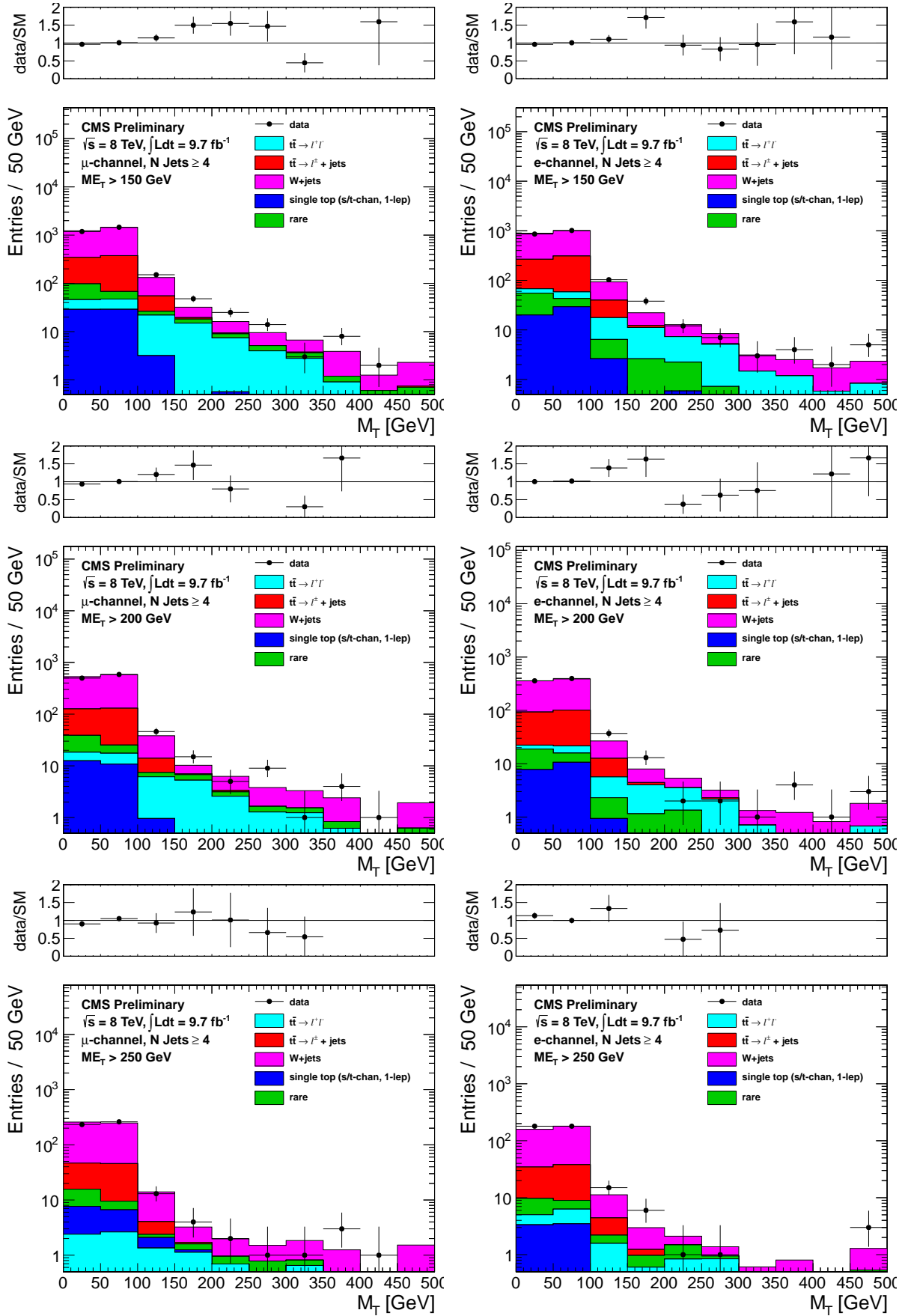


Figure 10: Comparison of the  $M_T$  distribution in data vs. MC for events with a leading muon (left) and leading electron (right) satisfying the requirements of CR1. The  $E_T^{\text{miss}}$  requirements used are 150 GeV (top), 200 GeV (middle) and 250 GeV (bottom).

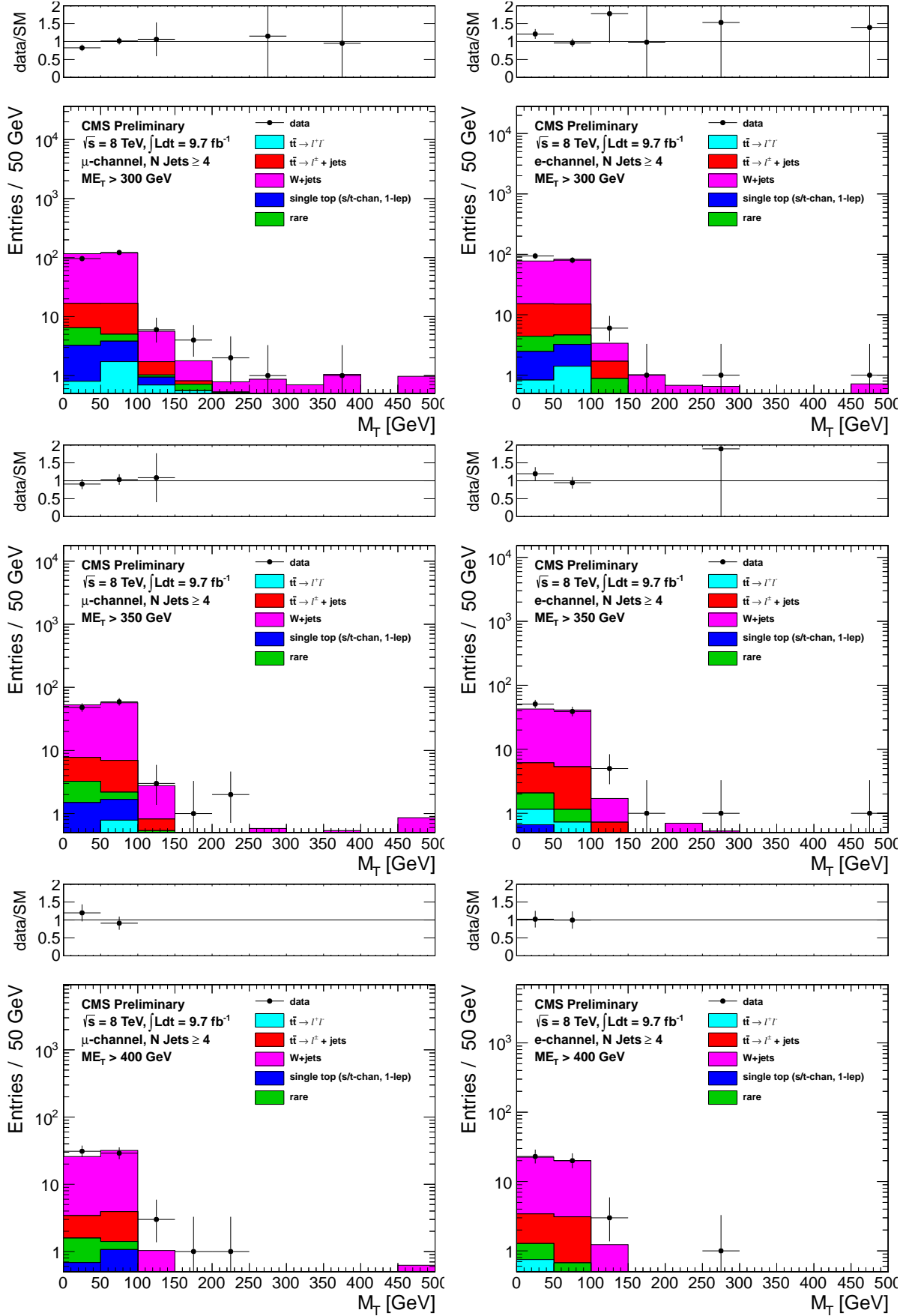


Figure 11: Comparison of the  $M_T$  distribution in data vs. MC for events with a leading muon (left) and leading electron (right) satisfying the requirements of CR1. The  $E_T^{\text{miss}}$  requirements used are 300 GeV (top), 350 GeV (middle) and 400 GeV (bottom).

## 6.2 Single Lepton Top MC Modelling Validation from CR2

The  $M_T$  tail for single-lepton top events ( $t\bar{t} \rightarrow \ell + \text{jets}$  and single top) is dominated by jet resolution effects. The  $W$  cannot be far off-shell because  $M_W < M_{\text{top}}$ . The modeling of the  $M_T$  tail from jet resolution effects is studied using  $Z$ +jets data and MC samples.

$Z$  events are selected by requiring 2 good leptons (satisfying ID and isolation requirements) and requiring the  $M_{\ell\ell}$  to be in the range 81–101 GeV. To reduce  $t\bar{t}$  backgrounds, events with a CSV tag are removed. The negative lepton is treated as a neutrino and so is added to the MET:  $E_T^{\text{miss}} \rightarrow p_T(\ell^-) + E_T^{\text{miss}}$ , and the  $M_T$  is recalculated with the positive lepton  $M_T(\ell^+, E_T^{\text{miss}})$ . The resulting “pseudo- $M_T$ ” is dominated by jet resolution effects, since no off-shell  $Z$  production enters the sample due to the  $M_{\ell\ell}$  requirement. This section describes how well the MC predicts the tail of “pseudo- $M_T$ ”.

The underlying distributions are shown in Fig. 12 and 13. Just as in CR1, there is an excess in the tails.

We then perform the exact same type of Data/MC comparison and analysis as described for CR1 in Section 6.1. For CR1 we collected the data/MC tail information in Table 13 ; the equivalent for CR2 is Table 14 (for CR2 the statistics are not sufficient to split electrons and muons). The last line of Table 14 gives the data/MC scale factor for the  $t\bar{t}$  lepton + jets  $M_T$  tail ( $SFR_{\text{top}}$ ). This is calculated in the same way as  $SFR_{\text{wjets}}$  of Table 13.

Sample	CR2PRESEL0	CR2PRESEL1	CR2A	CR2B	CR2C	CR2D	CR2E
MC	$36 \pm 2$	$30 \pm 2$	$18 \pm 1$	$30 \pm 2$	$13 \pm 1$	$5 \pm 0$	$2 \pm 0$
Data	56	43	32	40	21	12	2
Data/MC	$1.56 \pm 0.23$	$1.44 \pm 0.24$	$1.77 \pm 0.34$	$1.32 \pm 0.22$	$1.65 \pm 0.37$	$2.65 \pm 0.79$	$0.99 \pm 0.71$
DY MC	$27 \pm 2$	$23 \pm 2$	$14 \pm 2$	$25 \pm 3$	$11 \pm 2$	$3 \pm 1$	$1 \pm 1$
DY Data	$47 \pm 8$	$36 \pm 7$	$28 \pm 6$	$35 \pm 6$	$19 \pm 5$	$11 \pm 3$	$1 \pm 1$
DY Data/MC	$1.75 \pm 0.31$	$1.58 \pm 0.32$	$2.00 \pm 0.47$	$1.38 \pm 0.31$	$1.78 \pm 0.56$	$3.29 \pm 1.73$	$0.98 \pm 1.20$
$SFR_{\text{top}}$	$1.66 \pm 0.40$	$1.51 \pm 0.35$	$1.89 \pm 0.56$	$1.35 \pm 0.28$	$1.71 \pm 0.51$	$2.97 \pm 1.26$	$0.98 \pm 0.71$

Table 14: Yields in  $M_T$  tail comparing the  $Z$ +jets MC prediction (after applying SFs) to data without subtracting the non- $Z$ +jets components (top table) and with subtracting the non- $Z$ +jets components (bottom table). CR2PRESEL refers to a sample with  $E_T^{\text{miss}} > 50$  GeV and  $M_T > 150$  GeV.

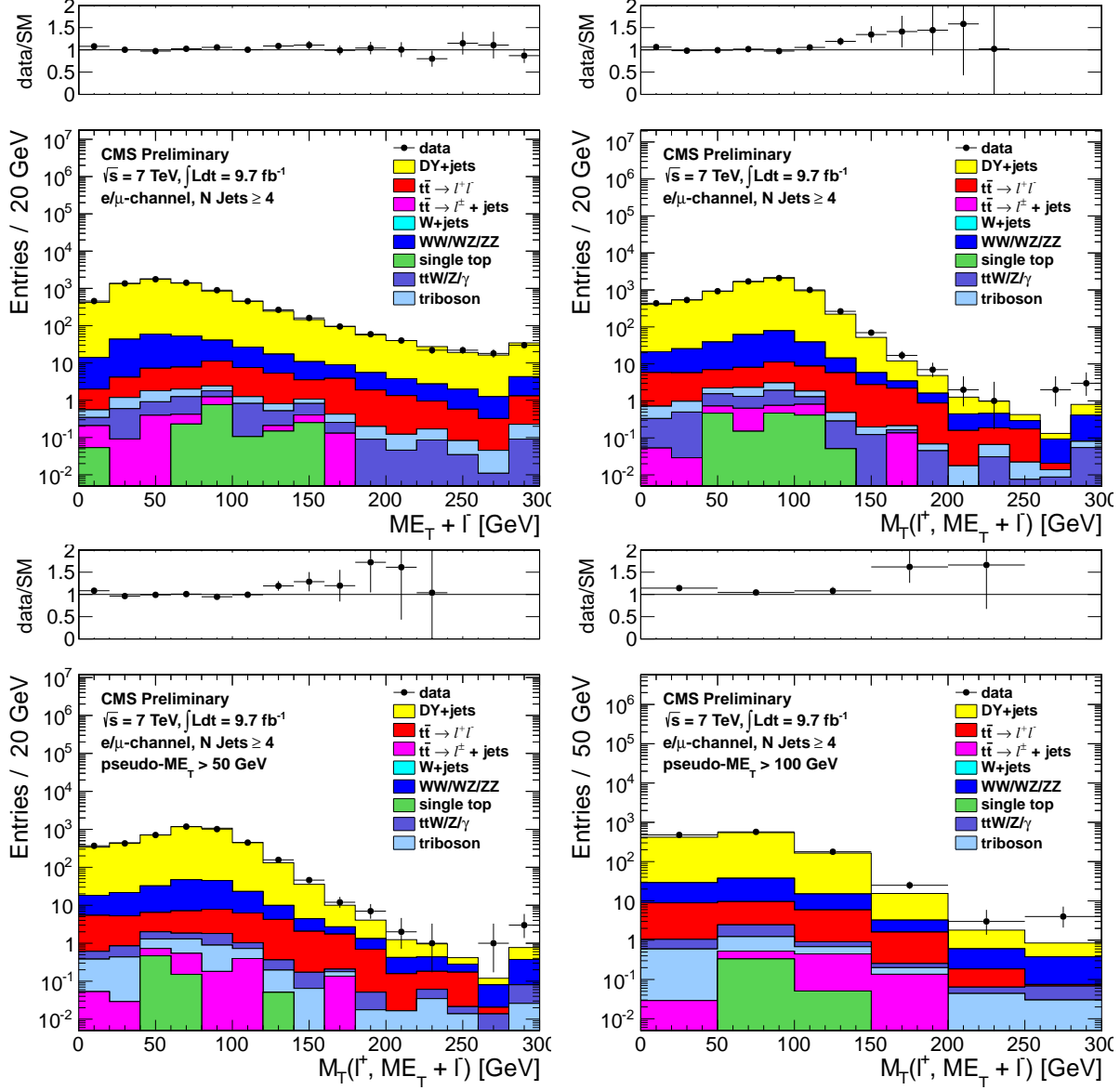


Figure 12: Comparison of the pseudo- $E_T^{\text{miss}}$  (top, left), pseudo- $M_T$  (top, right and bottom) distributions in data vs. MC for events satisfying the requirements of CR2, combining both the muon and electron channels. The pseudo- $M_T$  distributions are shown before any additional requirements (top, right) and after requiring pseudo- $E_T^{\text{miss}} > 50$  GeV (bottom, left) and pseudo- $E_T^{\text{miss}} > 100$  GeV (bottom, right) .

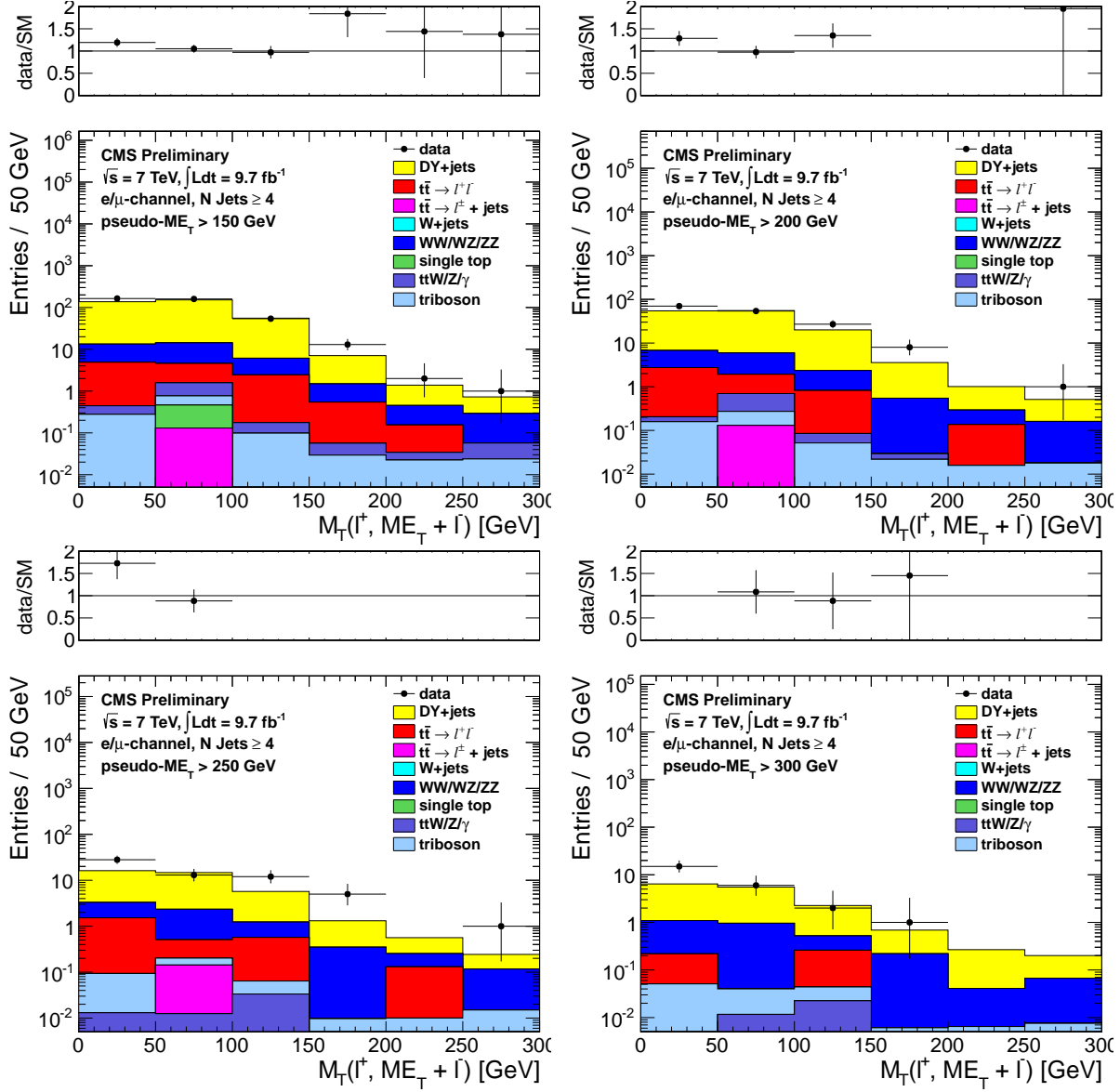


Figure 13: Comparison of the  $M_T$  distribution in data vs. MC for events satisfying the requirements of CR2, combining both the muon and electron channels. The pseudo- $E_T^{\text{miss}}$  requirements used are 150 GeV (top, left), 200 GeV (top, right), 250 GeV (bottom, left) and 300 GeV (bottom, right).

## 6.3 Dilepton studies in CR4

### 6.3.1 Modeling of Additional Hard Jets in Top Dilepton Events

Dilepton  $t\bar{t}$  events have 2 jets from the top decays, so additional jets from radiation or higher order contributions are required to enter the signal sample. In this Section we develop an algorithm to be applied to all  $t\bar{t} \rightarrow \ell\ell$  MC samples to ensure that the distribution of extra jets is properly modelled.

The modeling of additional jets in  $t\bar{t}$  events is checked in a  $t\bar{t} \rightarrow \ell\ell$  control sample, selected by requiring

- exactly 2 selected electrons or muons with  $p_T > 20$  GeV
- $E_T^{\text{miss}} > 50$  GeV
- $\geq 1$  b-tagged jet
- Z-veto ( $|m_{\ell\ell} - 91| > 15$  GeV)

Figure 14 shows a comparison of the jet multiplicity distribution in data and MC for this two-lepton control sample. After requiring at least 1 b-tagged jet, most of the events have 2 jets, as expected from the dominant process  $t\bar{t} \rightarrow \ell\ell$ . There is also a significant fraction of events with additional jets. The 3-jet sample is mainly comprised of  $t\bar{t}$  events with 1 additional emission and similarly the  $\geq 4$ -jet sample contains primarily  $t\bar{t} + \geq 2$  jet events.

It should be noted that in the case of  $t\bar{t} \rightarrow \ell\ell$  events with a single reconstructed lepton, the other lepton may be mis-reconstructed as a jet. For example, a hadronic tau may be mis-identified as a jet (since no  $\tau$  identification is used). In this case only 1 additional jet from radiation may suffice for a  $t\bar{t} \rightarrow \ell\ell$  event to enter the signal sample. As a result, both the samples with  $t\bar{t} + 1$  jet and  $t\bar{t} + \geq 2$  jets are relevant for estimating the top dilepton background in the signal region.

Table 15 shows scale factors ( $K_3$  and  $K_4$ ) used to correct the fraction of events with additional jets in MC to the observed fraction in data. These scale factors are calculated from Fig. 14 as follows:

- $N_2$  = data yield minus non-dilepton  $t\bar{t}$  MC yield for  $N_{\text{jets}} = 1$  or 2.
- $N_3$  = data yield minus non-dilepton  $t\bar{t}$  MC yield for  $N_{\text{jets}} = 3$
- $N_4$  = data yield minus non-dilepton  $t\bar{t}$  MC yield for  $N_{\text{jets}} \geq 4$
- $M_2$  = dilepton  $t\bar{t}$  MC yield for  $N_{\text{jets}} = 1$  or 2
- $M_3$  = dilepton  $t\bar{t}$  MC yield for  $N_{\text{jets}} = 3$
- $M_4$  = dilepton  $t\bar{t}$  MC yield for  $N_{\text{jets}} \geq 4$

then

- $SF_2 = N_2/M_2$
- $SF_3 = N_3/M_3$
- $SF_4 = N_4/M_4$
- $K_3 = SF_3/SF_2$
- $K_4 = SF_4/SF_2$

This insures that  $K_3 M_3 / (M_2 + K_3 M_3 + K_4 M_4) = N_3 / (N_2 + N_3 + N_4)$  and similarly for the  $\geq 4$  jet bin.

Table 15 also shows the values of  $K_3$  and  $K_4$  when the  $E_T^{\text{miss}}$  cut in the control sample definition is changed from 50 GeV to 100 GeV and 150 GeV. This demonstrates that there is no statistically significant dependence of  $K_3$  and  $K_4$  on the  $E_T^{\text{miss}}$  cut.

The factors  $K_3$  and  $K_4$  (derived with the 100 GeV  $E_T^{\text{miss}}$  cut) are applied to the  $t\bar{t} \rightarrow \ell\ell$  MC throughout the entire analysis, i.e. whenever  $t\bar{t} \rightarrow \ell\ell$  MC is used to estimate or subtract a yield or distribution.

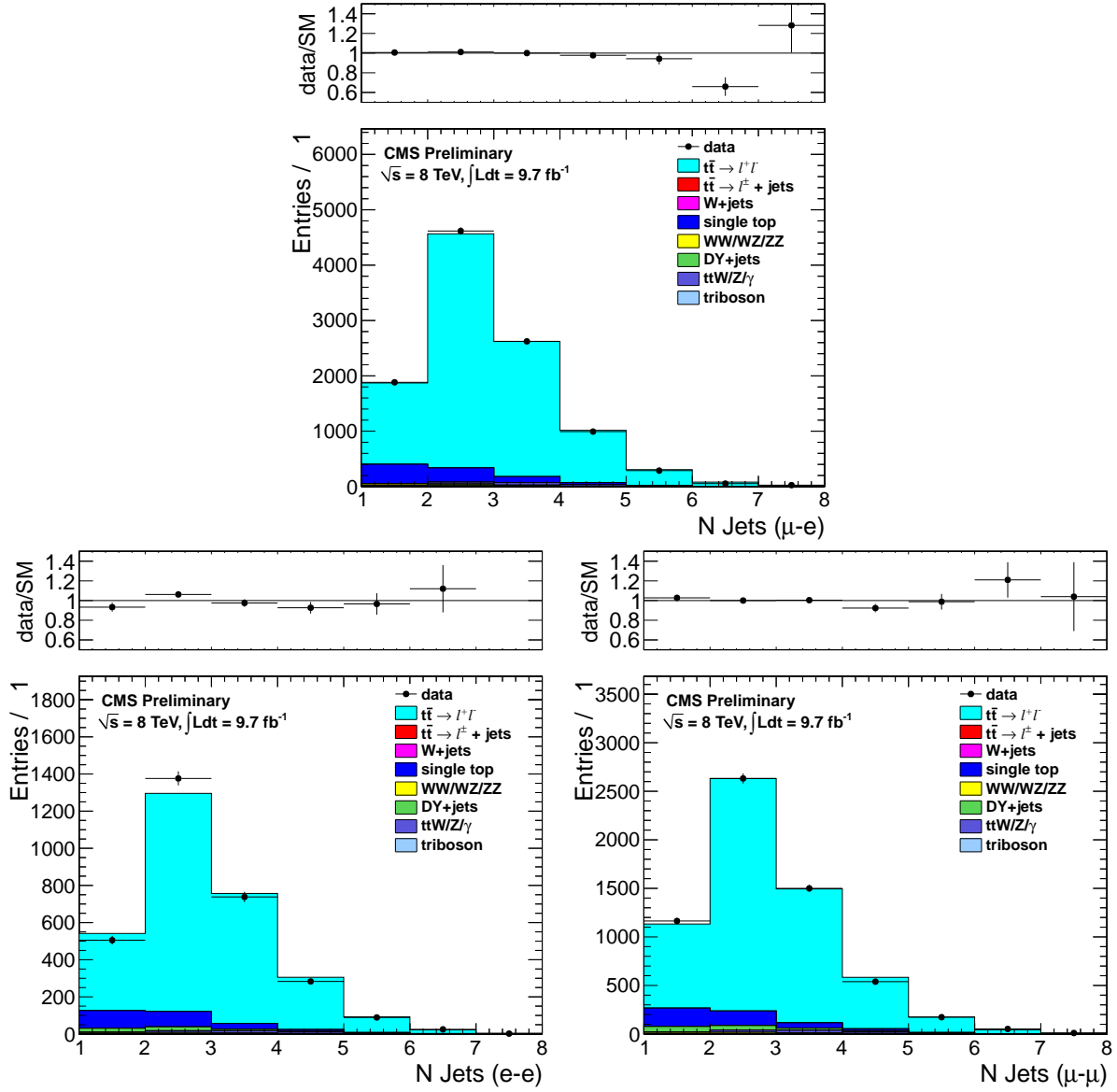


Figure 14: Comparison of the jet multiplicity distribution in data and MC for dilepton events in the  $e\mu$  (top),  $e-e$  (bottom left) and  $\mu\mu$  (bottom right) channels.

349 To be explicit, whenever Powheg is used, the Powheg  $K_3$  and  $K_4$  are used; whenever default MadGraph  
350 is used, the MadGraph  $K_3$  and  $K_4$  are used, etc. In order to do so, it is first necessary to count the  
351 number of additional jets from radiation and exclude leptons mis-identified as jets. A jet is considered a  
352 mis-identified lepton if it is matched to a generator-level second lepton with sufficient energy to satisfy  
353 the jet  $p_T$  requirement ( $p_T > 30$  GeV). Then  $t\bar{t} \rightarrow \ell\ell$  events that need two radiation jets to enter our  
354 selection are scaled by  $K_4$ , while those that only need one radiation jet are scaled by  $K_3$ .

Jet Multiplicity Sample	$E_T^{\text{miss}}$ cut for data/MC scale factors		
	50 GeV	100 GeV	150 GeV
N jets = 3 (sensitive to $t\bar{t} + 1$ extra jet from radiation)	$K_3 = 0.98 \pm 0.02$	$K_3 = 1.01 \pm 0.03$	$K_3 = 1.00 \pm 0.08$
N jets $\geq 4$ (sensitive to $t\bar{t} + \geq 2$ extra jets from radiation)	$K_4 = 0.94 \pm 0.02$	$K_4 = 0.93 \pm 0.04$	$K_4 = 1.00 \pm 0.08$

Table 15: Data/MC scale factors used to account for differences in the fraction of events with additional hard jets from radiation in  $t\bar{t} \rightarrow \ell\ell$  events. The values derived with the 100 GeV  $E_T^{\text{miss}}$  cut are applied to the  $t\bar{t} \rightarrow \ell\ell$  MC throughout the analysis.



### 6.3.2 Validation of the “Physics” Modelling of the $t\bar{t} \rightarrow \ell\ell$ MC in CR4

As mentioned above,  $t\bar{t} \rightarrow$  dileptons where one of the leptons is somehow lost constitutes the main background. The object of this test is to validate the  $M_T$  distribution of this background by looking at the  $M_T$  distribution of well identified dilepton events. We construct a transverse mass variable from the leading lepton and the  $E_T^{\text{miss}}$ . We distinguish between events with leading electrons and leading muons.

The  $t\bar{t}$  MC is corrected using the  $K_3$  and  $K_4$  factors from Section 6.3.1. It is also normalized to the total data yield separately for the  $E_T^{\text{miss}}$  requirements of the various signal regions. These normalization factors are listed in Table 16 and are close to unity.

The underlying  $E_T^{\text{miss}}$  and  $M_T$  distributions are shown in Figures 15 and 16. The data-MC agreement is quite good. Quantitatively, this is also shown in Table 17. This is a **very** important Table. It shows that for well identified  $t\bar{t} \rightarrow \ell\ell$ , the MC can predict the  $M_T$  tail. Since the main background is also  $t\bar{t} \rightarrow \ell\ell$  except with one “missed” lepton, this is a key test.

Sample	CR4PRESEL	CR4A	CR4B	CR4C	CR4D	CR4E	CR4F
$\mu$ Data/MC-SF	$1.01 \pm 0.03$	$0.96 \pm 0.04$	$0.99 \pm 0.07$	$1.05 \pm 0.13$	$0.91 \pm 0.20$	$1.10 \pm 0.34$	$1.50 \pm 0.67$
e Data/MC-SF	$0.99 \pm 0.03$	$0.99 \pm 0.05$	$0.91 \pm 0.08$	$0.84 \pm 0.13$	$0.70 \pm 0.18$	$0.73 \pm 0.29$	$0.63 \pm 0.38$

Table 16: Data/MC scale factors for total yields, applied to compare the shapes of the distributions. The uncertainties are statistical only.

Sample	CR4PRESEL	CR4A	CR4B	CR4C	CR4D	CR4E	CR4F
$\mu$ MC	$256 \pm 14$	$152 \pm 11$	$91 \pm 9$	$26 \pm 5$	$6 \pm 2$	$4 \pm 2$	$2 \pm 1$
$\mu$ Data	251	156	98	27	8	6	4
$\mu$ Data/MC SF	$0.98 \pm 0.08$	$1.02 \pm 0.11$	$1.08 \pm 0.16$	$1.04 \pm 0.28$	$1.29 \pm 0.65$	$1.35 \pm 0.80$	$2.10 \pm 1.72$
e MC	$227 \pm 13$	$139 \pm 11$	$73 \pm 8$	$21 \pm 4$	$5 \pm 2$	$2 \pm 1$	$1 \pm 1$
e Data	219	136	72	19	2	1	1
e Data/MC SF	$0.96 \pm 0.09$	$0.98 \pm 0.11$	$0.99 \pm 0.16$	$0.92 \pm 0.29$	$0.41 \pm 0.33$	$0.53 \pm 0.62$	$0.76 \pm 0.96$
$\mu$ +e MC	$483 \pm 19$	$291 \pm 16$	$164 \pm 13$	$47 \pm 7$	$11 \pm 3$	$6 \pm 2$	$3 \pm 2$
$\mu$ +e Data	470	292	170	46	10	7	5
$\mu$ +e Data/MC SF	$0.97 \pm 0.06$	$1.00 \pm 0.08$	$1.04 \pm 0.11$	$0.99 \pm 0.20$	$0.90 \pm 0.37$	$1.11 \pm 0.57$	$1.55 \pm 1.04$

Table 17: Yields in  $M_T$  tail comparing the MC prediction (after applying SFs) to data. The uncertainties are statistical only.

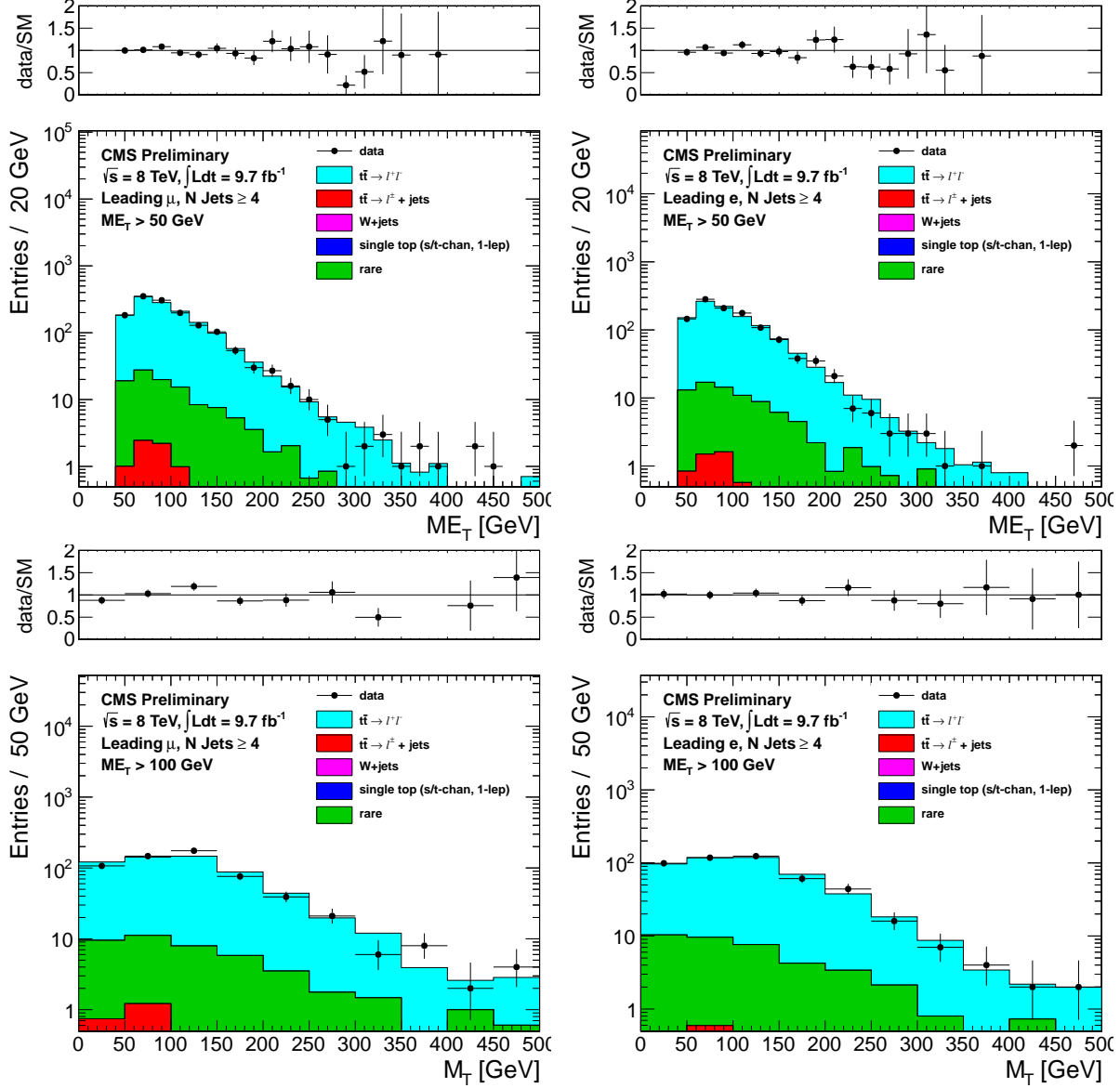


Figure 15: Comparison of the  $E_T^{\text{miss}}$  (top) and  $M_T$  for  $E_T^{\text{miss}} > 100$  (bottom) distributions in data vs. MC for events with a leading muon (left) and leading electron (right) satisfying the requirements of CR4.

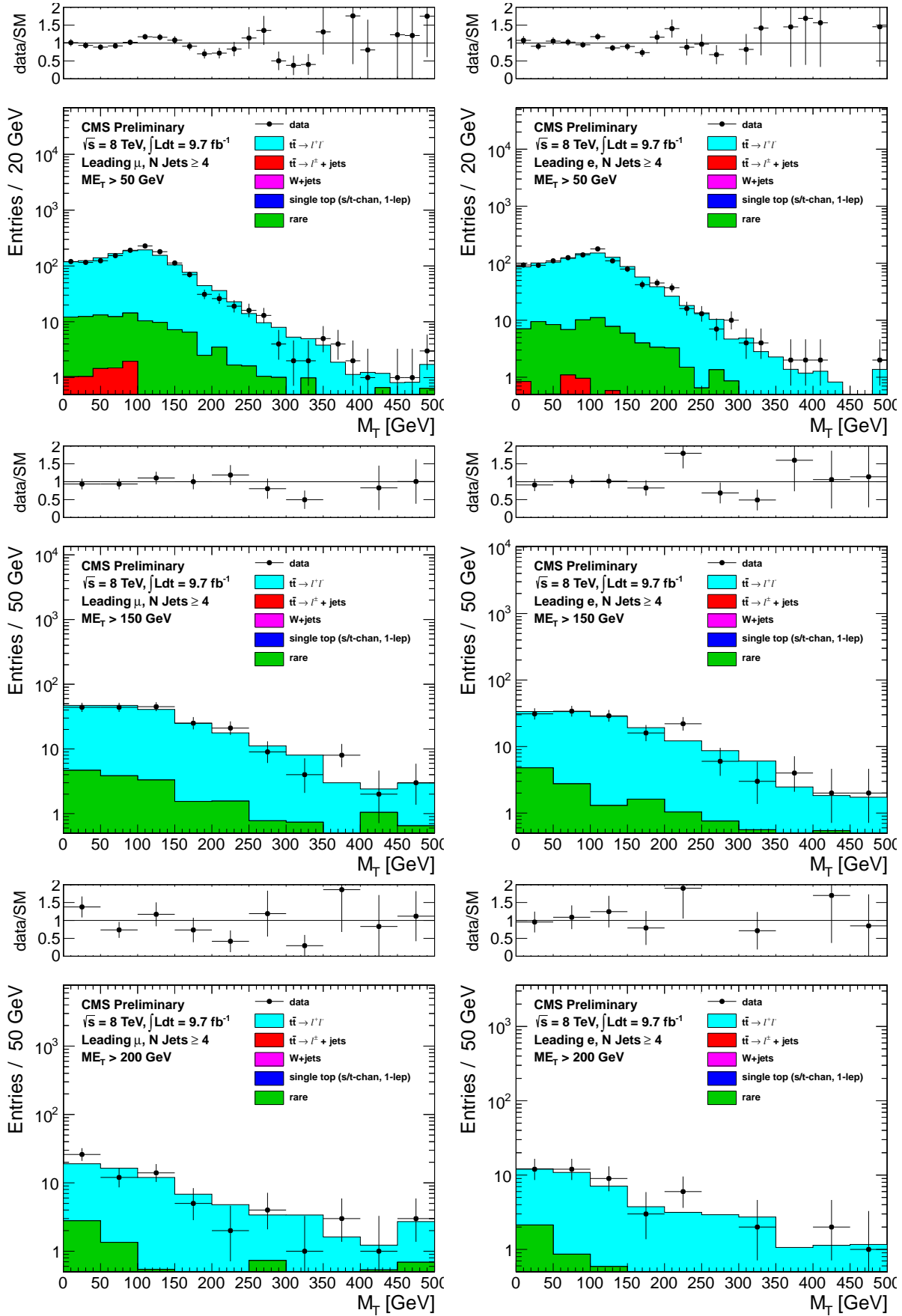


Figure 16: Comparison of the  $M_T$  distribution in data vs. MC for events with a leading muon (left) and leading electron (right) satisfying the requirements of CR4. The  $E_T^{\text{miss}}$  requirements used are 50 GeV (top), 200 GeV (middle) and 250 GeV (bottom).

## 6.4 Test of control region with isolated track in CR5

This CR consists of events that pass all cuts but fail the isolated track veto cut. These events (especially in the tail of  $M_T$ ) are predominantly  $t\bar{t}$  dileptons. Thus the test in this control region is similar to that performed in CR4 and described in Section 6.3.2. There is some non-trivial complementarity because CR5 also includes events with taus and events with electrons or muons below the threshold of the CR4 selection. Also, this test is somewhat sensitive to the simulation of the track isolation requirement, since the number of dilepton events in CR5 depends on the (in)efficiency of that cut.

In CR5 there is also a significant component of  $t\bar{t} \rightarrow \ell + \text{jets}$ , where one of the jets fluctuates to an isolated track. This component dominates at low  $M_T$  and is not necessarily well reproduced quantitatively by the simulation. This makes the normalization of the top MC a little bit tricky. We define a “pre-veto” sample as the sample of events that pass all cuts without any isolated track requirements. This sample is dominated by  $t\bar{t} \rightarrow \ell + \text{jets}$ . We normalize the dilepton component of the top MC to that sample. This is done by normalizing the total  $t\bar{t}$  MC to the  $M_T$  peak region,  $50 < M_T < 80$  GeV in this sample.

Next we define a “post-veto” sample as the events that have an isolated track. The  $t\bar{t} \rightarrow \ell + \text{jets}$  component is normalized in this sample, again by normalizing to the  $M_T$  peak region. These normalization factors are summarized in Table 18.

The post-veto  $t\bar{t} \rightarrow \ell\ell$  is taken from MC, but with scale factor obtained by the normalization of the “pre-veto” sample.

The underlying  $E_T^{\text{miss}}$  and  $M_T$  distributions are shown in Figures 17 and 18. The data-MC agreement is quite good. Quantitatively, this is also shown in Table 19. This is the second key test of the  $t\bar{t} \rightarrow \ell\ell$  modeling

Sample	CR5PRESEL	CR5A	CR5B	CR5C	CR5D	CR5E	CR5F	CR5G
$\mu$ pre-veto $M_T$ -SF	$1.05 \pm 0.01$	$1.02 \pm 0.02$	$0.95 \pm 0.03$	$0.90 \pm 0.05$	$0.98 \pm 0.08$	$0.97 \pm 0.13$	$0.85 \pm 0.18$	$0.92 \pm 0.31$
$\mu$ post-veto $M_T$ -SF	$1.25 \pm 0.04$	$1.17 \pm 0.07$	$1.05 \pm 0.12$	$0.85 \pm 0.19$	$0.84 \pm 0.30$	$1.07 \pm 0.54$	$1.38 \pm 1.14$	$0.68 \pm 2.05$
e pre-veto $M_T$ -SF	$1.01 \pm 0.01$	$0.95 \pm 0.02$	$0.95 \pm 0.03$	$0.94 \pm 0.06$	$0.85 \pm 0.09$	$0.84 \pm 0.13$	$1.05 \pm 0.23$	$1.04 \pm 0.33$
e post-veto $M_T$ -SF	$1.21 \pm 0.04$	$1.12 \pm 0.07$	$1.25 \pm 0.14$	$1.17 \pm 0.27$	$2.01 \pm 0.64$	$1.71 \pm 0.99$	$2.79 \pm 2.04$	$0.81 \pm 1.58$

Table 18:  $M_T$  peak Data/MC scale factors. The pre-veto SFs are applied to the  $t\bar{t} \rightarrow \ell\ell$  sample, while the post-veto SFs are applied to the single lepton samples. The raw MC is used for backgrounds from rare processes. The uncertainties are statistical only.

Sample	CR5PRESEL	CR5A	CR5B	CR5C	CR5D	CR5E	CR5F	CR5G
$\mu$ MC	$490 \pm 9$	$299 \pm 7$	$155 \pm 6$	$49 \pm 3$	$19 \pm 2$	$7 \pm 1$	$3 \pm 1$	$2 \pm 1$
$\mu$ Data	514	311	167	57	12	4	2	1
$\mu$ Data/MC SF	$1.05 \pm 0.05$	$1.04 \pm 0.06$	$1.08 \pm 0.09$	$1.17 \pm 0.17$	$0.64 \pm 0.20$	$0.54 \pm 0.29$	$0.66 \pm 0.49$	$0.58 \pm 0.62$
e MC	$405 \pm 8$	$239 \pm 7$	$130 \pm 5$	$43 \pm 3$	$16 \pm 2$	$8 \pm 1$	$6 \pm 2$	$3 \pm 1$
e Data	427	248	120	38	14	4	3	2
e Data/MC SF	$1.06 \pm 0.06$	$1.04 \pm 0.07$	$0.93 \pm 0.09$	$0.89 \pm 0.16$	$0.86 \pm 0.25$	$0.52 \pm 0.28$	$0.54 \pm 0.35$	$0.76 \pm 0.60$
$\mu$ +e MC	$894 \pm 12$	$538 \pm 10$	$284 \pm 8$	$92 \pm 4$	$35 \pm 3$	$15 \pm 2$	$9 \pm 2$	$4 \pm 1$
$\mu$ +e Data	941	559	287	95	26	8	5	3
$\mu$ +e Data/MC SF	$1.05 \pm 0.04$	$1.04 \pm 0.05$	$1.01 \pm 0.07$	$1.04 \pm 0.12$	$0.74 \pm 0.16$	$0.53 \pm 0.20$	$0.58 \pm 0.29$	$0.69 \pm 0.43$

Table 19: Yields in  $M_T$  tail comparing the MC prediction (after applying SFs) to data. The uncertainties are statistical only.

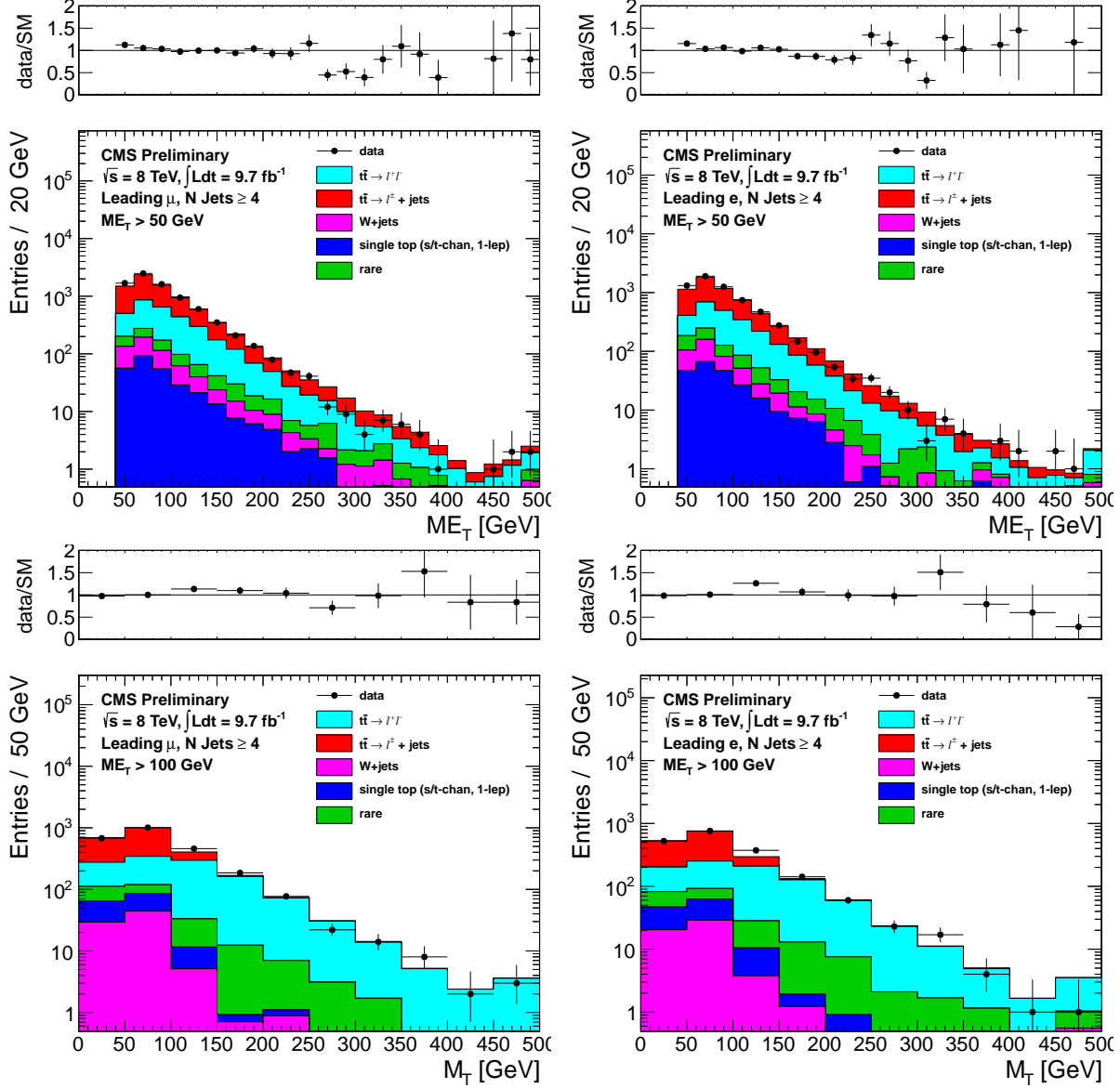


Figure 17: Comparison of the  $E_T^{\text{miss}}$  (top) and  $M_T$  for  $E_T^{\text{miss}} > 100$  (bottom) distributions in data vs. MC for events with a leading muon (left) and leading electron (right) satisfying the requirements of CR5.

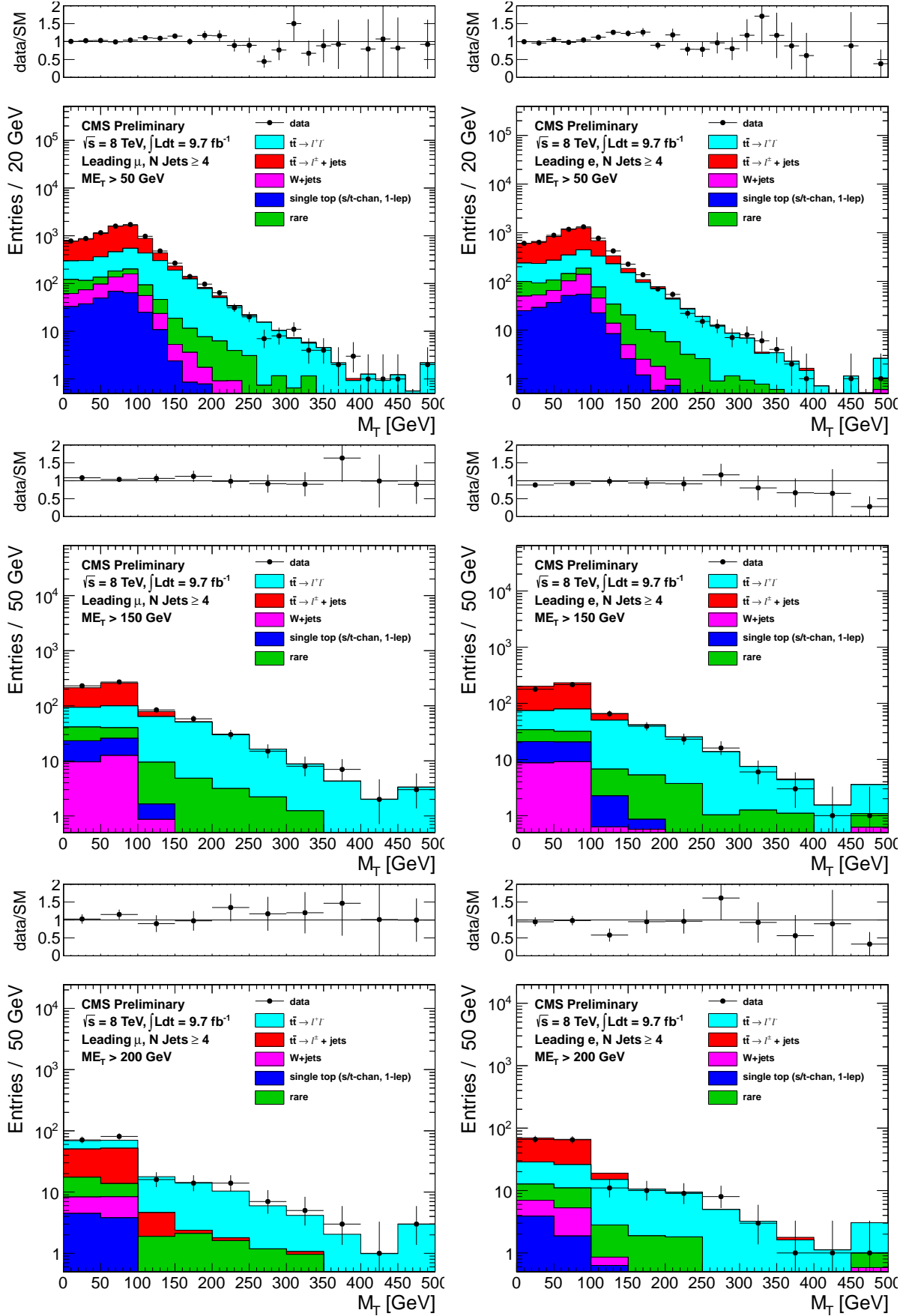


Figure 18: Comparison of the  $M_T$  distribution in data vs. MC for events with a leading muon (left) and leading electron (right) satisfying the requirements of CR5. The  $E_T^{\text{miss}}$  requirements used are 50 GeV (top), 150 GeV (middle) and 200 GeV (bottom).

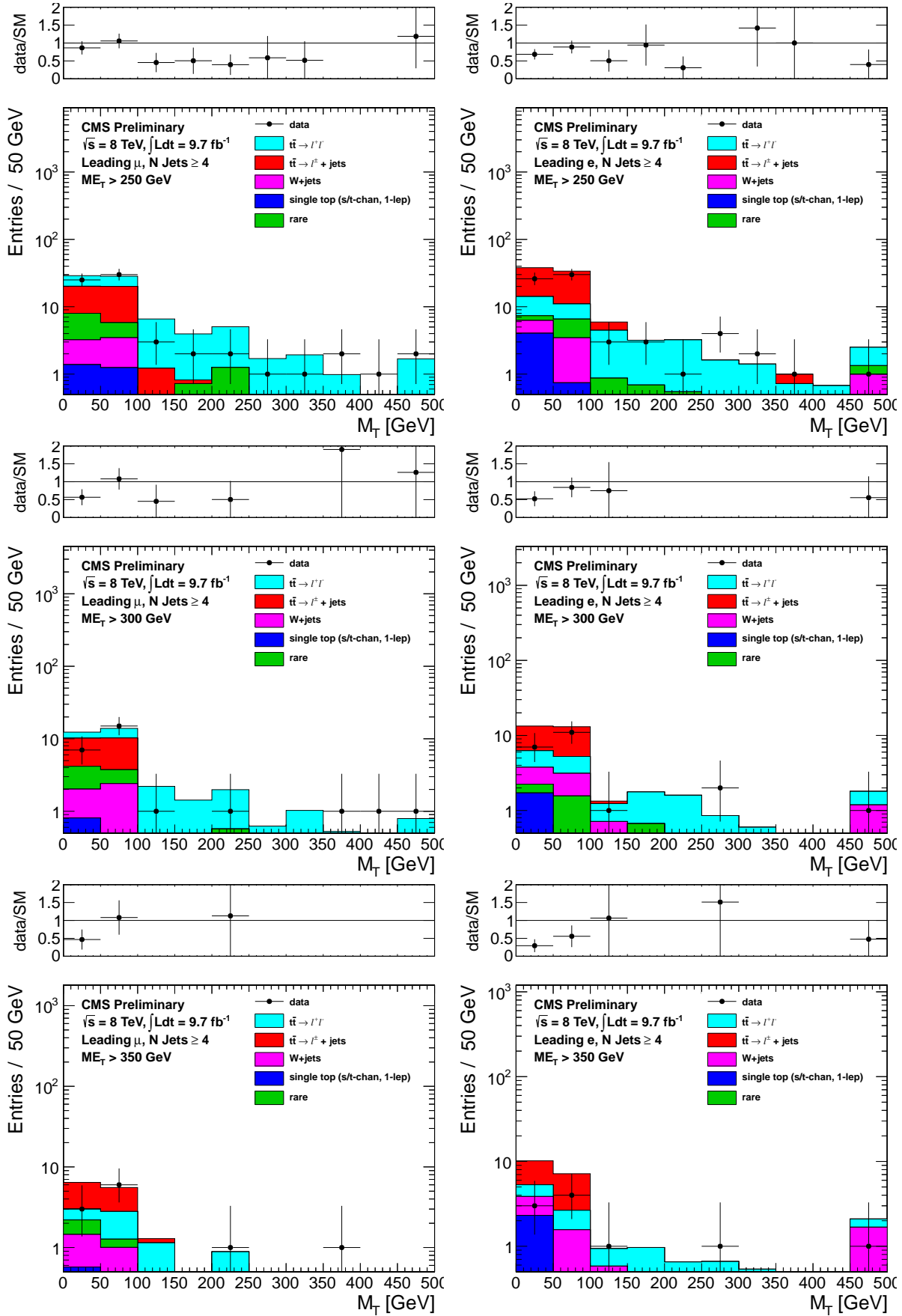


Figure 19: Comparison of the  $M_T$  distribution in data vs. MC for events with a leading muon (left) and leading electron (right) satisfying the requirements of CR5. The  $E_T^{\text{miss}}$  requirements used are 250 GeV (top), 300 GeV (middle) and 350 GeV (bottom).

## 7 Other Backgrounds

Additional background contributions from rare processes include

- $t\bar{t}$  in association with a boson,  $t\bar{t} + WZ/\gamma^*$
- $Z/\gamma^* + \text{Jets}$
- diboson,  $WW/WZ/ZZ$
- triboson,  $WWW/WWZ/WZZ/ZZZ$
- dilepton single top,  $tW$ .

These backgrounds are small, contributing at the  $\sim 5\%$  level and their predictions are taken from MC, normalized to the corresponding cross sections. A 50% systematic uncertainty is assigned for all these backgrounds. Note that these backgrounds are not double-counted because the contribution to the  $M_T$  peak region is subtracted off when deriving the  $M_T$  peak data/MC scale factors.

Backgrounds from QCD are expected to be small in the signal regions with large  $M_T$  and  $E_T^{\text{miss}}$ .

## 8 Tail-to-Peak ratio for lepton + jets top and W events

An important component of the background calculation is the ratio of the number of events with  $M_T$  in the signal region to the number of events with  $50 < M_T < 80$  GeV. As discussed in Section 2.1, these ratios are different for  $W + \text{jets}$  and top events.

Sample	SRA	SRB	SRC	SRD	SRE	SRF	SRG
$R_{top}^\mu$	$0.015 \pm 0.001$	$0.035 \pm 0.002$	$0.021 \pm 0.002$	$0.021 \pm 0.004$	$0.025 \pm 0.007$	$0.015 \pm 0.009$	$0.021 \pm 0.015$
$R_{wjet}^\mu$	$0.040 \pm 0.001$	$0.071 \pm 0.003$	$0.062 \pm 0.004$	$0.064 \pm 0.006$	$0.065 \pm 0.009$	$0.067 \pm 0.012$	$0.065 \pm 0.016$
$R_{top}^e$	$0.015 \pm 0.001$	$0.031 \pm 0.002$	$0.026 \pm 0.003$	$0.025 \pm 0.005$	$0.009 \pm 0.005$	$0.021 \pm 0.012$	$0.034 \pm 0.024$
$R_{wjet}^e$	$0.040 \pm 0.002$	$0.075 \pm 0.004$	$0.067 \pm 0.005$	$0.063 \pm 0.007$	$0.061 \pm 0.010$	$0.067 \pm 0.015$	$0.070 \pm 0.021$

Table 20: Ratio of MC events in the  $M_T$ -tail over events in the  $M_T$ -peak for  $t\bar{t} \rightarrow \ell + \text{jets}$  (also used for 1-lepton single top) and  $W + \text{jets}$ . These are derived before applying the b-tagging requirement.

The MC value of these ratios are shown in Table 20. In addition the studies of CR1 and CR2 (Sections 6.1 and 6.2) lead to data/MC scale factors  $SFR_{wjets}$  (Table 13) and  $SFR_{top}$  (Table 14)



## 9 Background Prediction

Here we give the details of how we arrive at the background prediction in a given signal region. We concentrate on the method used to arrive at the central value of the background prediction. The systematic uncertainties will be discussed in Section 10. The actual results for the BG prediction will be given in Section 11.

As mentioned in Section 2, we normalize the main  $t\bar{t}$  background to the  $M_T$  peak. This is actually a bit tricky because we want to minimize the effect of the isolated track veto on lepton + jets events, which may not be terribly well reproduced. Thus, we define two normalization region in the  $M_T$  peak ( $50 < M_T < 80$  GeV), one before and one after the application of the isolated track veto.

The event counts in pre-veto and post-veto normalization regions are given in Tables 21 and 22. The data-MC agreement in these two tables is quite good, and this is certainly a good thing.

Sample	SRA	SRB	SRC	SRD	SRE	SRF	SRG
Muon							
$t\bar{t} \rightarrow \ell\ell$	$371 \pm 6$	$120 \pm 4$	$43 \pm 2$	$17 \pm 1$	$8 \pm 1$	$4 \pm 1$	$1 \pm 0$
$t\bar{t} \rightarrow \ell + \text{jets} \ \& \ \text{single top} \ (1\ell)$	$3666 \pm 21$	$1088 \pm 12$	$355 \pm 7$	$127 \pm 4$	$50 \pm 3$	$22 \pm 2$	$8 \pm 1$
$W + \text{jets}$	$316 \pm 8$	$113 \pm 5$	$46 \pm 3$	$21 \pm 2$	$11 \pm 1$	$5 \pm 1$	$2 \pm 1$
Rare	$117 \pm 5$	$48 \pm 3$	$16 \pm 2$	$6 \pm 1$	$2 \pm 1$	$1 \pm 0$	$1 \pm 0$
Total	$4470 \pm 24$	$1369 \pm 13$	$461 \pm 8$	$171 \pm 5$	$71 \pm 3$	$33 \pm 2$	$13 \pm 1$
Data	4538	1304	418	168	69	28	12
Electron							
$t\bar{t} \rightarrow \ell\ell$	$290 \pm 6$	$98 \pm 3$	$35 \pm 2$	$13 \pm 1$	$6 \pm 1$	$3 \pm 1$	$1 \pm 0$
$t\bar{t} \rightarrow \ell + \text{jets} \ \& \ \text{single top} \ (1\ell)$	$2899 \pm 19$	$861 \pm 10$	$282 \pm 6$	$104 \pm 4$	$42 \pm 2$	$16 \pm 2$	$8 \pm 1$
$W + \text{jets}$	$252 \pm 28$	$87 \pm 4$	$35 \pm 3$	$18 \pm 2$	$8 \pm 1$	$4 \pm 1$	$2 \pm 1$
Rare	$89 \pm 5$	$34 \pm 3$	$15 \pm 2$	$7 \pm 1$	$3 \pm 1$	$0 \pm 0$	$0 \pm 0$
Total	$3530 \pm 35$	$1079 \pm 12$	$367 \pm 7$	$142 \pm 5$	$60 \pm 3$	$24 \pm 2$	$11 \pm 1$
Data	3358	1022	346	122	51	25	12
Muon+Electron Combined							
$t\bar{t} \rightarrow \ell\ell$	$661 \pm 9$	$218 \pm 5$	$78 \pm 3$	$30 \pm 2$	$14 \pm 1$	$7 \pm 1$	$3 \pm 1$
$t\bar{t} \rightarrow \ell + \text{jets} \ \& \ \text{single top} \ (1\ell)$	$6565 \pm 28$	$1949 \pm 16$	$637 \pm 9$	$231 \pm 5$	$92 \pm 4$	$39 \pm 2$	$16 \pm 2$
$W + \text{jets}$	$568 \pm 29$	$199 \pm 6$	$81 \pm 4$	$38 \pm 3$	$19 \pm 2$	$9 \pm 1$	$4 \pm 1$
Rare	$206 \pm 7$	$82 \pm 4$	$31 \pm 3$	$14 \pm 2$	$5 \pm 1$	$2 \pm 0$	$1 \pm 0$
Total	$8000 \pm 42$	$2448 \pm 18$	$828 \pm 11$	$314 \pm 7$	$131 \pm 4$	$56 \pm 3$	$24 \pm 2$
Data	7896	2326	764	290	120	53	24

Table 21: Preveto MC and data yields in  $M_T$  peak region. The n-jets k-factors have been applied to the  $t\bar{t} \rightarrow \ell\ell$ . The uncertainties are statistical only. These MC and data yields are used to derive data/MC SFs, the pre-veto  $M_T$ -SFs, shown in Table 23.

Sample	SRA	SRB	SRC	SRD	SRE	SRF	SRG
Muon							
$t\bar{t} \rightarrow \ell\ell$	$139 \pm 4$	$46 \pm 2$	$16 \pm 1$	$7 \pm 1$	$3 \pm 1$	$1 \pm 0$	$1 \pm 0$
$t\bar{t} \rightarrow \ell + \text{jets} \ \& \ \text{single top} \ (1\ell)$	$3273 \pm 20$	$974 \pm 11$	$321 \pm 6$	$113 \pm 4$	$45 \pm 2$	$21 \pm 2$	$8 \pm 1$
$W + \text{jets}$	$294 \pm 8$	$105 \pm 5$	$42 \pm 3$	$19 \pm 2$	$10 \pm 1$	$5 \pm 1$	$2 \pm 1$
Rare	$83 \pm 4$	$34 \pm 3$	$11 \pm 1$	$4 \pm 1$	$2 \pm 1$	$1 \pm 0$	$1 \pm 0$
Total	$3789 \pm 22$	$1160 \pm 12$	$391 \pm 7$	$143 \pm 4$	$60 \pm 3$	$28 \pm 2$	$11 \pm 1$
Data	3790	1098	358	143	59	24	11
Electron							
$t\bar{t} \rightarrow \ell\ell$	$116 \pm 4$	$40 \pm 2$	$14 \pm 1$	$5 \pm 1$	$2 \pm 0$	$1 \pm 0$	$1 \pm 0$
$t\bar{t} \rightarrow \ell + \text{jets} \ \& \ \text{single top} \ (1\ell)$	$2595 \pm 18$	$774 \pm 10$	$258 \pm 6$	$97 \pm 4$	$40 \pm 2$	$15 \pm 1$	$7 \pm 1$
$W + \text{jets}$	$236 \pm 28$	$82 \pm 4$	$33 \pm 3$	$17 \pm 2$	$8 \pm 1$	$4 \pm 1$	$2 \pm 1$
Rare	$62 \pm 4$	$23 \pm 2$	$9 \pm 1$	$4 \pm 1$	$2 \pm 1$	$0 \pm 0$	$0 \pm 0$
Total	$3009 \pm 34$	$919 \pm 11$	$315 \pm 7$	$123 \pm 4$	$51 \pm 3$	$21 \pm 2$	$10 \pm 1$
Data	2788	837	288	92	39	19	10
Muon+Electron Combined							
$t\bar{t} \rightarrow \ell\ell$	$255 \pm 5$	$86 \pm 3$	$30 \pm 2$	$12 \pm 1$	$5 \pm 1$	$2 \pm 1$	$1 \pm 0$
$t\bar{t} \rightarrow \ell + \text{jets} \ \& \ \text{single top} \ (1\ell)$	$5869 \pm 27$	$1747 \pm 15$	$579 \pm 9$	$209 \pm 5$	$85 \pm 3$	$36 \pm 2$	$15 \pm 2$
$W + \text{jets}$	$529 \pm 29$	$188 \pm 6$	$75 \pm 4$	$36 \pm 3$	$18 \pm 2$	$9 \pm 1$	$4 \pm 1$
Rare	$145 \pm 6$	$58 \pm 4$	$21 \pm 2$	$8 \pm 1$	$3 \pm 1$	$1 \pm 0$	$1 \pm 0$
Total	$6797 \pm 40$	$2079 \pm 17$	$705 \pm 10$	$265 \pm 6$	$111 \pm 4$	$49 \pm 3$	$21 \pm 2$
Data	6578	1935	646	235	98	43	21

Table 22: MC and data yields in  $M_T$  peak region after full selection. The n-jets k-factors have been applied to the  $t\bar{t} \rightarrow \ell\ell$ . The uncertainties are statistical only. These MC and data yields are used to derive data/MC SFs, the post-veto  $M_T$ -SFs, shown in Table 23.

The dominant dilepton background is normalized to the pre-veto normalization region. A pre-veto scale factor ( $SF_{pre}$ ) is defined as a common scale factors that needs to be applied to the  $t\bar{t}$ , single-top, and  $W$  + jets MC to make the data yield in the pre-veto normalization agree with the MC prediction (the small rare MC component is held fixed). Then, the dilepton background prediction is obtained by multiplying the dilepton BG Monte Carlo by  $SF_{pre}$ .

The  $t\bar{t}$  lepton + jet BG is normalized to post-veto normalization region. A post-veto scale factor ( $SF_{post}$ ) is defined in (almost) the same way as the pre-veto scale factor. The difference here is that this scale factor applies only to the lepton + jets components and not the dilepton component, since that component is already rescaled by  $SF_{pre}$ . This procedure minimizes the reliance on the understanding of the isolated track veto.

The pre-veto and post-veto SF are shown in Table 23.

Sample	SRA	SRB	SRC	SRD	SRE	SRF	SRG
$\mu$ pre-veto $M_T$ -SF	$1.02 \pm 0.02$	$0.95 \pm 0.03$	$0.90 \pm 0.05$	$0.98 \pm 0.08$	$0.97 \pm 0.13$	$0.85 \pm 0.18$	$0.92 \pm 0.31$
$\mu$ post-veto $M_T$ -SF	$1.00 \pm 0.02$	$0.95 \pm 0.03$	$0.91 \pm 0.05$	$1.00 \pm 0.09$	$0.99 \pm 0.13$	$0.85 \pm 0.18$	$0.96 \pm 0.31$
$\mu$ veto $M_T$ -SF	$0.98 \pm 0.01$	$0.99 \pm 0.01$	$1.01 \pm 0.02$	$1.02 \pm 0.04$	$1.02 \pm 0.06$	$1.00 \pm 0.09$	$1.04 \pm 0.11$
e pre-veto $M_T$ -SF	$0.95 \pm 0.02$	$0.95 \pm 0.03$	$0.94 \pm 0.06$	$0.85 \pm 0.09$	$0.84 \pm 0.13$	$1.05 \pm 0.23$	$1.04 \pm 0.33$
e post-veto $M_T$ -SF	$0.92 \pm 0.02$	$0.91 \pm 0.03$	$0.91 \pm 0.06$	$0.74 \pm 0.08$	$0.75 \pm 0.13$	$0.91 \pm 0.22$	$1.01 \pm 0.33$
e veto $M_T$ -SF	$0.97 \pm 0.01$	$0.96 \pm 0.02$	$0.97 \pm 0.03$	$0.87 \pm 0.05$	$0.89 \pm 0.08$	$0.86 \pm 0.11$	$0.97 \pm 0.14$

Table 23:  $M_T$  peak Data/MC scale factors. The pre-veto SFs are applied to the  $t\bar{t} \rightarrow \ell\ell$  sample, while the post-veto SFs are applied to the single lepton samples. The veto SF is shown for comparison across channels. The raw MC is used for backgrounds from rare processes. The uncertainties are statistical only.

Then the  $t\bar{t}$  lepton + jet BG is obtained by taking the number of MC-predicted  $t\bar{t}$  lepton + jets in the post-veto normalization region, scaling it by  $SF_{post}$ , multiplying it by the tail-to-peak ratio  $R_{top}$  of Table 20, and finally the data-MC scale factor  $SFR_{top}$  from Table 14.

The single top background is obtained in exactly the same way as the  $t\bar{t}$  lepton + jet BG, using the same tail-to-peak ratio and the same data-MC scale-factor. The  $W$  background is done in a similar way, but using a different tail-to-peak ratio ( $R_{wjets}$  of Table 20), and a different data-MC scale factor ( $SFR_{wjet}$  from Table 13).

Other (small) backgrounds are taken straight from Monte Carlo, as described in Section 7.

Sample	SRA	SRB	SRC	SRD	SRE	SRF	SRG
Muon							
$t\bar{t} \rightarrow \ell\ell$	$326 \pm 6$	$193 \pm 5$	$66 \pm 3$	$23 \pm 2$	$9 \pm 1$	$4 \pm 1$	$2 \pm 1$
$t\bar{t} \rightarrow \ell + \text{jets \& single top } (1\ell)$	$54 \pm 3$	$38 \pm 2$	$8 \pm 1$	$3 \pm 1$	$1 \pm 1$	$1 \pm 0$	$0 \pm 0$
$W + \text{jets}$	$17 \pm 2$	$8 \pm 1$	$3 \pm 1$	$2 \pm 1$	$0 \pm 0$	$0 \pm 0$	$0 \pm 0$
Rare	$33 \pm 2$	$23 \pm 2$	$9 \pm 1$	$5 \pm 1$	$3 \pm 1$	$1 \pm 0$	$1 \pm 0$
Total	$430 \pm 7$	$262 \pm 6$	$86 \pm 3$	$33 \pm 2$	$14 \pm 1$	$6 \pm 1$	$4 \pm 1$
Electron							
$t\bar{t} \rightarrow \ell\ell$	$261 \pm 5$	$153 \pm 4$	$54 \pm 2$	$19 \pm 1$	$7 \pm 1$	$2 \pm 1$	$1 \pm 0$
$t\bar{t} \rightarrow \ell + \text{jets \& single top } (1\ell)$	$41 \pm 2$	$28 \pm 2$	$7 \pm 1$	$3 \pm 1$	$1 \pm 0$	$1 \pm 0$	$1 \pm 0$
$W + \text{jets}$	$11 \pm 2$	$7 \pm 1$	$3 \pm 1$	$2 \pm 1$	$0 \pm 0$	$0 \pm 0$	$0 \pm 0$
Rare	$26 \pm 2$	$16 \pm 2$	$7 \pm 1$	$3 \pm 1$	$1 \pm 0$	$0 \pm 0$	$0 \pm 0$
Total	$340 \pm 6$	$204 \pm 5$	$71 \pm 3$	$26 \pm 2$	$8 \pm 1$	$4 \pm 1$	$2 \pm 1$
Muon+Electron Combined							
$t\bar{t} \rightarrow \ell\ell$	$587 \pm 8$	$346 \pm 6$	$120 \pm 4$	$42 \pm 2$	$16 \pm 1$	$7 \pm 1$	$4 \pm 1$
$t\bar{t} \rightarrow \ell + \text{jets \& single top } (1\ell)$	$95 \pm 3$	$67 \pm 3$	$15 \pm 1$	$6 \pm 1$	$2 \pm 1$	$1 \pm 1$	$1 \pm 0$
$W + \text{jets}$	$29 \pm 2$	$15 \pm 2$	$6 \pm 1$	$3 \pm 1$	$1 \pm 0$	$0 \pm 0$	$0 \pm 0$
Rare	$59 \pm 3$	$38 \pm 3$	$16 \pm 2$	$8 \pm 1$	$4 \pm 1$	$2 \pm 0$	$1 \pm 0$
Total	$770 \pm 10$	$466 \pm 7$	$157 \pm 4$	$59 \pm 3$	$22 \pm 2$	$10 \pm 1$	$6 \pm 1$

Table 24: MC yields in  $M_T$  tail region after full selection. The n-jets k-factors have been applied to the  $t\bar{t} \rightarrow \ell\ell$ . The uncertainties are statistical only. Note these values are only used for the rare backgrounds prediction.

## 10 Systematic Uncertainties on the Background

In this Section we discuss the systematic uncertainty on the BG prediction. This prediction is assembled from the event counts in the peak region of the transverse mass distribution as well as Monte Carlo with a number of correction factors, as described previously. The final uncertainty on the prediction is built up from the uncertainties in these individual components. The calculation is done for each signal region, for electrons and muons separately.

The choice to normalizing to the peak region of  $M_T$  has the advantage that some uncertainties, e.g., luminosity, cancel. It does however introduce complications because it couples some of the uncertainties in non-trivial ways. For example, the primary effect of an uncertainty on the rare MC cross-section is to introduce an uncertainty in the rare MC background estimate which comes entirely from MC. But this uncertainty also affects, for example, the  $t\bar{t} \rightarrow$  dilepton BG estimate because it changes the  $t\bar{t}$  normalization to the peak region (because some of the events in the peak region are from rare processes). These effects are carefully accounted for. Here we discuss the uncertainties one-by-one and comment on their impact on the overall result, at least to first order. Second order effects, such as the one described, are also included.

### 10.1 Statistical uncertainties on the event counts in the $M_T$ peak regions

These vary between 2% and 20%, depending on the signal region (different signal regions have different  $E_T^{\text{miss}}$  requirements, thus they also have different  $M_T$  regions used as control. Since the major backgrounds, eg,  $t\bar{t}$  are normalized to the peak regions, this fractional uncertainty is pretty much carried through all the way to the end. There is also an uncertainty from the finite MC event counts in the  $M_T$  peak regions. This is also included, but it is smaller.

Normalizing to the  $M_T$  peak has the distinct advantages that uncertainties on luminosity, cross-sections, trigger efficiency, lepton ID, cancel out. For the low statistics regions with high  $E_T^{\text{miss}}$  requirements, the price to pay in terms of event count is that statistical uncertainties start to become significant. In the future we may consider a different normalization strategy in the low statistics regions.

### 10.2 Uncertainty from the choice of $M_T$ peak region

This choice affects the scale factors of Table 23. If the  $M_T$  peak region is not well modelled, this would introduce an uncertainty.

We have tested this possibility by recalculating the post veto scale factors for a different choice of  $M_T$  peak region ( $40 < M_T < 100$  GeV instead of the default  $50 < M_T < 80$  GeV. This is shown in Table 25. The two results for the scale factors are very compatible. We do not take any systematic uncertainty for this possible effect.

### 10.3 Uncertainty on the Wjets cross-section and the rare MC cross-sections

These are taken as 50%, uncorrelated. The primary effect is to introduce a 50% uncertainty on the  $W +$  jets and rare BG background predictions, respectively. However they also have an effect on the other BGs via the  $M_T$  peak normalization in a way that tends to reduce the uncertainty. This is easy to understand: if the  $W$  cross-section is increased by 50%, then the  $W$  background goes up. But the number of  $M_T$  peak events attributed to  $t\bar{t}$  goes down, and since the  $t\bar{t}$  BG is scaled to the number of  $t\bar{t}$  events in the peak, the  $t\bar{t}$  BG goes down.

### 10.4 Scale factors for the tail-to-peak ratios for lepton + jets top and W events

These tail-to-peak ratios are described in Section 8. They are studied in CR1 and CR2. The studies are described in Sections 6.1 and 6.2), respectively, where we also give the uncertainty on the scale factors (see Tables 13 and 14, scale factors  $SFR_{\text{wjet}}$  and  $SFR_{\text{top}}$ ).

Sample	SRA	SRB	SRC	SRD	SRE	SRF	SRG
$50 \leq M_T \leq 80$							
$\mu$ pre-veto $M_T$ -SF	$1.02 \pm 0.02$	$0.95 \pm 0.03$	$0.90 \pm 0.05$	$0.98 \pm 0.08$	$0.97 \pm 0.13$	$0.85 \pm 0.18$	$0.92 \pm 0.31$
$\mu$ post-veto $M_T$ -SF	$1.00 \pm 0.02$	$0.95 \pm 0.03$	$0.91 \pm 0.05$	$1.00 \pm 0.09$	$0.99 \pm 0.13$	$0.85 \pm 0.18$	$0.96 \pm 0.31$
$\mu$ veto $M_T$ -SF	$0.98 \pm 0.01$	$0.99 \pm 0.01$	$1.01 \pm 0.02$	$1.02 \pm 0.04$	$1.02 \pm 0.06$	$1.00 \pm 0.09$	$1.04 \pm 0.11$
e pre-veto $M_T$ -SF	$0.95 \pm 0.02$	$0.95 \pm 0.03$	$0.94 \pm 0.06$	$0.85 \pm 0.09$	$0.84 \pm 0.13$	$1.05 \pm 0.23$	$1.04 \pm 0.33$
e post-veto $M_T$ -SF	$0.92 \pm 0.02$	$0.91 \pm 0.03$	$0.91 \pm 0.06$	$0.74 \pm 0.08$	$0.75 \pm 0.13$	$0.91 \pm 0.22$	$1.01 \pm 0.33$
e veto $M_T$ -SF	$0.97 \pm 0.01$	$0.96 \pm 0.02$	$0.97 \pm 0.03$	$0.87 \pm 0.05$	$0.89 \pm 0.08$	$0.86 \pm 0.11$	$0.97 \pm 0.14$
$40 \leq M_T \leq 100$							
$\mu$ pre-veto $M_T$ -SF	$1.02 \pm 0.01$	$0.97 \pm 0.02$	$0.91 \pm 0.05$	$0.95 \pm 0.06$	$0.97 \pm 0.10$	$0.80 \pm 0.14$	$0.74 \pm 0.22$
$\mu$ post-veto $M_T$ -SF	$1.00 \pm 0.01$	$0.96 \pm 0.02$	$0.90 \pm 0.04$	$0.98 \pm 0.07$	$1.00 \pm 0.11$	$0.80 \pm 0.15$	$0.81 \pm 0.24$
$\mu$ veto $M_T$ -SF	$0.98 \pm 0.01$	$0.99 \pm 0.01$	$0.99 \pm 0.02$	$1.03 \pm 0.03$	$1.03 \pm 0.05$	$1.01 \pm 0.08$	$1.09 \pm 0.09$
e pre-veto $M_T$ -SF	$0.97 \pm 0.01$	$0.93 \pm 0.02$	$0.94 \pm 0.04$	$0.81 \pm 0.06$	$0.86 \pm 0.10$	$0.95 \pm 0.17$	$1.06 \pm 0.26$
e post-veto $M_T$ -SF	$0.94 \pm 0.01$	$0.91 \pm 0.02$	$0.91 \pm 0.04$	$0.71 \pm 0.06$	$0.82 \pm 0.10$	$0.93 \pm 0.17$	$1.09 \pm 0.27$
e veto $M_T$ -SF	$0.97 \pm 0.01$	$0.98 \pm 0.01$	$0.97 \pm 0.02$	$0.88 \pm 0.04$	$0.95 \pm 0.06$	$0.98 \pm 0.08$	$1.03 \pm 0.09$

Table 25:  $M_T$  peak Data/MC scale factors. The pre-veto SFs are applied to the  $t\bar{t} \rightarrow \ell\ell$  sample, while the post-veto SFs are applied to the single lepton samples. The veto SF is shown for comparison across channels. The raw MC is used for backgrounds from rare processes. The uncertainties are statistical only.

## 10.5 Uncertainty on extra jet radiation for dilepton background

As discussed in Section 6.3.1, the jet distribution in  $t\bar{t} \rightarrow$  dilepton MC is rescaled by the factors  $K_3$  and  $K_4$  to make it agree with the data. The 3% uncertainties on  $K_3$  and  $K_4$  comes from data/MC statistics. This result directly in a 3% uncertainty on the dilepton background, which is by far the most important one.

## 10.6 Uncertainty from MC statistics

This affects mostly the  $t\bar{t} \rightarrow \ell\ell$  background estimate, which is taken from Monte Carlo with appropriate correction factors. This uncertainty is negligible in the low  $E_T^{\text{miss}}$  signal regions, and grows to about 15% in SRG.

## 10.7 Uncertainty on the $t\bar{t} \rightarrow \ell\ell$ Acceptance

The  $t\bar{t}$  background prediction is obtained from MC, with corrections derived from control samples in data. The uncertainty associated with the theoretical modeling of the  $t\bar{t}$  production and decay is estimated by comparing the background predictions obtained using alternative MC samples. It should be noted that the full analysis is performed with the alternative samples under consideration, including the derivation of the various data-to-MC scale factors. The variations considered are

- Top mass: The alternative values for the top mass differ from the central value by 5 GeV:  $m_{\text{top}} = 178.5$  GeV and  $m_{\text{top}} = 166.5$  GeV.
- Jet-parton matching scale: This corresponds to variations in the scale at which the Matrix Element partons from Madgraph are matched to Parton Shower partons from Pythia. The nominal value is  $x_q > 20$  GeV. The alternative values used are  $x_q > 10$  GeV and  $x_q > 40$  GeV.
- Renormalization and factorization scale: The alternative samples correspond to variations in the scale  $\times 2$  and  $\times 0.5$ . The nominal value for the scale used is  $Q^2 = m_{\text{top}}^2 + \sum_{\text{jets}} p_T^2$ .
- Alternative generators: Samples produced with different generators, Powheg (our default) and Madgraph.
- Modeling of taus: The alternative sample does not include Tauola and is otherwise identical to the Powheg sample. This effect was studied earlier using 7 TeV samples and found to be negligible.
- The PDF uncertainty is estimated following the PDF4LHC recommendations. The events are reweighted using alternative PDF sets for CT10 and MSTW2008 and the uncertainties for each

are derived using the alternative eigenvector variations and the “master equation”. In addition, the NNPDF2.1 set with 100 replicas. The central value is determined from the mean and the uncertainty is derived from the  $1\sigma$  range. The overall uncertainty is derived from the envelope of the alternative predictions and their uncertainties. This effect was studied earlier using 7 TeV samples and found to be negligible.

$\Delta/N$ [%]	Madgraph	Mass Up	Mass Down	Scale Up	Scale Down	Match Up	Match Down
SRA	2	2	5	12	7	0	2
SRB	6	0	6	5	12	5	6

Table 26: Relative difference in  $t\bar{t} \rightarrow \ell\ell$  predictions for alternative MC samples in the higher statistics regions SRA and SRB. These differences are based on the central values of the predictions. For a fuller picture of the situation, including statistical uncertainties, see Fig. 20.

In Fig. 20 we compare the alternate MC  $t\bar{t} \rightarrow \ell\ell$  background predictions for regions A through E. We can make the following observations based on this Figure.

- In the tighter signal regions we are running out of statistics.
- Within the limited statistics, there is no evidence that the situation changes as we go from signal region A to signal region E. Therefore, we assess a systematic based on the relatively high statistics test in signal region A, and apply the same systematic uncertainty to all other regions.
- In order to fully (as opposed as  $1\sigma$ ) cover the alternative MC variations in region A we would have to take a systematic uncertainty of  $\approx 10\%$ . This would be driven by the scale up/scale down variations, see Table 26.

Sample	K3	K4
Powheg	$1.01 \pm 0.03$	$0.93 \pm 0.04$
Madgraph	$1.01 \pm 0.04$	$0.92 \pm 0.04$
Mass Up	$1.00 \pm 0.04$	$0.92 \pm 0.04$
Mass Down	$1.06 \pm 0.04$	$0.99 \pm 0.05$
Scale Up	$1.14 \pm 0.04$	$1.23 \pm 0.06$
Scale Down	$0.89 \pm 0.03$	$0.74 \pm 0.03$
Match Up	$1.02 \pm 0.04$	$0.97 \pm 0.04$
Match Down	$1.02 \pm 0.04$	$0.91 \pm 0.04$

Table 27:  $E_T^{\text{miss}} > 100$  GeV: Data/MC scale factors used to account for differences in the fraction of events with additional hard jets from radiation in  $t\bar{t} \rightarrow \ell\ell$  events.

However, we have two pieces of information indicating that the scale up/scale down variations are inconsistent with the data. These are described below.

The first piece of information is that the jet multiplicity in the scale up/scale down sample is the most inconsistent with the data. This is shown in Table 27, where we tabulate the  $K_3$  and  $K_4$  factors of Section 6.3.1 for different  $t\bar{t}$  MC samples. The data/MC disagreement in the  $N_{jets}$  distribution for the scale up/scale down samples is also shown in Fig. 21 and 22. This should be compared with the equivalent  $N_{jets}$  plots for the default Powheg MC, see Fig. 14, which agrees much better with data.

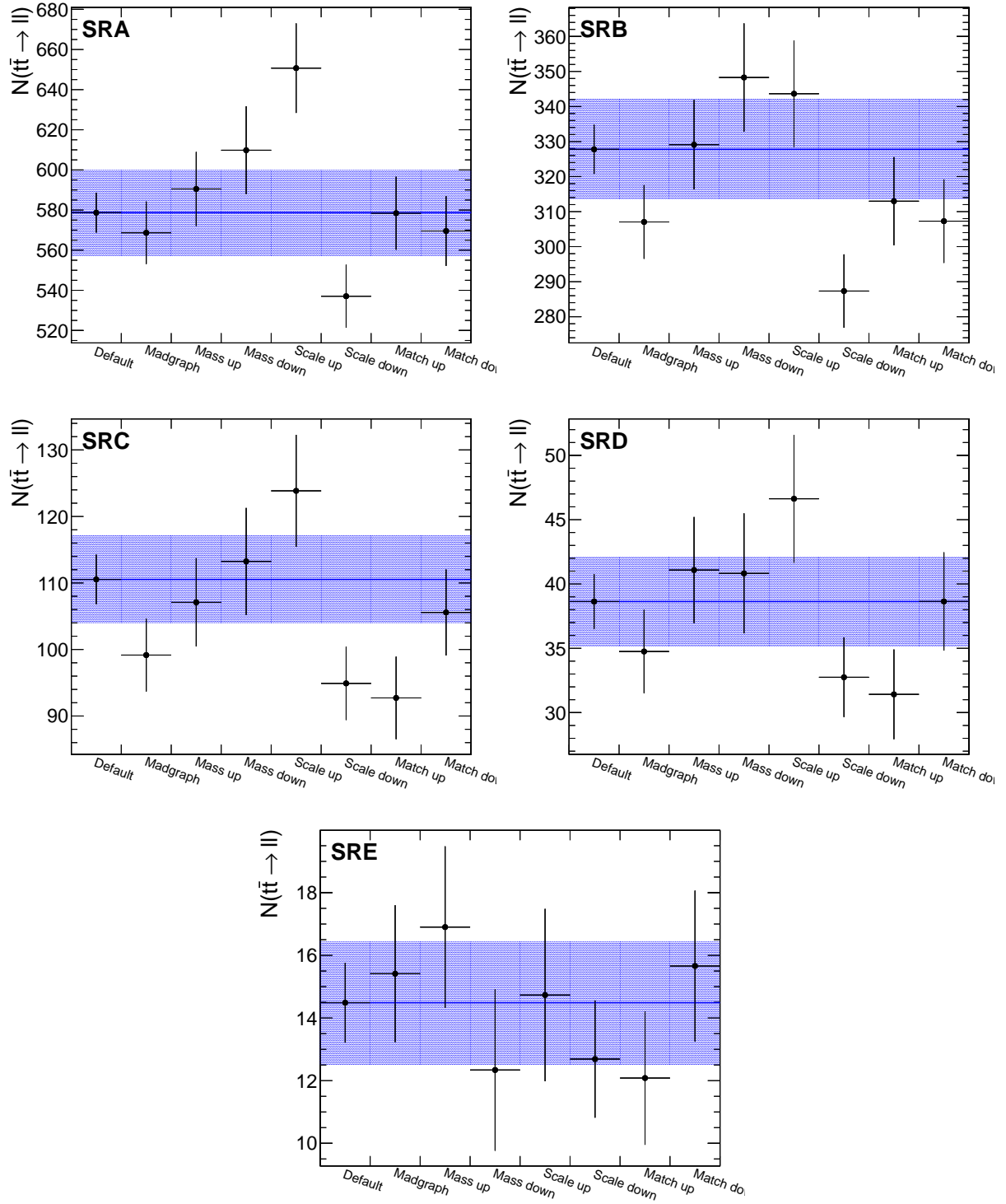


Figure 20: Comparison of the  $t\bar{t} \rightarrow \ell\ell$  central prediction with those using alternative MC samples. The blue band corresponds to the total statistical error for all data and MC samples. The alternative sample predictions are indicated by the datapoints. The uncertainties on the alternative predictions correspond to the uncorrelated statistical uncertainty from the size of the alternative sample only. Note the suppressed vertical scales.



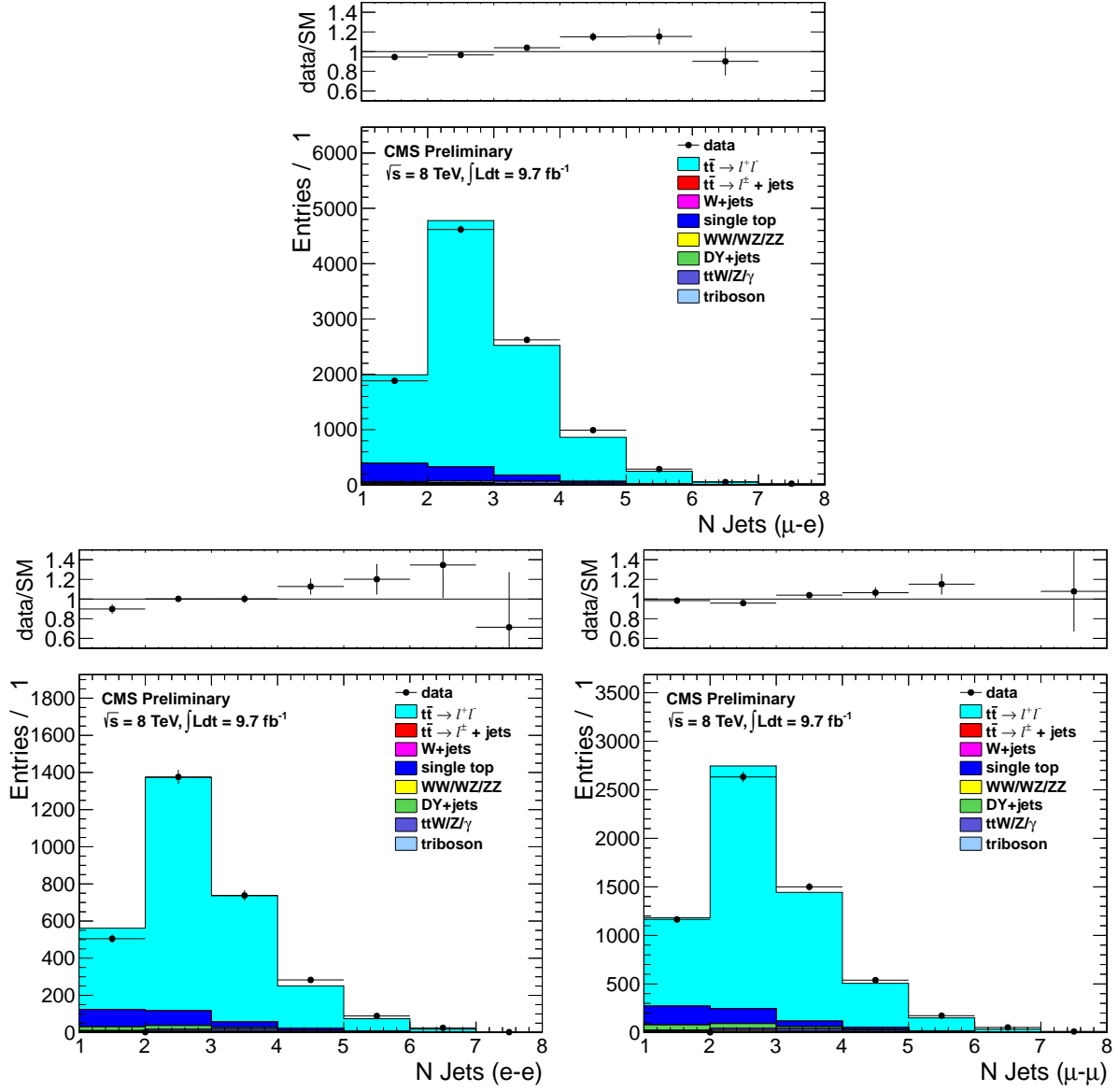


Figure 21: SCALE UP: Comparison of the jet multiplicity distribution in data and MC for dilepton events in the  $e\mu$  (top),  $e-e$  (bottom left) and  $\mu\mu$  (bottom right) channels.

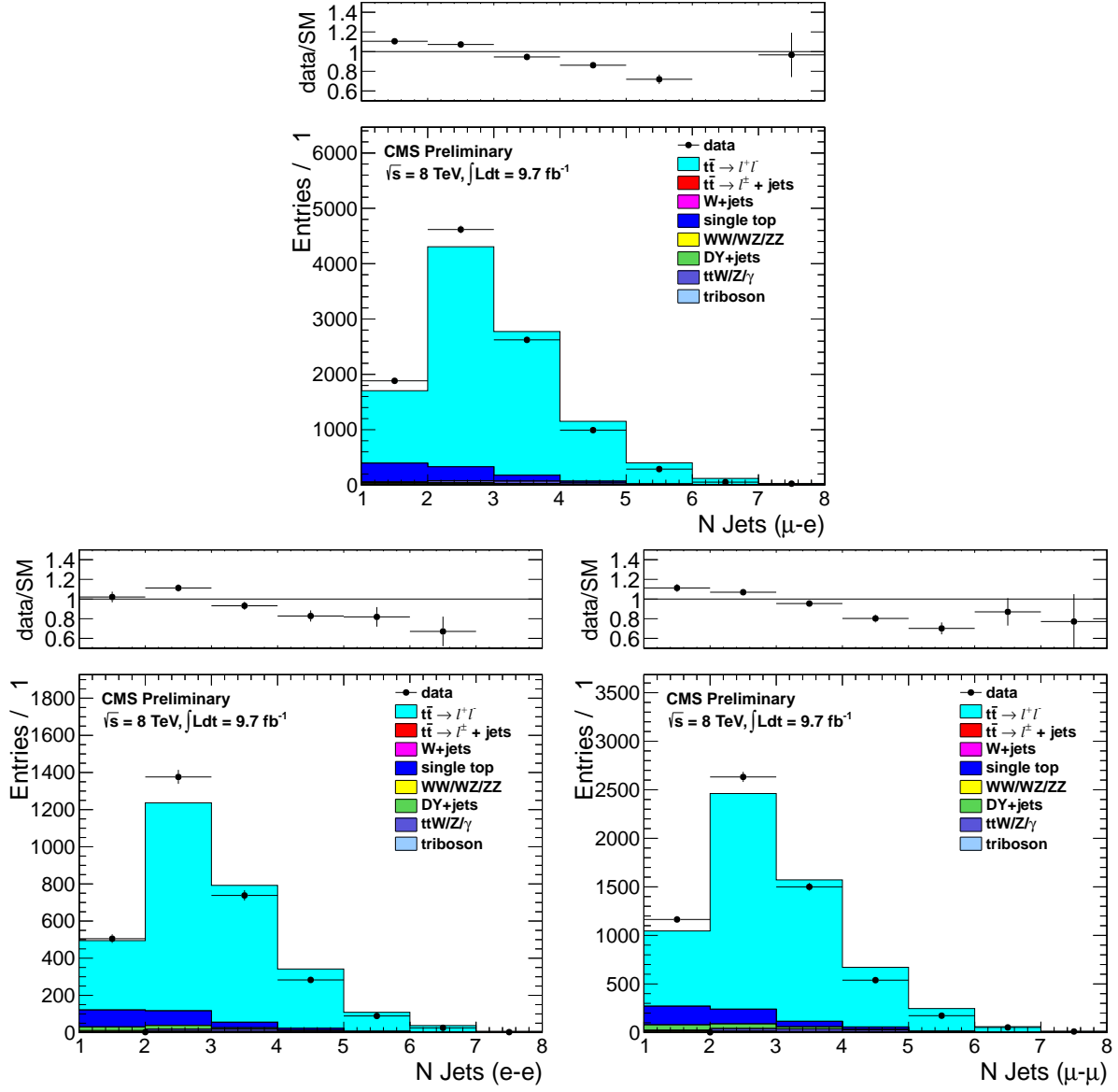


Figure 22: SCALE DOWN: Comparison of the jet multiplicity distribution in data and MC for dilepton events in the  $e\mu$  (top),  $e-e$  (bottom left) and  $\mu\mu$  (bottom right) channels.

The second piece of information is that we have performed closure tests in CR5 using the alternative MC samples. These are exactly the same tests as the one performed in Section 6.4 on the Powheg sample. As we argued previously, this is a very powerful test of the background calculation. The results of this test are summarized in Table 28. Concentrating on the relatively high statistics CR5A region, we see for all  $t\bar{t}$  MC samples except scale up/scale down we obtain closure within  $1\sigma$ . The scale up/scale down tests closes worse, only within  $2\sigma$ . This again is evidence that the scale up/scale down variations are in disagreement with the data.

Sample	CR5PRESEL	CR5A	CR5B	CR5C	CR5D	CR5E
POWHEG						
$\mu$ Data/MC SF	$1.05 \pm 0.05$	$1.04 \pm 0.06$	$1.08 \pm 0.09$	$1.17 \pm 0.17$	$0.64 \pm 0.20$	$0.54 \pm 0.29$
$e$ Data/MC SF	$1.06 \pm 0.06$	$1.04 \pm 0.07$	$0.93 \pm 0.09$	$0.89 \pm 0.16$	$0.86 \pm 0.25$	$0.52 \pm 0.28$
$\mu+e$ Data/MC SF	$1.05 \pm 0.04$	$1.04 \pm 0.05$	$1.01 \pm 0.07$	$1.04 \pm 0.12$	$0.74 \pm 0.16$	$0.53 \pm 0.20$
MADGRAPH						
$\mu$ Data/MC SF	$1.05 \pm 0.05$	$1.06 \pm 0.07$	$1.08 \pm 0.10$	$1.21 \pm 0.19$	$0.64 \pm 0.21$	$0.43 \pm 0.24$
$e$ Data/MC SF	$1.06 \pm 0.06$	$1.04 \pm 0.08$	$0.97 \pm 0.10$	$0.97 \pm 0.18$	$1.10 \pm 0.34$	$0.68 \pm 0.38$
$\mu+e$ Data/MC SF	$1.06 \pm 0.04$	$1.05 \pm 0.05$	$1.03 \pm 0.07$	$1.10 \pm 0.13$	$0.83 \pm 0.18$	$0.53 \pm 0.21$
MASS UP						
$\mu$ Data/MC SF	$1.04 \pm 0.06$	$1.04 \pm 0.07$	$1.07 \pm 0.10$	$1.20 \pm 0.19$	$0.57 \pm 0.18$	$0.56 \pm 0.31$
$e$ Data/MC SF	$1.04 \pm 0.06$	$1.05 \pm 0.08$	$1.01 \pm 0.11$	$1.12 \pm 0.22$	$1.02 \pm 0.33$	$0.61 \pm 0.34$
$\mu+e$ Data/MC SF	$1.04 \pm 0.04$	$1.04 \pm 0.05$	$1.04 \pm 0.07$	$1.17 \pm 0.15$	$0.74 \pm 0.17$	$0.58 \pm 0.23$
MASS DOWN						
$\mu$ Data/MC SF	$1.02 \pm 0.06$	$1.02 \pm 0.07$	$1.04 \pm 0.10$	$1.25 \pm 0.21$	$0.82 \pm 0.28$	$0.94 \pm 0.56$
$e$ Data/MC SF	$1.06 \pm 0.06$	$1.02 \pm 0.08$	$0.95 \pm 0.11$	$0.91 \pm 0.18$	$1.07 \pm 0.35$	$0.59 \pm 0.33$
$\mu+e$ Data/MC SF	$1.04 \pm 0.04$	$1.02 \pm 0.05$	$1.00 \pm 0.07$	$1.09 \pm 0.14$	$0.94 \pm 0.22$	$0.72 \pm 0.30$
SCALE UP						
$\mu$ Data/MC SF	$0.94 \pm 0.05$	$0.94 \pm 0.07$	$0.99 \pm 0.10$	$1.24 \pm 0.21$	$0.71 \pm 0.24$	$0.69 \pm 0.39$
$e$ Data/MC SF	$0.94 \pm 0.06$	$0.89 \pm 0.07$	$0.81 \pm 0.09$	$0.77 \pm 0.15$	$0.84 \pm 0.27$	$0.49 \pm 0.28$
$\mu+e$ Data/MC SF	$0.94 \pm 0.04$	$0.91 \pm 0.05$	$0.91 \pm 0.07$	$1.00 \pm 0.13$	$0.77 \pm 0.18$	$0.57 \pm 0.23$
SCALE DOWN						
$\mu$ Data/MC SF	$1.11 \pm 0.06$	$1.10 \pm 0.07$	$1.24 \pm 0.12$	$1.26 \pm 0.20$	$0.64 \pm 0.21$	$0.70 \pm 0.39$
$e$ Data/MC SF	$1.16 \pm 0.07$	$1.20 \pm 0.09$	$1.00 \pm 0.11$	$1.02 \pm 0.19$	$1.02 \pm 0.32$	$0.53 \pm 0.29$
$\mu+e$ Data/MC SF	$1.13 \pm 0.04$	$1.14 \pm 0.06$	$1.13 \pm 0.08$	$1.15 \pm 0.14$	$0.80 \pm 0.18$	$0.60 \pm 0.23$
MATCH UP						
$\mu$ Data/MC SF	$1.06 \pm 0.06$	$1.06 \pm 0.07$	$1.20 \pm 0.11$	$1.42 \pm 0.23$	$0.70 \pm 0.23$	$0.63 \pm 0.35$
$e$ Data/MC SF	$1.06 \pm 0.06$	$1.04 \pm 0.08$	$0.97 \pm 0.11$	$0.93 \pm 0.18$	$1.25 \pm 0.41$	$0.63 \pm 0.36$
$\mu+e$ Data/MC SF	$1.06 \pm 0.04$	$1.06 \pm 0.05$	$1.09 \pm 0.08$	$1.18 \pm 0.15$	$0.92 \pm 0.21$	$0.63 \pm 0.25$
MATCH DOWN						
$\mu$ Data/MC SF	$1.08 \pm 0.06$	$1.06 \pm 0.07$	$1.14 \pm 0.11$	$1.17 \pm 0.19$	$0.59 \pm 0.19$	$0.45 \pm 0.25$
$e$ Data/MC SF	$1.05 \pm 0.06$	$0.99 \pm 0.08$	$0.86 \pm 0.09$	$0.78 \pm 0.15$	$0.79 \pm 0.25$	$0.50 \pm 0.28$
$\mu+e$ Data/MC SF	$1.07 \pm 0.04$	$1.03 \pm 0.05$	$1.00 \pm 0.07$	$0.98 \pm 0.12$	$0.68 \pm 0.15$	$0.48 \pm 0.18$

Table 28: Ratio of yields in  $M_T$  tail comparing the MC prediction (after applying SFs) to data. The uncertainties are statistical only.

Based on the two observations above, we argue that the MC scale up/scale down variations are too extreme. We feel that a reasonable choice would be to take one-half of the scale up/scale down variations in our MC. This factor of  $1/2$  would then bring the discrepancy in the closure test of Table 28 for the scale up/scale down variations from about  $2\sigma$  to about  $1\sigma$ .

Then, going back to Table 26, and reducing the scale up/scale down variations by a factor 2, we can see that a systematic uncertainty of 6% would fully cover all of the variations from different MC samples in SRA and SRB. **Thus, we take a 6% systematic uncertainty, constant as a function of signal region, as the systematic due to alternative MC models.** Note that this 6% is also consistent with the level at which we are able to test the closure of the method in CR5 for the high statistics regions (Table 28).

## 10.8 Uncertainty from the isolated track veto

This is the uncertainty associated with how well the isolated track veto performance is modeled by the Monte Carlo. This uncertainty only applies to the fraction of dilepton BG events that have a second  $e/\mu$  or a one prong  $\tau \rightarrow h$ , with  $P_T > 10$  GeV in  $|\eta| < 2.4$ . This fraction is about 1/3, see Table 29. The uncertainty for these events is 6% and is obtained from tag-and-probe studies, see Section 10.8.1.

Sample	SRA	SRB	SRC	SRD	SRE	SRF	SRG
$\mu$ Frac. $t\bar{t} \rightarrow \ell\ell$ with true iso. trk.	$0.32 \pm 0.03$	$0.30 \pm 0.03$	$0.32 \pm 0.06$	$0.34 \pm 0.10$	$0.35 \pm 0.16$	$0.40 \pm 0.24$	$0.50 \pm 0.32$
$e$ Frac. $t\bar{t} \rightarrow \ell\ell$ with true iso. trk.	$0.32 \pm 0.03$	$0.31 \pm 0.04$	$0.33 \pm 0.06$	$0.38 \pm 0.11$	$0.38 \pm 0.19$	$0.60 \pm 0.31$	$0.61 \pm 0.45$

Table 29: Fraction of  $t\bar{t} \rightarrow \ell\ell$  events with a true isolated track.

### 10.8.1 Isolated Track Veto: Tag and Probe Studies

In this section we compare the performance of the isolated track veto in data and MC using tag-and-probe studies with samples of  $Z \rightarrow ee$  and  $Z \rightarrow \mu\mu$ . The purpose of these studies is to demonstrate that the efficiency to satisfy the isolated track veto requirements is well-reproduced in the MC, since if this were not the case we would need to apply a data-to-MC scale factor in order to correctly predict the  $t\bar{t} \rightarrow \ell\ell$  background.

This study addresses possible data vs. MC discrepancies for the **efficiency** to identify (and reject) events with a second **genuine** lepton ( $e$ ,  $\mu$ , or  $\tau \rightarrow 1$ -prong). It does not address possible data vs. MC discrepancies in the fake rate for rejecting events without a second genuine lepton; this is handled separately in the top normalization procedure by scaling the  $t\bar{t} \rightarrow \ell + \text{jets}$  contribution to match the data in the  $M_T$  peak after applying the isolated track veto.

Furthermore, we test the data and MC isolated track veto efficiencies for electrons and muons since we are using a Z tag-and-probe technique, but we do not directly test the performance for hadronic tracks from  $\tau$  decays. The performance for hadronic  $\tau$  decay products may differ from that of electrons and muons for two reasons. First, the  $\tau$  may decay to a hadronic track plus one or two  $\pi^0$ 's, which may decay to  $\gamma\gamma$  followed by a photon conversion. As shown in Figure 28, the isolation distribution for charged tracks from  $\tau$  decays that are not produced in association with  $\pi^0$ 's are consistent with that from  $e$ 's and  $\mu$ 's. Since events from single prong  $\tau$  decays produced in association with  $\pi^0$ 's comprise a small fraction of the total sample, and since the kinematics of  $\tau$ ,  $\pi^0$  and  $\gamma \rightarrow e^+e^-$  decays are well-understood, we currently demonstrate that the isolation is well-reproduced for electrons and muons only. Second, hadronic tracks may undergo nuclear interactions and hence their tracks may not be reconstructed. As discussed above, independent studies show that the MC reproduces the hadronic tracking efficiency within 4%, leading to a total background uncertainty of less than 0.5% (after taking into account the fraction of the total background due to hadronic  $\tau$  decays with  $p_T > 10$  GeV tracks), and we hence regard this effect as negligible.

The tag-and-probe studies are performed in the full data sample, and compared with the DYJets mad-graph sample. All events must contain a tag-probe pair (details below) with opposite-sign and satisfying the Z mass requirement 76–106 GeV. We compare the distributions of absolute track isolation for probe electrons/muons in data vs. MC. The contributions to this isolation sum are from ambient energy in the event from underlying event, pile-up and jet activity, and hence do not depend on the  $p_T$  of the probe lepton. We therefore restrict the probe  $p_T$  to be  $> 30$  GeV in order to suppress fake backgrounds with steeply-falling  $p_T$  spectra. To suppress non-Z backgrounds (in particular  $t\bar{t}$ ) we require  $E_T^{\text{miss}} < 30$  GeV and 0 b-tagged events. The specific criteria for tags and probes for electrons and muons are:

- Electrons

- Tag criteria

- \* Electron passes full analysis ID/iso selection
- \*  $p_T > 30$  GeV,  $|\eta| < 2.1$
- \* Matched to the single electron trigger HLT\_Ele27\_WP80\_v\*

- Probe criteria

595           \* Electron passes full analysis ID selection  
 596           \*  $p_T > 30$  GeV  
 597   • Muons  
 598       – Tag criteria  
 599           \* Muon passes full analysis ID/iso selection  
 600           \*  $p_T > 30$  GeV,  $|\eta| < 2.1$   
 601           \* Matched to 1 of the 2 single muon triggers  
 602               · HLT\_IsoMu30\_v\*  
 603               · HLT\_IsoMu30\_eta2p1\_v\*  
 604       – Probe criteria  
 605           \* Muon passes full analysis ID selection  
 606           \*  $p_T > 30$  GeV

607   The absolute track isolation distributions for passing probes are displayed in Fig. 23. In general we observe  
 608   good agreement between data and MC. To be more quantitative, we compare the data vs. MC efficiencies  
 609   to satisfy absolute track isolation requirements varying from  $> 1$  GeV to  $> 5$  GeV, as summarized in  
 610   Table 30. In the  $\geq 0$  and  $\geq 1$  jet bins where the efficiencies can be tested with statistical precision, the  
 611   data and MC efficiencies agree within 6%, and we apply this as a systematic uncertainty on the isolated  
 612   track veto efficiency. For the higher jet multiplicity bins the statistical precision decreases, but we do not  
 613   observe any evidence for a data vs. MC discrepancy in the isolated track veto efficiency.

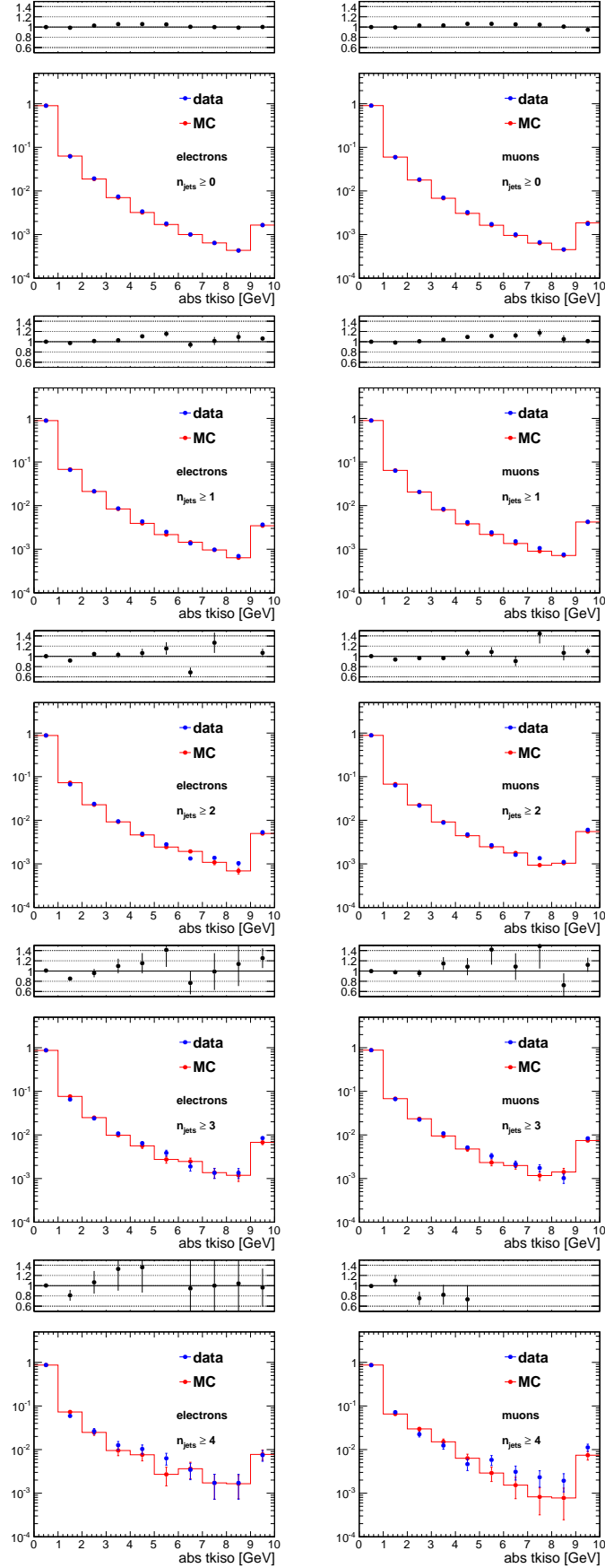


Figure 23: Comparison of the absolute track isolation in data vs. MC for electrons (left) and muons (right) for events with the  $N_{\text{jets}}$  requirement varied from  $N_{\text{jets}} \geq 0$  to  $N_{\text{jets}} \geq 4$ .

e + $\geq 0$ jets	> 1 GeV	> 2 GeV	> 3 GeV	> 4 GeV	> 5 GeV
data	$0.098 \pm 0.0002$	$0.036 \pm 0.0001$	$0.016 \pm 0.0001$	$0.009 \pm 0.0001$	$0.006 \pm 0.0000$
mc	$0.097 \pm 0.0002$	$0.034 \pm 0.0001$	$0.016 \pm 0.0001$	$0.009 \pm 0.0001$	$0.005 \pm 0.0000$
data/mc	$1.00 \pm 0.00$	$1.04 \pm 0.00$	$1.04 \pm 0.01$	$1.03 \pm 0.01$	$1.02 \pm 0.01$
$\mu$ + $\geq 0$ jets	> 1 GeV	> 2 GeV	> 3 GeV	> 4 GeV	> 5 GeV
data	$0.094 \pm 0.0001$	$0.034 \pm 0.0001$	$0.016 \pm 0.0001$	$0.009 \pm 0.0000$	$0.006 \pm 0.0000$
mc	$0.093 \pm 0.0001$	$0.033 \pm 0.0001$	$0.015 \pm 0.0001$	$0.009 \pm 0.0000$	$0.006 \pm 0.0000$
data/mc	$1.01 \pm 0.00$	$1.03 \pm 0.00$	$1.03 \pm 0.01$	$1.03 \pm 0.01$	$1.02 \pm 0.01$
e + $\geq 1$ jets	> 1 GeV	> 2 GeV	> 3 GeV	> 4 GeV	> 5 GeV
data	$0.110 \pm 0.0005$	$0.044 \pm 0.0003$	$0.022 \pm 0.0002$	$0.014 \pm 0.0002$	$0.009 \pm 0.0002$
mc	$0.110 \pm 0.0005$	$0.042 \pm 0.0003$	$0.021 \pm 0.0002$	$0.013 \pm 0.0002$	$0.009 \pm 0.0001$
data/mc	$1.00 \pm 0.01$	$1.04 \pm 0.01$	$1.06 \pm 0.02$	$1.08 \pm 0.02$	$1.06 \pm 0.03$
$\mu$ + $\geq 1$ jets	> 1 GeV	> 2 GeV	> 3 GeV	> 4 GeV	> 5 GeV
data	$0.106 \pm 0.0004$	$0.043 \pm 0.0003$	$0.023 \pm 0.0002$	$0.014 \pm 0.0002$	$0.010 \pm 0.0001$
mc	$0.106 \pm 0.0004$	$0.042 \pm 0.0003$	$0.021 \pm 0.0002$	$0.013 \pm 0.0002$	$0.009 \pm 0.0001$
data/mc	$1.00 \pm 0.01$	$1.04 \pm 0.01$	$1.06 \pm 0.01$	$1.08 \pm 0.02$	$1.07 \pm 0.02$
e + $\geq 2$ jets	> 1 GeV	> 2 GeV	> 3 GeV	> 4 GeV	> 5 GeV
data	$0.117 \pm 0.0012$	$0.050 \pm 0.0008$	$0.026 \pm 0.0006$	$0.017 \pm 0.0005$	$0.012 \pm 0.0004$
mc	$0.120 \pm 0.0012$	$0.048 \pm 0.0008$	$0.025 \pm 0.0006$	$0.016 \pm 0.0005$	$0.011 \pm 0.0004$
data/mc	$0.97 \pm 0.01$	$1.05 \pm 0.02$	$1.05 \pm 0.03$	$1.07 \pm 0.04$	$1.07 \pm 0.05$
$\mu$ + $\geq 2$ jets	> 1 GeV	> 2 GeV	> 3 GeV	> 4 GeV	> 5 GeV
data	$0.111 \pm 0.0010$	$0.048 \pm 0.0007$	$0.026 \pm 0.0005$	$0.018 \pm 0.0004$	$0.013 \pm 0.0004$
mc	$0.115 \pm 0.0010$	$0.048 \pm 0.0006$	$0.025 \pm 0.0005$	$0.016 \pm 0.0004$	$0.012 \pm 0.0003$
data/mc	$0.97 \pm 0.01$	$1.01 \pm 0.02$	$1.04 \pm 0.03$	$1.09 \pm 0.04$	$1.09 \pm 0.04$
e + $\geq 3$ jets	> 1 GeV	> 2 GeV	> 3 GeV	> 4 GeV	> 5 GeV
data	$0.123 \pm 0.0031$	$0.058 \pm 0.0022$	$0.034 \pm 0.0017$	$0.023 \pm 0.0014$	$0.017 \pm 0.0012$
mc	$0.131 \pm 0.0030$	$0.055 \pm 0.0020$	$0.030 \pm 0.0015$	$0.020 \pm 0.0013$	$0.015 \pm 0.0011$
data/mc	$0.94 \pm 0.03$	$1.06 \pm 0.06$	$1.14 \pm 0.08$	$1.16 \pm 0.10$	$1.17 \pm 0.12$
$\mu$ + $\geq 3$ jets	> 1 GeV	> 2 GeV	> 3 GeV	> 4 GeV	> 5 GeV
data	$0.121 \pm 0.0025$	$0.055 \pm 0.0018$	$0.033 \pm 0.0014$	$0.022 \pm 0.0011$	$0.017 \pm 0.0010$
mc	$0.120 \pm 0.0024$	$0.052 \pm 0.0016$	$0.029 \pm 0.0012$	$0.019 \pm 0.0010$	$0.014 \pm 0.0009$
data/mc	$1.01 \pm 0.03$	$1.06 \pm 0.05$	$1.14 \pm 0.07$	$1.14 \pm 0.08$	$1.16 \pm 0.10$
e + $\geq 4$ jets	> 1 GeV	> 2 GeV	> 3 GeV	> 4 GeV	> 5 GeV
data	$0.129 \pm 0.0080$	$0.070 \pm 0.0061$	$0.044 \pm 0.0049$	$0.031 \pm 0.0042$	$0.021 \pm 0.0034$
mc	$0.132 \pm 0.0075$	$0.059 \pm 0.0053$	$0.035 \pm 0.0041$	$0.025 \pm 0.0035$	$0.017 \pm 0.0029$
data/mc	$0.98 \pm 0.08$	$1.18 \pm 0.15$	$1.26 \pm 0.20$	$1.24 \pm 0.24$	$1.18 \pm 0.28$
$\mu$ + $\geq 4$ jets	> 1 GeV	> 2 GeV	> 3 GeV	> 4 GeV	> 5 GeV
data	$0.136 \pm 0.0067$	$0.064 \pm 0.0048$	$0.041 \pm 0.0039$	$0.029 \pm 0.0033$	$0.024 \pm 0.0030$
mc	$0.130 \pm 0.0063$	$0.065 \pm 0.0046$	$0.035 \pm 0.0034$	$0.020 \pm 0.0026$	$0.013 \pm 0.0022$
data/mc	$1.04 \pm 0.07$	$0.99 \pm 0.10$	$1.19 \pm 0.16$	$1.47 \pm 0.25$	$1.81 \pm 0.37$

Table 30: Comparison of the data vs. MC efficiencies to satisfy the indicated requirements on the absolute track isolation, and the ratio of these two efficiencies. Results are indicated separately for electrons and muons and for various jet multiplicity requirements.

# 11 Results

The results of the search, still blinded are shown in Table 31. The  $M_T$  distributions, still blinded, for increasing values of  $E_T^{\text{miss}}$  are shown in Fig 24,25,26.

Sample	SRA	SRB	SRC	SRD	SRE	SRF	SRG
Muon							
$t\bar{t} \rightarrow \ell\ell$	$330.6 \pm 24.5$	$183.4 \pm 14.7$	$59.5 \pm 5.8$	$22.5 \pm 2.9$	$9.0 \pm 1.7$	$3.7 \pm 1.0$	$2.2 \pm 0.9$
$t\bar{t} \rightarrow \ell + \text{jets \& single top } (1\ell)$	$92.8 \pm 27.5$	$41.0 \pm 8.6$	$11.5 \pm 3.5$	$7.7 \pm 3.4$	$0.7 \pm 0.6$	$0.3 \pm 0.2$	$0.2 \pm 0.2$
$W + \text{jets}$	$19.2 \pm 4.5$	$10.0 \pm 2.2$	$3.1 \pm 1.0$	$1.2 \pm 0.6$	$0.6 \pm 0.4$	$0.4 \pm 0.3$	$0.2 \pm 0.2$
Rare	$33.2 \pm 16.6$	$22.7 \pm 11.4$	$9.0 \pm 4.5$	$4.8 \pm 2.4$	$2.9 \pm 1.5$	$1.2 \pm 0.6$	$1.0 \pm 0.5$
Total	$475.8 \pm 39.3$	$257.2 \pm 19.2$	$83.2 \pm 7.9$	$36.2 \pm 5.1$	$13.3 \pm 2.3$	$5.5 \pm 1.2$	$3.6 \pm 1.0$
Data	?	?	?	?	?	?	?
Electron							
$t\bar{t} \rightarrow \ell\ell$	$248.1 \pm 18.8$	$144.4 \pm 11.9$	$51.1 \pm 5.3$	$16.2 \pm 2.4$	$5.5 \pm 1.2$	$2.5 \pm 0.8$	$1.3 \pm 0.5$
$t\bar{t} \rightarrow \ell + \text{jets \& single top } (1\ell)$	$68.0 \pm 20.2$	$31.2 \pm 6.6$	$9.3 \pm 2.8$	$4.9 \pm 2.1$	$0.5 \pm 0.4$	$0.2 \pm 0.2$	$0.2 \pm 0.2$
$W + \text{jets}$	$14.3 \pm 3.3$	$7.5 \pm 1.7$	$2.4 \pm 0.8$	$0.8 \pm 0.4$	$0.4 \pm 0.3$	$0.3 \pm 0.2$	$0.1 \pm 0.2$
Rare	$25.8 \pm 12.9$	$15.8 \pm 7.9$	$7.1 \pm 3.6$	$2.9 \pm 1.5$	$0.7 \pm 0.4$	$0.3 \pm 0.2$	$0.1 \pm 0.1$
Total	$356.2 \pm 29.6$	$198.9 \pm 15.1$	$69.9 \pm 6.7$	$24.7 \pm 3.5$	$7.1 \pm 1.3$	$3.4 \pm 0.9$	$1.7 \pm 0.6$
Data	?	?	?	?	?	?	?
Muon+Electron Combined							
$t\bar{t} \rightarrow \ell\ell$	$578.7 \pm 42.7$	$327.8 \pm 25.5$	$110.6 \pm 10.1$	$38.7 \pm 4.7$	$14.5 \pm 2.4$	$6.2 \pm 1.5$	$3.5 \pm 1.2$
$t\bar{t} \rightarrow \ell + \text{jets \& single top } (1\ell)$	$160.8 \pm 47.7$	$72.2 \pm 15.1$	$20.8 \pm 6.3$	$12.6 \pm 5.4$	$1.2 \pm 0.9$	$0.6 \pm 0.4$	$0.4 \pm 0.3$
$W + \text{jets}$	$33.5 \pm 8.0$	$17.5 \pm 4.1$	$5.5 \pm 1.9$	$2.0 \pm 1.2$	$1.0 \pm 0.7$	$0.7 \pm 0.5$	$0.3 \pm 0.4$
Rare	$59.0 \pm 29.5$	$38.5 \pm 19.3$	$16.1 \pm 8.1$	$7.7 \pm 3.9$	$3.6 \pm 1.8$	$1.5 \pm 0.8$	$1.1 \pm 0.6$
Total	$832.0 \pm 68.5$	$456.1 \pm 33.5$	$153.0 \pm 13.8$	$60.9 \pm 8.1$	$20.3 \pm 3.2$	$8.9 \pm 1.8$	$5.3 \pm 1.4$
Data	?	?	?	?	?	?	?

Table 31: The result of the search.



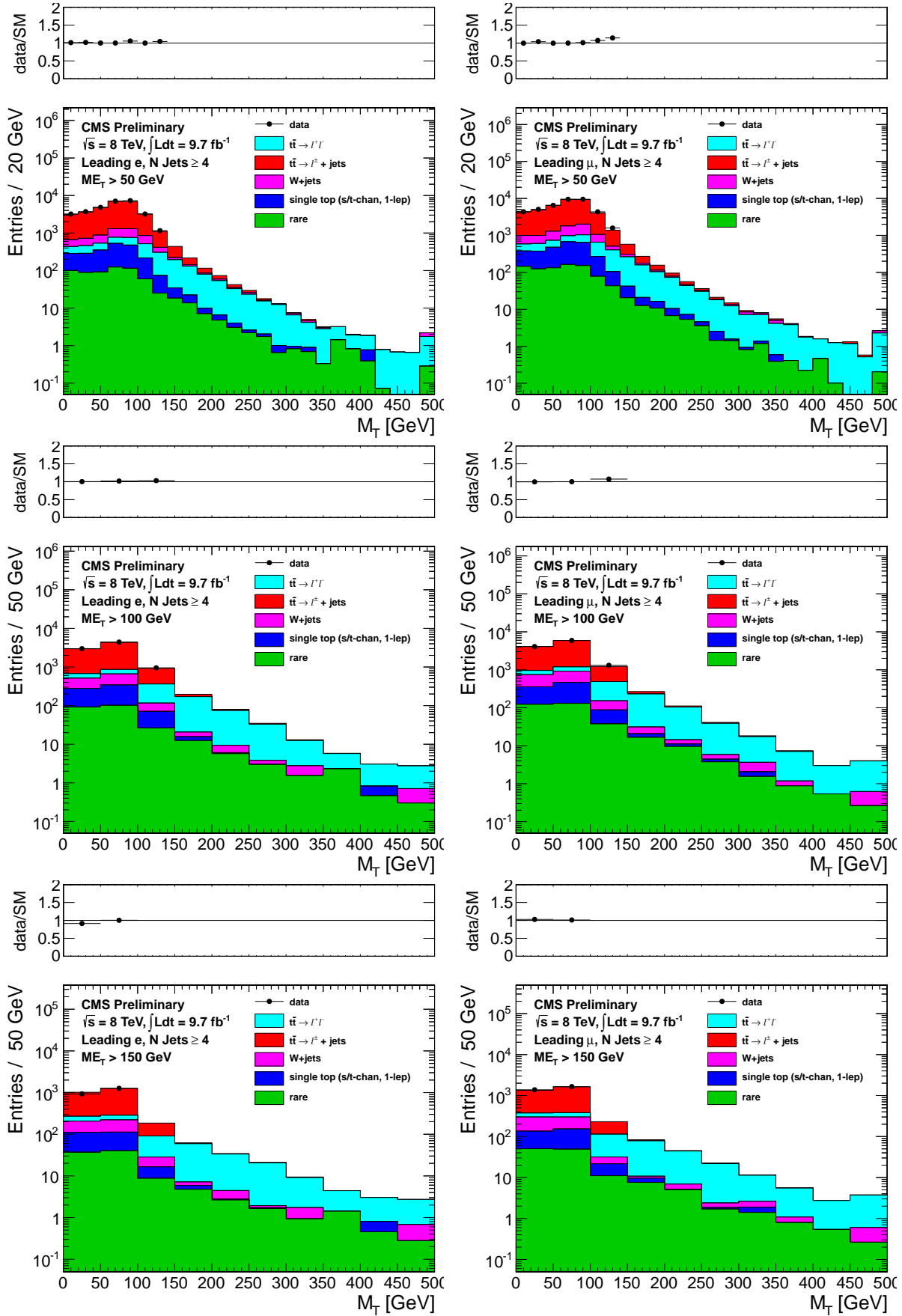


Figure 24:  $M_T$  in the data compared to SM Monte Carlo, for increasing values of  $E_T^{\text{miss}}$ . Note that the MC tails have not been rescaled at this point.

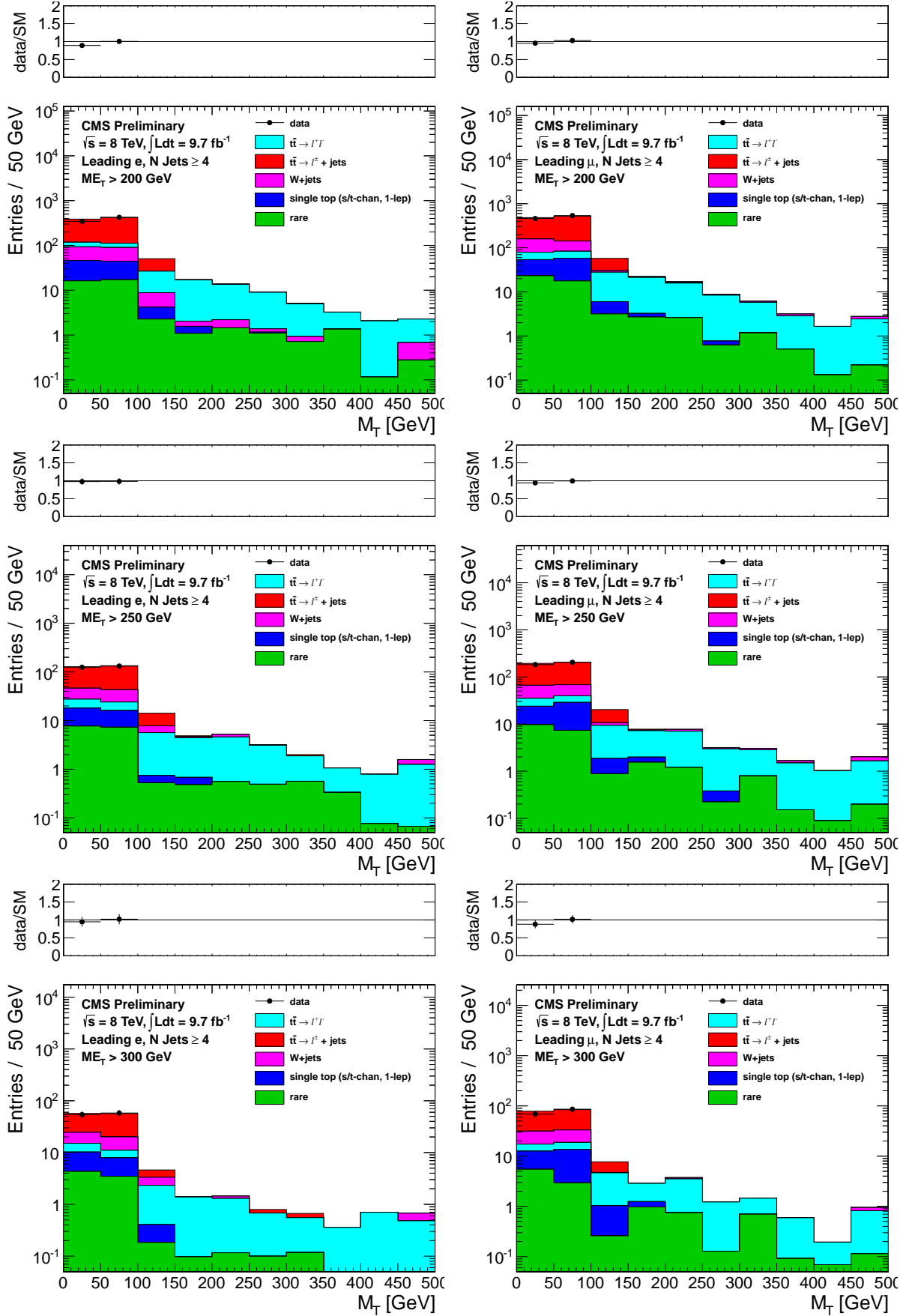


Figure 25:  $M_T$  in the data compared to SM Monte Carlo, for increasing values of  $E_T^{\text{miss}}$ . Note that the MC tails have not been rescaled at this point.

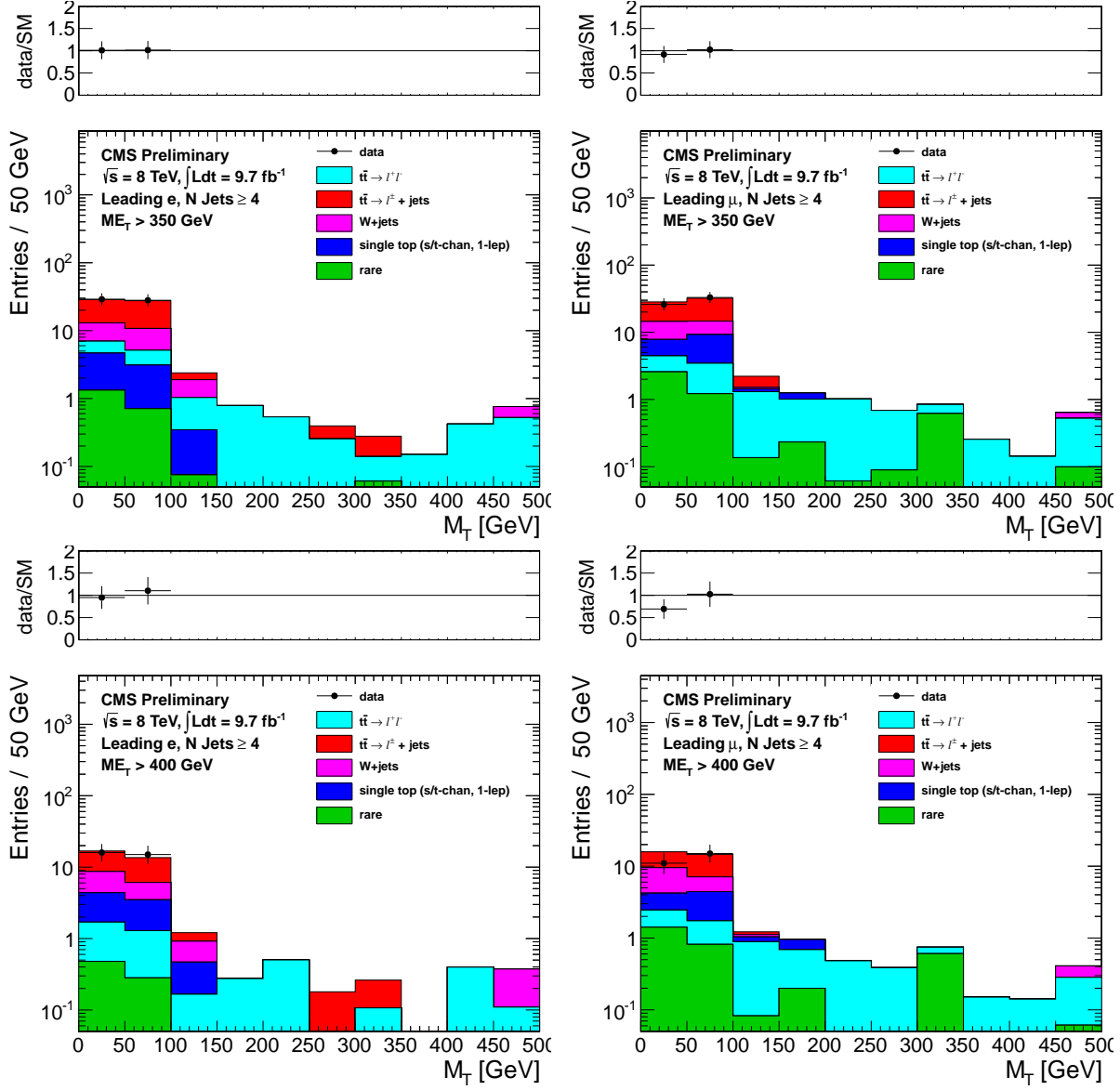


Figure 26:  $M_T$  in the data compared to SM Monte Carlo, for increasing values of  $E_T^{\text{miss}}$ . Note that the MC tails have not been rescaled at this point.



## References

- [1] <https://twiki.cern.ch/twiki/bin/view/LHCPhysics/SUSYCrossSections8TeVstopsbottom>
- [2] T. Plehn *et al.*, JHEP 1208(2012) 091.
- [3] These are measured by the Florida group in the context of the same sign and ewk-ino analyses.

## A Performance of the Isolation Requirement

The last requirement used in the analysis is an isolated track veto. This selection criteria rejects events containing a track of  $p_T > 10$  GeV with relative track isolation  $\sum p_T/p_T(trk)$  in a cone of size  $R = 0.3 < 0.1$ . It may be noted that only tracks consistent with the vertex with highest  $\sum p_T^2$  are considered in order to reduce the impact of spurious tracks, for example from pileup interactions. This requirement has very good performance. Figure 27 shows the efficiency for rejecting dilepton events compared to the efficiency for selecting single lepton events for various cone sizes and cut values. The chosen working point provides a signal efficiency of  $\epsilon(sig) = 92\%$  for a background rejection of  $\epsilon(bkg) = 53\%$  in MC. With "signal" ("background") we are referring to  $t\bar{t} \rightarrow \ell + \text{jets}$  ( $t\bar{t} \rightarrow \ell\ell$ ).

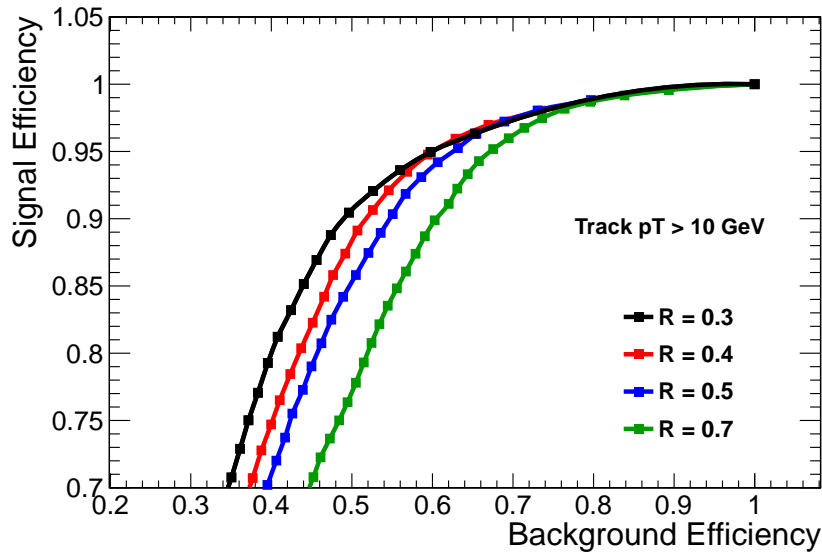


Figure 27: Comparison of the performance in terms of signal (single lepton events) efficiency and background (dilepton events) rejection for various cone sizes and cut values. The current isolation requirement uses a cone of size  $\Delta R = 0.3$  and a cut value of 0.1, corresponding to  $\epsilon(sig) = 92\%$  for  $\epsilon(bkg) = 53\%$ .

It should be emphasized that the isolated track veto has a different impact on the samples with a single lepton (mainly  $t\bar{t} \rightarrow \ell + \text{jets}$  and  $W + \text{jets}$ ) and that with two leptons (mainly  $t\bar{t} \rightarrow \ell\ell$ ). For the dilepton background, the veto rejects events which have a genuine second lepton. Thus the performance may be understood as an efficiency  $\epsilon_{iso\ trk}$  to identify the isolated track. In the case of the single lepton background, the veto rejects events which do not have a genuine second lepton, but rather which contain a "fake" isolated track. The isolated track veto thus effectively scales the single lepton sample by  $(1 - \epsilon_{fake})$ , where  $\epsilon_{fake}$  is the probability to identify an isolated track with  $p_T > 10$  GeV in events which contain no genuine second lepton. It is thus necessary to study the isolated track efficiency  $\epsilon(trk)$  and  $\epsilon_{fake}$  in order to fully characterize the veto performance.

The veto efficiency for dilepton events is calculated using the tag and probe method in Z events. A good lepton satisfying the full ID and isolation criteria and matched to a trigger object serves as the tag. The probe is defined as a track with  $p_T > 10$  GeV that has opposite charge to the tag and has an invariant mass with the probe consistent with the Z mass.

The variable used to study the performance of the veto is the absolute track isolation, since it removes the dependence of the isolation variable on the  $p_T$  of the object under consideration. This is particularly

useful because the underlying  $p_T$  distribution is different for second leptons in  $t\bar{t} \rightarrow \ell\ell$  events compared to Z events, particularly due to the presence of  $\tau$ s that have softer decay products. As shown in Figure 28, the absolute isolation is consistent between Z + 4 jet events and  $t\bar{t} \rightarrow \ell\ell$  events, including leptons from W and  $\tau$  decays. This supports the notion that the isolation, defined as the energy surrounding the object under consideration, depends only on the environment of the object and not on the object itself. The isolation is thus sensitive to the ambient pileup and jet activity in the event, which is uncorrelated with the lepton  $p_T$ . It is thus justified to use tag and probe in Z + 4 jet events, where the jet activity is similar to  $t\bar{t} \rightarrow \ell\ell$  events in our  $N_{\text{jets}} > 4$  signal region, in order to estimate the performance of the isolation requirement for the various leptonic categories of  $t\bar{t} \rightarrow \ell\ell$  events.

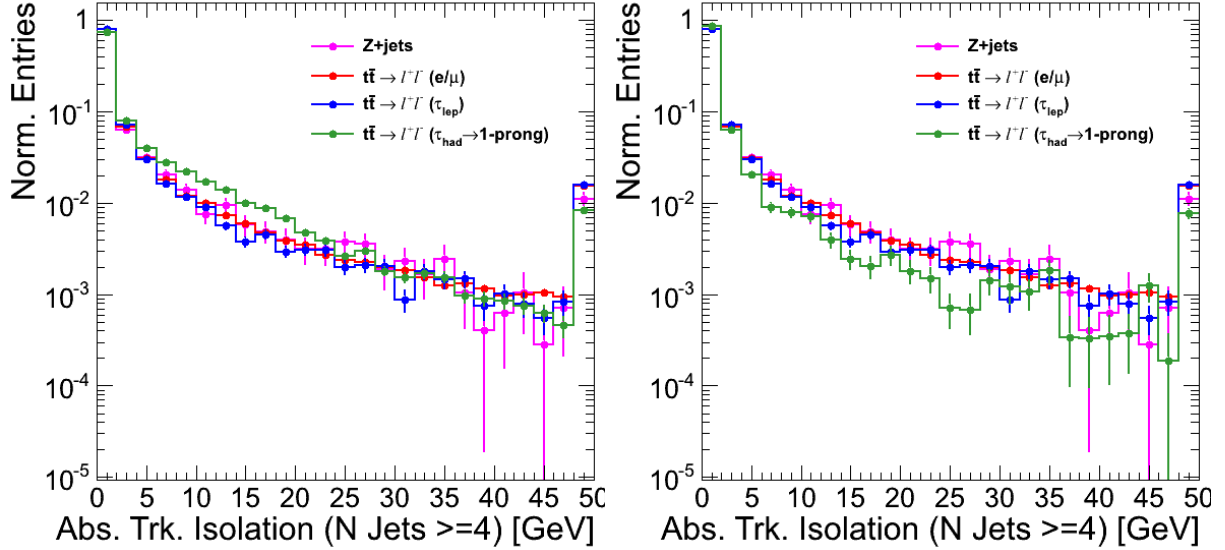


Figure 28: Comparison of absolute track isolation for track probes in Z + 4 jet and  $t\bar{t} \rightarrow \ell\ell$  events for different lepton types. The isolation variables agree across samples, except for single prong  $\tau$ s, that tend to be slightly less isolated (left). The agreement across isolation distributions is recovered after removing single prong  $\tau$  events produced in association with  $\pi^0$ s from the sample (right).

## B Additional CR Data and MC Comparisons

This appendix shows some additional comparisons of the data and MC background samples for various CRs. Figure 29 shows some additional components of the  $M_T$ , the lepton  $p_T$  and the azimuthal angle between the lepton and the  $E_T^{\text{miss}}$  for CR1 (Section 6.1). Figure 30 shows the equivalent distributions for CR2 (Section 6.2), the positive lepton  $p_T$  and the angle between this lepton and the pseudo- $E_T^{\text{miss}}$ . Similarly, figure 33 shows the lepton  $p_T$  and the azimuthal angle between the lepton and the  $E_T^{\text{miss}}$  for CR5 (Section 6.4). Figures 31 and 32 provide some data and MC comparisons of the  $t\bar{t} \rightarrow \ell\ell$  control sample CR4 (Section 6.3) for various kinematic distributions: leading lepton  $p_T$  and eta, as well as the angles between the two leptons and between the leading lepton and the  $E_T^{\text{miss}}$ . These distributions show quite good agreement between data and MC. More quantitative information is included in the section discussing each control region.

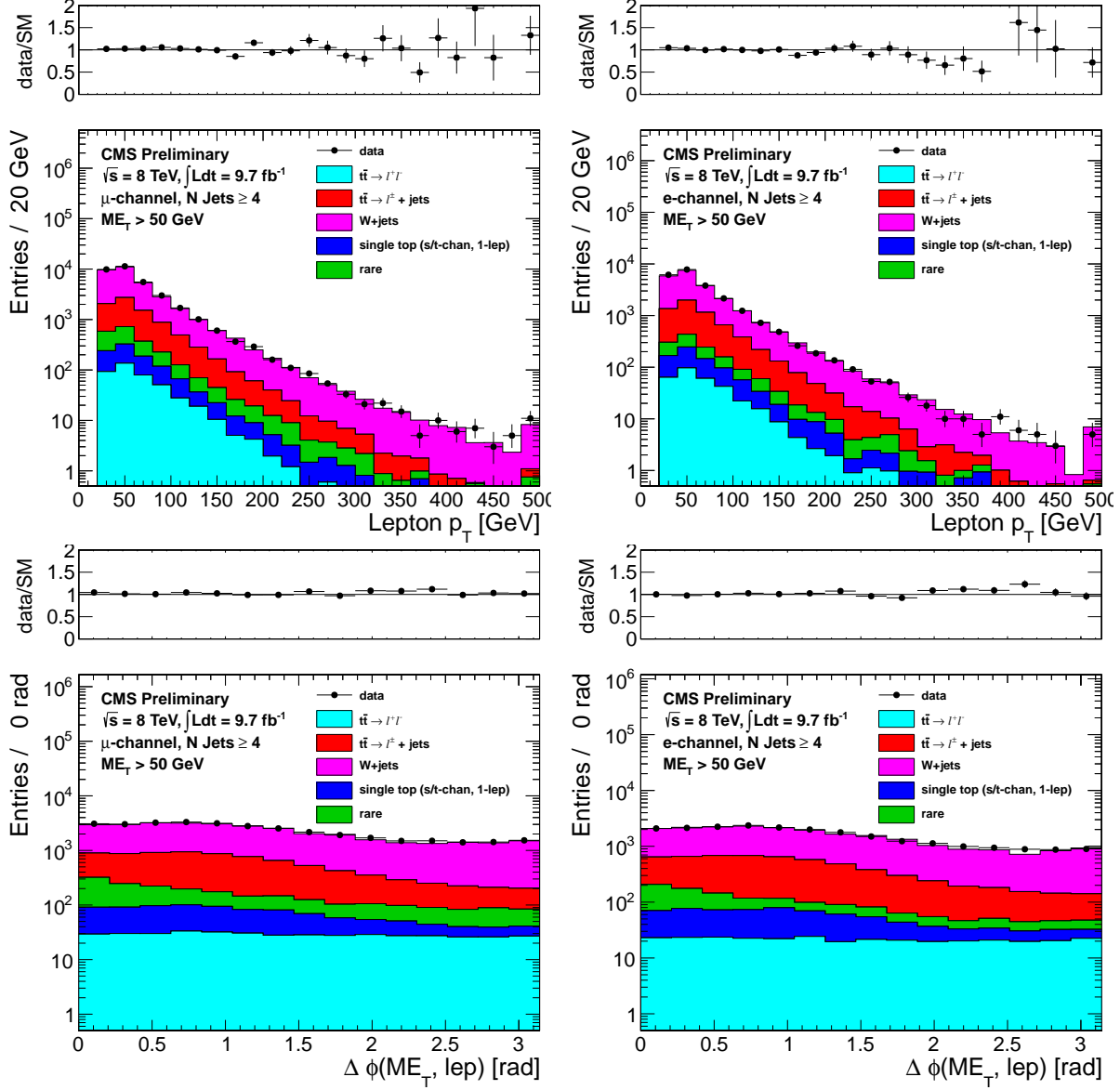


Figure 29: Comparison of the lepton  $p_T$  (top) and azimuthal angle between the  $E_T^{\text{miss}}$  and the lepton (bottom) for data vs. MC for events with a leading muon (left) and leading electron (right) satisfying the requirements of CR1.

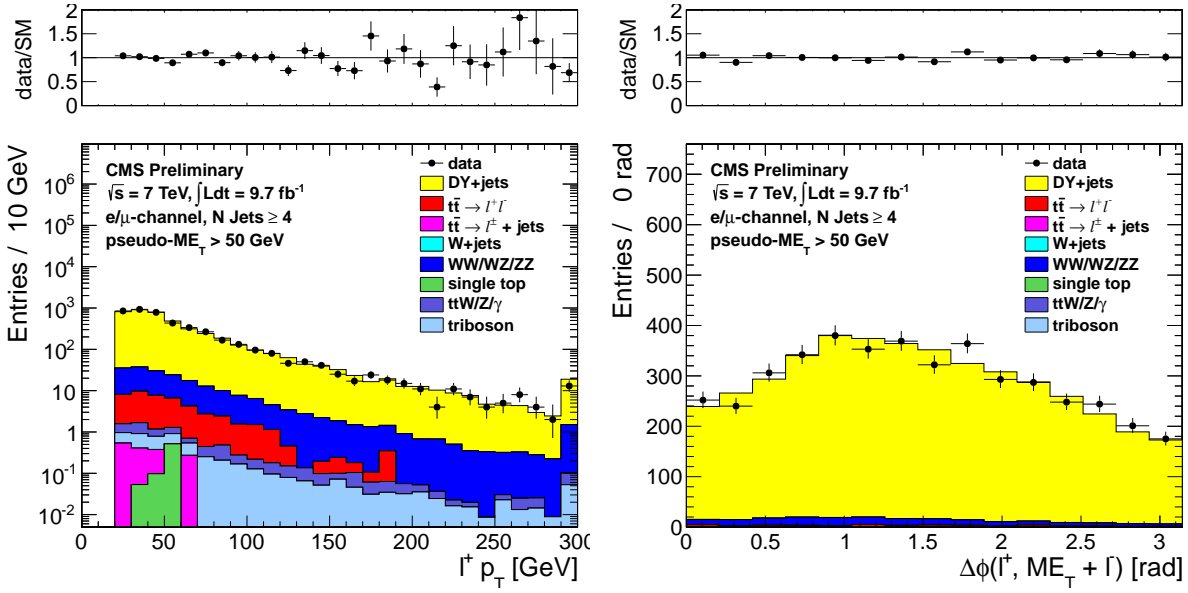


Figure 30: Comparison of the positive lepton  $p_T$  (left) and the azimuthal angle between this lepton and the pseudo- $E_T^{\text{miss}}$  (right) distributions in data vs. MC for events satisfying the requirements of CR2, combining both the muon and electron channels.



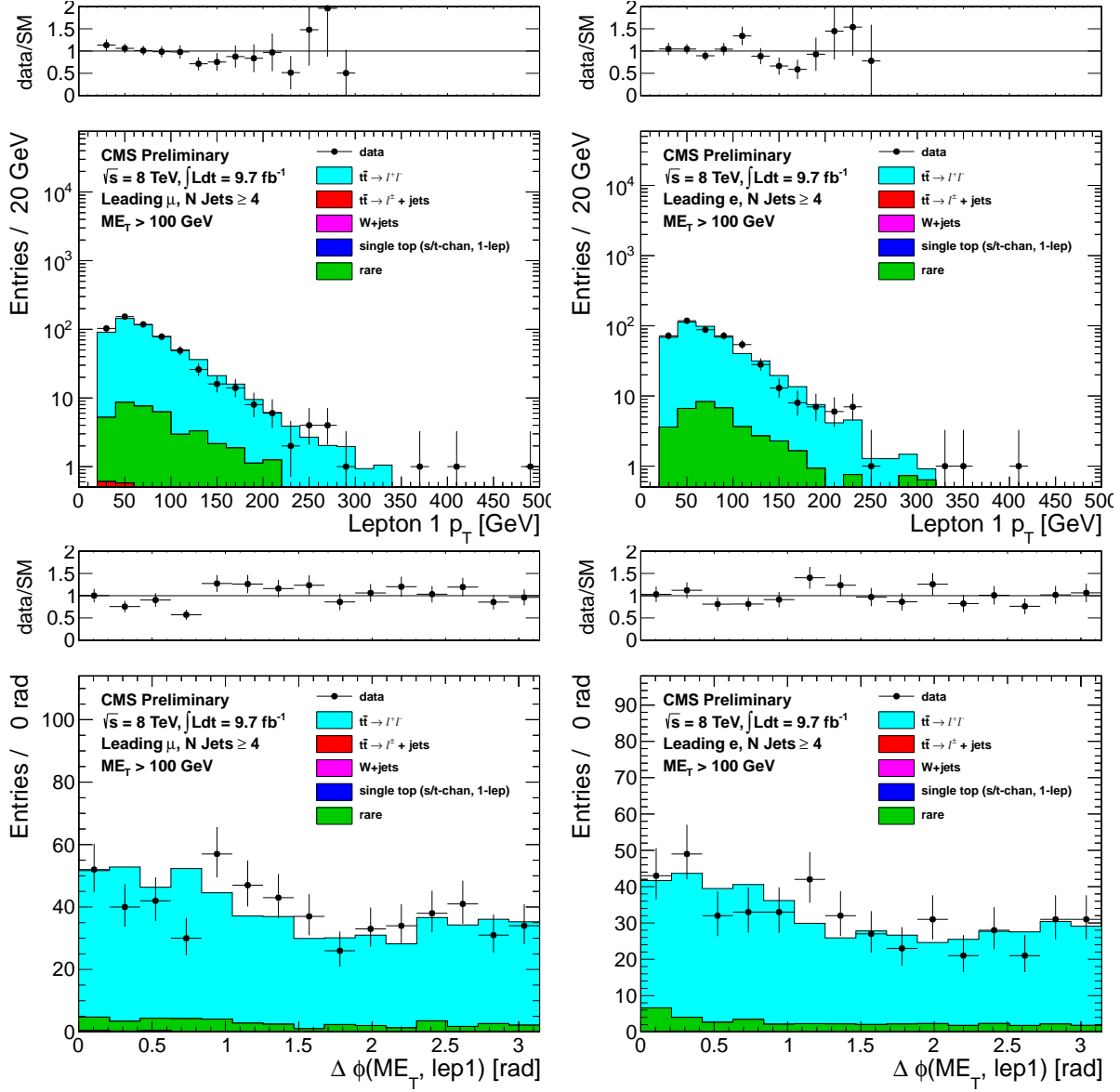


Figure 31: Comparison of the leading lepton  $p_T$  (top) and azimuthal angle between the leading lepton and the  $E_T^{\text{miss}}$  for  $E_T^{\text{miss}} > 100 \text{ GeV}$  distributions in data vs. MC for events with a leading muon (left) and leading electron (right) satisfying the requirements of CR4.

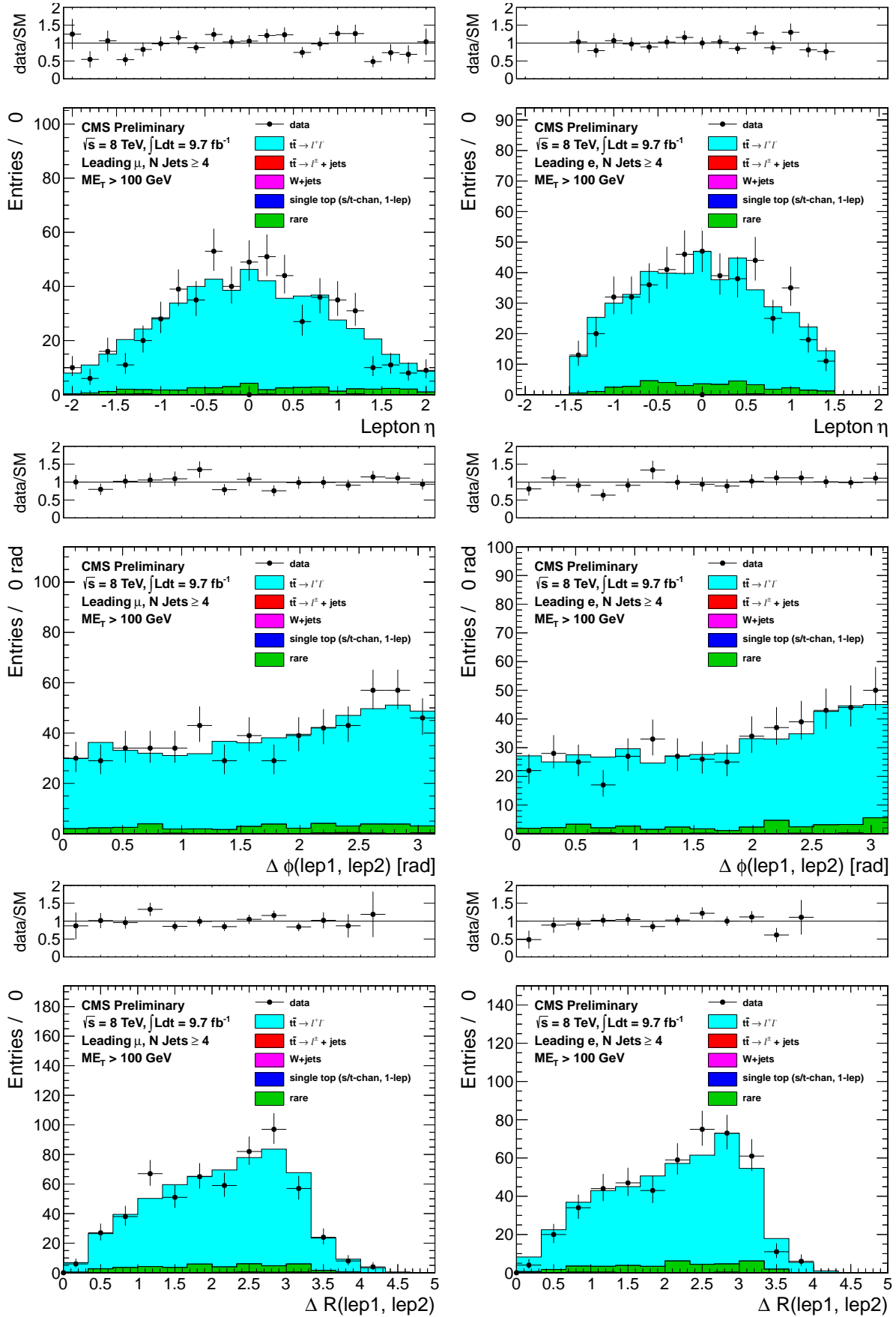


Figure 32: Comparison of the leading lepton  $\eta$  (top), difference in the azimuthal angle (center) and  $\Delta R$  separation (bottom) between the two leptons for  $E_T^{\text{miss}} > 100 \text{ GeV}$  distributions in data vs. MC for events with a leading muon (left) and leading electron (right) satisfying the requirements of CR4.

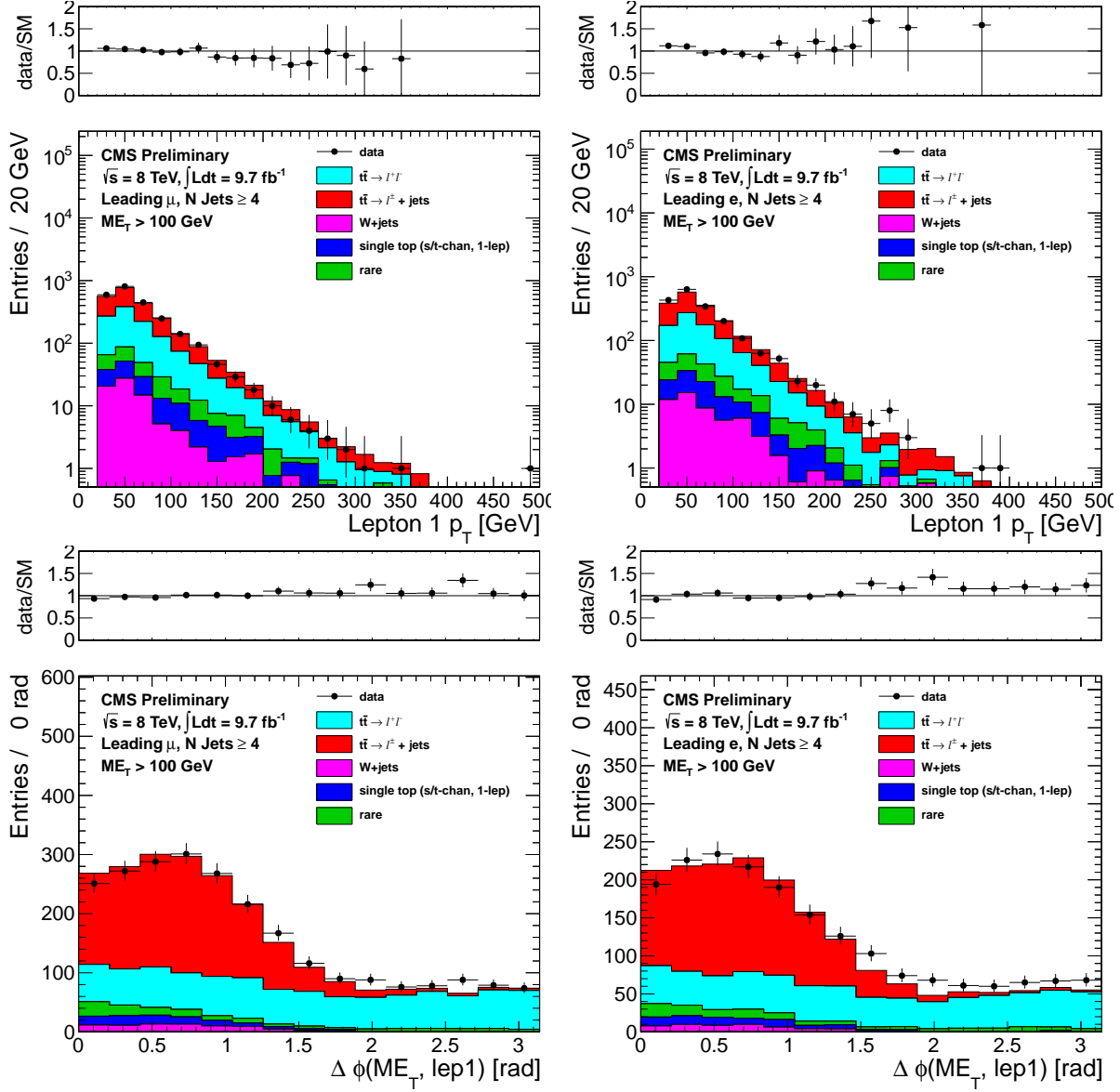


Figure 33: Comparison of the lepton  $p_T$  (top) and azimuthal angle between the  $E_T^{\text{miss}}$  and the lepton (bottom) for data vs. MC for  $E_T^{\text{miss}} > 100 \text{ GeV}$  for events with a leading muon (left) and leading electron (right) satisfying the requirements of CR5.

## C Glossary of abbreviations

$R_{wjet}^e, R_{wjet}^\mu, R_{wjet}$

Monte Carlo ratio of  $W + \text{jet}$  events in the  $M_T$  tail to the  $M_T$  peak. Separately for electrons and muons, or combined.

$R_{top}^e, R_{top}^\mu, R_{top}$

Monte Carlo ratio of  $t\bar{t}$  or single-top  $\ell + \text{jets}$  events in the  $M_T$  tail to the  $M_T$  peak. Separately for electrons and muons, or combined.

$SFR_{wjet}^e, SFR_{wjet}^\mu, SFR_{wjet}$

Data/MC scale factors for  $R_{wjet}^e, R_{wjet}^\mu, R_{wjet}$

$SFR_{top}^e, SFR_{top}^\mu, SFR_{top}$

Data/MC scale factors for  $R_{top}^e, R_{top}^\mu, R_{top}$

$K_3$  and  $K_4$

Scale factors for  $t\bar{t} \rightarrow \ell\ell$  events with one or two extra jets from radiation

$SF_{pre}$  and  $SF_{post}$

Scale factors to be applied to MC to normalize to the yields in the  $M_T$  control region before and after the application of the isolated track veto.